PERFORMANCE EVALUATION AND STABILITY ANALYSIS OF MULTI-LAYERED COVER SYSTEM FOR NEAR-SURFACE HAZARDOUS WASTE DISPOSAL FACILITY

Thesis Submitted in Partial Fulfilment of

the Requirements for the Degree of

Doctor of Philosophy

in Civil Engineering

by

Sudheer Kumar Yamsani

(Roll No. 136104005)

DEPARTMENT OF CIVIL ENGINEERING
INDIAN INSTITUTE OF TECHNOLOGY GUWAHATI
GUWAHATI-781039, INDIA

June 2018

CERTIFICATE

This is to certify that the thesis titled "**Performance Evaluation and Stability Analysis of Multi-Layered Cover System for Near-Surface Hazardous Waste Disposal Facility**" submitted by **Sudheer Kumar Yamsani** to Indian Institute of Technology Guwahati, for the award of the degree of **Doctor of Philosophy** is a record of bonafide research work carried out by him under my supervision and guidance. The thesis work, in my opinion, has reached the requisite standard fulfilling the requirement for the degree of **Doctor of Philosophy**.

Dr. S. Sreedeep
Professor
Department of Civil Engineering
Indian Institute of Technology Guwahati
Assam-781039, India.

DECLARATION

I hereby declare that this written submission represents my ideas in my own words and wherever others ideas and words have been included; I have adequately cited and referenced the original sources. I also declare that I have adhered to all principles of academic honesty and integrity and have not misinterpreted or fabricated or falsified any idea/ data/ fact/ source in my submission. This thesis, in any way, does not purport to endorse any proprietary products or technologies.

Sudheer Kumar Yamsani

(136104005)

ABSTRACT

Substantial change in human habitat lead to exponential rise in hazardous wastes that necessitate a stable and sustainable-engineered disposal facility. Near surface disposal facility (NSDF) with multi-layered liners and covers could help in containing such hazardous wastes thereby protecting the environment. Performance of liners is partly understood and numerous studies are in progress however, the performance assessment of multi-layered cover system (MLCS) is at its nascent stage. This study hence focused to reduce constraints influencing performance and stability of MLCS. The key issues with different layers of MLCS include erosion, desiccation, degradation, and infiltration (performance indices) of surface soil, clogging of filter and drainage layers, infiltration into barrier layers, and translational stability. Observing the influence of soil type and compaction state on performance indices of surface layer in MLCS, attempt was made to identify appropriate soil type and optimal zone of compaction satisfying performance markers suggested in literature. Results portrayed that soil with moderate plasticity exhibit optimal performance while those with low plasticity were prone to higher erosion and infiltration. High plastic soils result in high shrinkage and prone to desiccation. In addition, it was observed that the compacting soil at optimum water contents to higher densities would enhance its performance. Long-term hydraulic performance of different soil-geotextile systems were investigated using standard method and attempt was made to evolve a quick method for such long-term studies using geotechnical centrifuge. The study brings out the efficiency of centrifugation in quick evaluation of long-term hydraulic performance of different soil-geotextile systems. Lack of combined strength and seepage based design criteria for selection of drainage layer materials motivated in identifying optimal relative density and particle size of aggregates used in drainage layers.

Further, the existing method for translation stability analysis of uniformly laid cover soil over geotextile layer was extended for its applicability in MLCS and used for developing design charts for different scenario encountered in its life. Field studies on pilot MLCS found vegetation cover as the best means for resisting surface erosion. Empirically estimated and observed soil loss has shown great agreement when considered on annual basis however showed noticeable difference in temporal variation. Further studies are needed in evaluating field performance of MLCS and appropriateness of erosion estimation methods.

Keywords: Multi-layered cover system (MLCS), performance, stability, erosion, strength.

ACKNOWLEDGEMENTS

"Salutations to the respected teachers who open the spiritual eyes of those blind, due to ignorance, with the ointment of knowledge."

I would like to express my sincere gratitude and heartfelt thanks to my supervisor Dr. Sreedeep. S for his excellent technical guidance. I am always indebted to him for the freedom that he had given me to work at my schedule throughout this journey. He took keen interest right from the beginning of the research work until its completion. I am thankful for his generous nature and all his precious time that he spent with me during the entire course of my study. I am highly grateful to him for the valuable guidance and precious advice that will go a long way in moulding my career.

I am grateful to the doctoral committee members Dr. Subashisa Dutta, Dr. Arindam Dey, Dr. T.V. Bharat, and Dr. Kartha for their constructive comments, insightful inputs, and suggestions from the early stages of this research. I would also like to thank Dr. R. R. Rakesh, scientific officer, Bhabha Atomic Research Centre (BARC) for his timely inputs. The final shape of the thesis would not have been possible without their valuable feedback. I extend my thanks to the examiners of this thesis for their invaluable suggestions that helped in improving the thesis.

I highly appreciate Ministry of Human Resource Development (MHRD), India for providing me the fellowship. I am also thankful to Bhabha Atomic Research Centre (BARC), Govt. of India, for their financial support. I thank Director of the Institute, Head of the Civil Engineering Department, Dean Academics, and Dean R&D of IIT Guwahati for strengthening the research environment of the Institute to conduct my research. I also extend thanks to lab staff: Mr. Hariram Upadhyay and lab attendants: Mr. Karun Chandra Bhuyan, Mr. Raju, and Mr. Madav for their help during the experimentation phase.

I would like to thank Mrs. Malaya, Mrs. Poly, Mr Abhijeet Deka, Mr. Abhijeet rout, Mrs. Yagom Gapak, Mr. Abhishek, Mr. Sanandam, Mr. Prashanth, Mr. Niranjan, Mr. Sunil, Mr. Anghuman, Mr. Himanshu, Mr. Manas, Mr. Vinay, Mr. Sandeep for their support in the experimentation work and valuable discussions in the laboratory. I especially thank Mr. Bhanu and Mr. Janarul for their help in various aspects of my thesis work.

I would like to thank my supervisor's family, Omar's family, Janarul's family, and innumerable friends who made my time at IIT Guwahati enjoyable and helped me not to miss my home. I especially thank Mr. Srikanth, Mr. Ashok, Mr. Rajesh, Mr. Kishore, Mr. Mahendra, Mr. Milind, Ms. Jumrik, Mrs. Jagori, Mr. Shiv, Mr. Suchit, Mr. Tharun, Mr. Pradeep, Mr. Romeo, Mr. Chiranjeeb, Mr. Partha, Mr. Priyanka, Mrs. Olympa, Mr. Harinarayan, Mr. Doordarshi, Mr. Rana, Mr. Krishanu, Mr. Debu, Mr. Satish, Mr. Shibaji, Mr. Phalgun, Mr. Naveen, Mr. Biplab for helping me at various times during my stay at IIT Guwahati.

I received incredible support and encouragement from my parents, my brother, and all other members of my family. They kept me motivated and gave me a free hand without letting me know what all difficulties they were facing. Without their great support and unconditional love, this thesis would not have been possible. I thank all of them from the bottom of my heart.

I thank the Almighty God for showering his blessings upon me that I could reach upto here.

Sudheer Kumar Yamsani

(136104005)

CONTENTS

Abstract ***iv***

Acknowledgements ***v***

List of figures ***xi***

List of tables ***xv***

Chapter 1 Introduction **1**

1.1 General 1

1.2 Significance of the study 2

1.3 Objective and scope of the study 2

1.4 Organization of thesis 3

Chapter 2 Literature review **5**

2.1 General 5

2.2 Multi-layer cover configuration 5

2.2.1 Surface layer 5

2.2.2 Geosynthetic filter 6

2.2.3 Drainage layer 6

2.2.4 Geomembrane /geosynthetic clay liner (GCL) barrier 7

2.2.5 Compacted clay barrier 7

2.2.6 Foundation layer 8

2.3 Different cover systems 8

2.4 Review of cover failures 11

2.5 Review on surface erosion 14

2.6 Review on slope stability analysis 22

2.7 Critical appraisal of the reviewed literature 27

Chapter 3 Evaluation of surface soil and its compaction state for MLCS **29**

3.1 General 29

3.2 Pin hole test 32

3.2.1 Pin hole method 32

3.2.2 Pin hole characteristics 36

3.3 Jet erosion test 41
3.3.1 Jet erosion characteristics 44
3.4 Mini disk infiltration test 49
3.4.1 Infiltration characteristics 51
3.5 Volumetric shrinkage test 53
3.5.1 Volumetric shrinkage characteristics 54
3.6 Unconfined compressive strength test 56
3.6.1 Unconfined compressive strength characteristics 57
3.7 Suitability of soil as surface layer of MLCS 58
3.8 Suitability of soil compaction state 59
3.9 Summary 60

Chapter 4 Hydraulic performance of filter and drainage layers 61

4.1 General 61
4.2 Hydraulic performance of geotextile filter layer 61
4.2.1 Long-term flow test 63
4.2.2 Geotechnical centrifuge modelling of long-term permeability test 65
4.3 Long-term flow behaviour at 1-g condition 70
4.3.1 Effect of soil type 70
4.3.2 Effect of geotextile type 71
4.4 Centrifuge modeling of long-term flow test 74
4.4.1 Long-term flow results corresponding to 72-g 74
4.4.2 Scale factors for permeability at equilibrium 76
4.5 Hydraulic-mechanical performance of drainage layer 77
4.5.1 Effect of displacement rate on shear characteristics 79
4.5.2 Effect of particle size and relative density on shear characteristics 81
4.5.3 Effect of particle size and relative density on seepage characteristics 82
4.5.4 Combined variation of shear strength and seepage characteristics 83
4.6 Summary 85

Chapter 5 Field performance of surface layer of multi-layered cover system 87

5.1 General 87
5.2 Materials 87
5.3 Methodology 89

5.3.1 Construction of MLCS 89
5.3.2 Rainfall simulator 93
5.3.3 Weather station 94
5.3.4 Vegetation measurements 97
5.3.5 Infiltration monitoring 99
5.3.6 Erosion monitoring 99
5.4 Revised Universal Soil Loss Equation (RUSLE) 100
5.4.1 Rainfall–runoff erosivity factor 101
5.4.2 Soil erodibility factor 101
5.4.3 Topographic factor 'LS' 102
5.4.4 Vegetation cover management factor 'C' 103
5.4.5 Support practice factor P 103
5.5 Results and discussion 104
5.5.1 Vegetation characteristics 104
5.5.2 Infiltration characteristics 105
5.5.3 Erosion characteristics 106
5.6 Soil loss estimation using RUSLE 109
5.7 Summary 111

Chapter 6 Translational slope stability analysis of MLCS 113

6.1 Preface 113
6.2 Analytical model 114
6.3 Analysis of critical FoS for cover system 118
6.4 Effect of slope inclination 119
6.5 Effect of length of MLCS 120
6.6 Alternate methods for enhancing stability of MLCS 121
6.6.1 Effect of interface friction angle (Use of improved materials) 121
6.6.2 Construction of toe-berm 122
6.6.3 Influence of veneer reinforcement on stability of MLCS 126
6.7 Factors leading to the reduction in slope stability of MLCS 127
6.7.1 Upward movement of compacting vehicle 128
6.7.2 Downward movement of compacting vehicle 130
6.7.3 Seepage forces (horizontal submergence) 132

6.7.4 Seismic forces 135
6.8 Summary 137

Chapter 7 Conclusions and future scope 139

7.1 General 139
7.2 Conclusions 139
7.3 Major contributions 140
7.4 Future scope 140

References 141

List of Publications 161

LIST OF FIGURES

Figure 2.1 Various cover systems installed in ALCD project, DOE, USEPA 9
Figure 3.1 Experimental program to evaluate surface soil and its compaction state for MLCS 30
Figure 3.2 Selected compactions states around compaction curve of best performing soil 32
Figure 3.3 Schematic representation of pin hole setup 33
Figure 3.4 Compaction procedure of pin hole sample 33
Figure 3.5 Provision of hole inside pin hole sample 33
Figure 3.6 Image of in-house fabricated pin hole testing apparatus 34
Figure 3.7 Figure depicting the filtration of sediment solutions 34
Figure 3.8 Shear stress versus erosion rate variation of different soil types 37
Figure 3.9 Variation of erosion rate with shear stress for different compaction states 39
Figure 3.10 Variation of critical shear stress against water content at different densities 40
Figure 3.11 Conceptual illustration of erosion phenomenon at different water contents 40
Figure 3.12 Variation of erodibility against water content for different densities 40
Figure 3.13 Erosion indices for different compaction states 41
Figure 3.14 Conceptual figure describing jet erosion test 41
Figure 3.15 Figure depicting the sample preparation for jet erosion test 42
Figure 3.16 Jet impact on the soil surface 43
Figure 3.17 Classification chart for jet erosion test (Hanson and Simon 2001) 44
Figure 3.18 Variation in jet erosion rate with shear stress for different soil types 45
Figure 3.19 Jet erosion characteristics of different soils 46
Figure 3.20 Variation in jet erosion rate with shear stress for different compaction states 48
Figure 3.21 Classification of jet erosion characteristics for different compaction states 49
Figure 3.22 Compaction recommendations using jet erosion classification 49
Figure 3.23 Pictorial representation of mini disk infiltrometer 50
Figure 3.24 Schematic representation of infiltration on samples of different diameter 50
Figure 3.25 Variation of infiltration rates at different compaction states 52
Figure 3.26 Shrinkage test of lab scale rectangular and circular compacted specimens 54
Figure 3.27 Figure depicting oven dried soil samples 54
Figure 3.28 Variation of volumetric shrinkage test at different compaction states 55
Figure 3.29 Unconfined compression test sample preparation and extraction 56

Figure 3.30 Variation of unconfined compressive strength at different compaction states 58
Figure 3.31 Variation in failure strain at different compaction states 58
Figure 3.32 Final zone of acceptance based on overall performance markers 59
Figure 4.1 Experimental program to evaluate performance of geotextile filter 62
Figure 4.2 Pictorial and microscopic representations of various geotextile samples 64
Figure 4.3 (a) Pictorial and (b) schematic representation of long-term permeability setup 65
Figure 4.4 Small-scale geotechnical centrifuge facility installed at IIT Guwahati 66
Figure 4.5 (a) Pictorial and (b) Schematic depiction of centrifugal long-term permeability setup 67
Figure 4.6 Effect of soil type on long-term permeability of different soil-geotextile combinations at 1-g condition 70
Figure 4.7 Effect of geotextile type on long-term permeability of different soil-geotextile combinations 72
Figure 4.8 Temporal variation of long-term permeability of different soil-geotextile combinations tested at 72-g centrifugation 75
Figure 4.9 Experimental program to evaluate guidelines for optimum drainage material 78
Figure 4.10 Variation of shear stress against displacement for different displacement rates 81
Figure 4.11 Variation of shear stress against normal stress for different size aggregates 82
Figure 4.12 Variation of shear stress against normal stress for different relative densities 82
Figure 4.13 Variation of permeability and angle of shear resistance for varying particle size 84
Figure 4.14 Variation of permeability and angle of shear resistance for varying relative density 84
Figure 5.1 Experimental program to evaluate field performance of surface layer in MLCS 87
Figure 5.2 Schematic representation of field cover system 90
Figure 5.3 Pictorial image of constructed field setup 90
Figure 5.4 Preparation of materials to be filled in multi-layer cover system 91
Figure 5.5 Construction of field cover system 93
Figure 5.6 Experimental setup for evaluating erosion and infiltration of surface soil in multi-layered cover system 93
Figure 5.7 Micro weather station used in this study 95
Figure 5.8 Weekly average climatic variations in the study area during the monitoring period 96

Figure 5.9 Schematic layout of measurement locations on the surface of MLCS 97
Figure 5.10 Schematic procedure for calculating vegetation index using image analysis 98
Figure 5.11 Overview of infiltration measurement locations around crack and vegetated area 99
Figure 5.12 Soil loss accumulated in the erosion collection chamber 100
Figure 5.13 Temporal variation in percentage vegetation cover on the surface layer of MLCS 104
Figure 5.14 Section of surface layer with mixture of green and dry grass 104
Figure 5.15 Temporal variation of weekly average infiltration against weekly total rainfall 105
Figure 5.16 Temporal variation of weekly average erosion rate against weekly total rainfall 106
Figure 5.17 Variation in soil loss depth due to erosion for a period of 12 months 107
Figure 5.18 Rill profile of a section describing influence of vegetation and boundary 108
Figure 5.19 Observed versus estimated soil loss for surface layer of filed pilot MLCS 110
Figure 6.1 Experimental program to evaluate translation slope stability of MLCS 114
Figure 6.2 Schematic outline of multi-layered cover system (MLCS) 115
Figure 6.3 Simplified MLCS for stability analysis along the n^{th} interface 116
Figure 6.4 Interactions of MLCS at the base of the passive wedge 117
Figure 6.5 Typical configuration of RCRA subtitle C cover system 118
Figure 6.6 Design curves for FoS of MLCS with change in slope 120
Figure 6.7 Design curves for FoS of MLCS with change in slope length 121
Figure 6.8 Design curves for FoS of MLCS with change in interface shear strength 122
Figure 6.9 Stability enhancement of MLCS using toe berm installation 123
Figure 6.10 Design curves for FoS of MLCS using toe berm of unit width at various vertical extents 124
Figure 6.11 Design curves for FoS of first interface in MLCS using toe berms of various width 125
Figure 6.12 Multi-layered cover system with tapered layers from toe to crest to enhance stability 125
Figure 6.13 Best suited reinforcing systems for selected MLCS configuration 126
Figure 6.14 Design curves for FoS of MLCS with change in tensile strength of reinforcements 127

Figure 6.15 Force distribution for compacting vehicle ascending the slope 129
Figure 6.16 Design curves for FoS of MLCS while compacting vehicle is ascending the slope 130
Figure 6.17 Force distribution for compacting vehicle descending the slope 131
Figure 6.18 Design curves for FoS of MLCS while compacting vehicle is descending the slope 132
Figure 6.19 Force distribution during horizontal submergence of slope 133
Figure 6.20 Force distribution for pseudo-static stability analysis 135
Figure 6.21 Design curves for FoS of MLCS with varying pseudo-static seismic coefficients 137

LIST OF TABLES

Table 3.1 Summary of basic geotechnical properties of selected soils 31

Table 3.2 Energy and flow rates corresponding to various rainfall forms 34

Table 3.3 Classification of erosion based on soil erosion rate index (Wan and Fell 2004) 36

Table 3.4 Pin hole characteristics of various soil types 36

Table 3.5 Energy and flow rates corresponding to various rainfall forms 42

Table 3.6 Jet erosion characteristics of various soil types 45

Table 3.7 Summary of overall performance markers of various soils 52

Table 4.1 Summary of basic properties of selected geotextiles 63

Table 4.2 Details of centrifuge 67

Table 4.3 Summary of long-term permeability characteristics of different soil-geotextile combinations at 1-g condition 73

Table 4.4 Summary of scale factors 76

Table 4.5 Summary of basic properties of aggregates selected for drainage layer in MLCS 78

Table 4.6 Permeability values of various particle sized aggregates 83

Table 4.7 Variation of permeability values with relative density of aggregates 83

Table 5.1 Summary of geotechnical properties of various cover soils 88

Table 5.2 Summary of general properties of geosynthetic specimens 89

Table 5.3 Configuration of multi-layered cover system 89

Table 5.4 Characteristics of simulated rainfall events 94

Table 5.5 Support practice factor P for various land use types 104

Table 5.6 Summary of rainfall–runoff erosivity and vegetation management factors 109

Table 5.7 Observed versus estimated soil loss for surface layer of filed pilot MLCS 110

Table 6.1 Details of different interfaces in multi-layered cover system (MLCS) 118

Table 6.2 Variation in FoS of MLCS with change in horizontal submergence ratio 135

Chapter 1
Introduction

1.1 General

Industrialization and urbanization has led to growth in hazardous contaminants that are radioactive in nature (EIA 2014). Safe and sustainable waste containment systems are of prime concern to prevent the ill effects posed by uncontrolled waste disposal in open lands (USEPA 1989). Near surface waste disposal facilities (NSDF) are one such schemes used for isolating the low and intermediate level radio-active waste from living habitat. NSDF includes multi-layered liners, covers, made of different soil composite systems, to inhibit contaminant interaction respectively from subsurface, and atmosphere. There are numerous studies that deal with design considerations of liner systems however, not many researchers have focused in evaluating performance and designs methods of cover systems (Albright et al. 2004; Benson et al. 2007), specifically for Indian subcontinent. Considering severe rainfalls and high temperature variations in tropical India, there is a great need to relook the performance of Multi-layered cover system (MLCS) for NSDF.

MLCS is usually made with layers of soils and geotextiles, each having definite role in waste isolation. The configuration of MLCS depends on type of waste and site conditions (Koerner and Daniel 1997). According to Landreth and Carson (1991), Resource conversation and recovery act (RCRA) subtitle 'C' MLCS configuration would likely perform better in climatic regions with high rainfall and intense temperatures (USEPA 2000, Dwyer 2003). It consists a surface layer made of locally available soil that helps in protecting other components of cover system, from direct interaction with atmospheric variants viz. rainfall, frost, radiation and temperatures. It is followed by a thin geotextile layer that protects the internal erosion of surface soil into drainage system present beneath. Drainage layer made of coarse sand or gravel helps in diverting infiltrated rainwater towards exit, thereby decreasing the hydraulic head over barrier layers. Multiple barrier layers made of composite geosynthetic clay liner (GCL) and conventional clay barrier are used for complete isolation of waste from atmosphere. Barriers essentially prevent waste-atmosphere interactions in two ways: venting waste gases/radiation into atmosphere and infiltrating water/oxygen into waste components (USEPA 1989). A thick layer of well-compacted locally available soil is used as foundation for these cover components, which prevents uneven in-situ settlements. Effective performance of individual components and

overall performance of MLCS in union of different components needs to be systematically evaluated before construction.

MLCS is generally built in mild to moderate slopes to prevent rain induced surface infiltration that might weaken the stability of it (USEPA 2015). Interface of soil-geotextiles or soil-soil components is always a weak layer prone to failure (Koerner and Hwu 1991; Koerner and Soong 2005; Bergado et al. 2006; Dixon et al. 2006). Constant soil-atmosphere interactions of surface layer induce erosion, infiltration, and desiccation, which subsequently reduce its performance (Daniel and Wu 1993; Benson et al. 2001; Piet et al. 2005). Clogging of geotextile filter beneath surface soil (Rowe 1998; Giroud et al. 2000; Koerner and Koerner 2013) and insufficient capacity of drainage layer (ITRC 2003; Merry et al. 2005; Tao et al. 2008) are other issues that are of prime consideration. For these reasons, this research attempts to evaluate the performance and stability of MLCS through systematic laboratory, field, analytical, and numerical studies.

1.2 Significance of the study

Critical assessment of literature indicated that there are relatively very few case studies associated to the long-term hydro-mechanical performance of cover systems. This is likely because the strong requirement of MLCS has been felt only recently, due to the attainment of full capacity of landfills and surface dumps. This is specifically true for hazardous radioactive shallow waste disposal facilities in developing countries like India (CPCB 2010). Though erosion is identified as a key restraint influencing performance of cover system, systematic assessment of erosion in surface soils is hardly attempted, particularly never attempted in wet-tropical Indian region. In addition, forensic investigation of existing municipal waste landfills indicates lack of sustainable cover system as prime reason for failure to happen (Suter et al. 1993; Siebecker 2005; Huvaj-Sarihan and Stark 2008; Zekkos et al. 2014; Lavigne et al. 2014). Considering the severity of contaminants in NSDF and the cost incurred in building these facilities, there is an immense need for a detailed study to orderly assess the performance and stability of MLCS.

1.3 Objective and scope of the study

The main objective of the study is to evaluate the performance of surface layer and overall stability of MLCS by controlled laboratory experiments and field studies. Following are the different scope of this study to achieve the objective:

1. Develop criterion for the performance evaluation of surface layer of MLCS by incorporating surface erosion.
2. Determination of long-term hydraulic performance of soil-geotextile filters and drainage layers of MLCS.
3. Evaluating field performance of MLCS affected by natural and simulated climatic conditions.
4. Translational stability analysis of MLCS under the influence of different anticipated field situations.

1.4 Organization of thesis

The thesis was presented in seven Chapters. Introduction, significance, objective, and scope of the study were presented in this chapter. Chapter 2 presents detailed literature review describing different types of landfill cover systems, hydraulic and stability performance studies of MLCS, forensic investigations detailing the limitations of cover systems lead to failure of landfills. Observing key constraints that influence long-term performance of cover systems, studies related to erosion, slope stability, performance of materials, design considerations of cover systems and many more were reviewed in this chapter. Chapter 3 includes the laboratory studies for evaluating the effect of soil type and compaction state on the performance of surface layer in MLCS. The performance of surface soil was assessed by evaluating index properties viz. erosion, infiltration, volumetric shrinkage (desiccation) and strength that represent major soil-atmosphere interaction mechanisms. Chapter 4 contains the performance of geotextile filter systems and drainage systems in cover systems. Performance of filter systems affected by change in soil type, gradation and geotextile type was presented. The efficacy of method for quick assessment of long-term hydraulic performance of soil-geotextile systems under accelerated gravity conditions was evaluated. Methodology for inclusion of combined shear and seepage characteristics in design of drainage layer was discussed in this chapter. Chapter 5 details the field studies involved in assessing the hydro-mechanical performance of pilot MLCS. The MLCS field model influenced by varying climatic conditions and simulated rainfall conditions was assessed in terms of its infiltration, erosion, and vegetation characteristics. Chapter 6 extends the analytical method for translational stability analysis for evaluating MLCS. The stability of multiple layers of cover system influenced by varying slope, material characteristics, stabilization methods, maintenance activities, and environmental factors was assessed using extended analytical method. Finally, the major conclusions and

contributions were summarized in Chapter 7. Recommendations for future work were also included in this chapter.

Chapter 2

Literature review

2.1 General

Multi-layered cover system (MLCS) is an important component of any landfill facility, which isolates various kinds of waste from direct atmospheric interaction thereby reducing the amount of effluents (leachate or greenhouse gases observed in surface dumps). Performance of MLCS mainly depends on efficiency of design (configuration of cover layers) that suits local climatic conditions and the materials that effectively associate with the atmospheric variations. Surface layer forms the essential part of MLCS, which is likely subjected to repeated erosion, infiltration, and desiccation influenced by cyclic changes in atmospheric conditions. Translational stability of covers is another major concern, as the interface between the contrasting materials used in different layers of MLCS is a weak layer prone to fail. Critical review of the literature indicates that there are not many studies, which deal with the field performance of pilot cover systems under extreme tropical climatic conditions (predominantly observed in Indian subcontinent). Such studies are essential for the long-term liability in post-closure performance of any landfill facility. This chapter hence deals with the review of existing literature that helps in understanding different configurations of landfill covers, problems associated with cover failure of existing landfill facilities, various cover performance studies, stability analysis under different scenario, erosion of surface soils, etc.

2.2 Multi-layer cover configuration

MLCS involve in multiple functions namely barrier, drainage, protection, self-stabilization, etc. Single material could not serve all the needs; hence, the MLCS essentially contains different layers of soils and geosynthetics, each having definite purpose to perform. In this part of literature, firstly, the different layers seen in various MLCSs are discussed in detail and later few commonly used MLCS configurations are discussed. The configuration of MLCS differs mainly based on the number of layers and thickness of layers present in it depending on the waste characteristics and site specifications.

2.2.1 Surface layer

A layer made of natural soil having relatively low permeability was placed at the top of the MLC for protecting bottom layers from being eroded due to continuous precipitation. The

surface layer was sloped at a grade of 3 to 5% for facilitating effective runoff. U.S. EPA recommends soil having maximum erodability of 2 ton/acre/yr to be used as surface layer. Surface layer essentially necessities a layer of vegetation to resist runoff-induced erosion. Drought resistant locally adaptable vegetation was recommended for vegetation layer for effective erosion control. In most of the case studies, the failure of cover system was attributed to the failure of top soil, by lack of resistance towards erosion and desiccation resulting in uncontrolled seepage into bottom layers (Koerner and Daniel, 1997).

2.2.1.1 Biotic barrier layer

In some cases, a high thickness soil layer can be provided below the surface protection layer and above drainage layer. Such a layer was made of cobbles or locally available soil which helps in preventing animal burrow and the root penetration into subsequent layers in case of vegetation cover system.

2.2.1.2 Vegetation layer

In instants of high erosion, a layer of vegetation is developed above surface protection layer to safeguard surface layer from rain and runoff induced erosion activity. Intense care need to be taken considering the extent of roots, not disturbing the function of protection and other layers present beneath. Site-specific effective vegetation needs to be identified considering local soil fertility that effective counters erosion process.

2.2.2 Geosynthetic filter

A geosynthetic filter made of woven or nonwoven geotextiles having hydraulic transmissivity more than 3×10^{-5} m^2/sec was used to restrict the flow of fine particles from surface layer along with infiltrating water that would clog drainage layer. Enough care needs to be considered in selection of appropriate filter that possess sufficient strength, enough roughness and essentially long-term compatibility with the soil present above it. Composite geosynthetic made of woven and non-woven geotextile components were proved relatively more efficient.

2.2.3 Drainage layer

A layer of high permeable coarse aggregates are laid below the surface and filter layer, to divert the infiltrating rainwater outside the cover system, thereby reducing the hydraulic head over the barrier layers present beneath. Hence, it is also referred as water diversion layer. The thickness and the type of aggregate were selected based on the climatic

conditions (peak rainfall of given site). Existing studies ignored cautious selection of aggregates considering the strength characteristics alongside seepage criteria. Moreover, use of aggregates may puncture the geomembrane layer present beneath, so usually it is supported with a blanket of fine sand with maximum particle size less than 3/8 inch having a minimum permeability 1 x 10^{-4} m/s. This provision would protect the geomembrane layer from punching action of coarse aggregates present in water diversion layer. It also promotes the stability of slope by increasing coordination between dissimilar layers. It also provides capillary effect between compacted clay and sand in dry seasons and hence reduces the possibility of desiccation.

2.2.3.1 Toe drain

Toe drain is one of the important component of cover system that takes care of the water infiltrated into the cover system. All the water that is infiltrated into cover system is diverted in to the toe drain through drainage or water diversion layer. Any problem in toe drain capacity or clogging will lead to pore pressure build-up followed by stability failure leading to bulk erosion or slope failure (Siebecker, 2005).

2.2.4 Geomembrane /geosynthetic clay liner (GCL) barrier

A layer of synthetic high tensile geomembrane of thickness more than 0.5 mm having very low permeability (almost negligible) was provided as a barrier layer to minimize downward seepage of water. Mostly the surfaces of geomembrane were smooth and cannot be stable while used in slope. To eliminate this problem, the geomembrane was sandwiched between two layers of high tensile geonets, thermally bonded. The layer of geonet above geomembrane also helps in promoting horizontal drainage of water along with increase in stability. In the absence of geomembrane, a layer of geosynthetic clay liner (GCL) is laid. GCL are prefabricated barrier made of geotextiles filled with compacted clay and binded within geomembranes. Use of composite GCLS is widely expanding considering the ease in construction and the quality in performance.

2.2.5 Compacted clay barrier

A thick compacted low permeable clay layer of minimum thickness 0.6 m, made of soil having permeability less than 1 x 10^{-9} m/s was provided as a final protection for infiltrating water. Utmost care need to be taken during design of this layer, as this is the final protection for water seepage. Problems such as desiccation, swelling, differential settlements may

occur in this layer, which need to be successfully countered. Mixtures of sands/ local soils with low permeable bentonites in different proportions were usually investigated to use in constructing these layers.

2.2.6 Foundation layer

A dense compacted sand/local soil layer was provided just above the waste as a foundation/prepared subgrade layer to protect the whole cover system from differential settlement of waste material and it promotes the stability of the slope. It sometimes also acts as gas collection layer. Gas collection layer is used in case of bio waste, household, agricultural, chemical, industrial waste isolation where, harmful gases would be produced due to continuous biological action. To collect these gases efficiently, a layer of gas collection was provided. This provision helps in maintaining barometric pressure levels, demoting differential settlements, protecting environment from greenhouse gases, protecting the upper layers from chemical degradation, etc. In some cases, where sulphate related wastes are present a layer of limestone was provided to protect formation of greenhouse gases to some extent.

2.3 Different cover systems

The United States Department of energy (DOE 2000) had worked on alternative landfill cover system (ALCS) that will be economic and efficient in various environmental conditions. In their work, they have constructed six different types of covers, each having defined limits and scheduled layers. The different types of covers constructed include two specified (by Resource Conservation and Recovery Act, U.S. RCRA) cover systems: RCRA subtitles C and D, four alternative cover systems: a GCL cover, a capillary barrier cover, an anisotropic barrier cover and an evapotranspiration soil cover is shown in the Figure 2.1. The construction procedure, design considerations, safety measures, performance results, etc. were explained in detail. The guidelines that are followed in cover construction include:

i) The permeability of the low permeable barrier layer has to be $1x10^{-7}$ cm/s or less.

ii) The permeability of the drainage sand layer has to be $1x10^{-2}$ cm/s or more.

iii) The permeability of the natural soil top layer has to be $1x10^{-5}$ cm/s or less.

iv) All the layers are sloped at a grade equal to 5%, in general 3% or more mild slope is suggested.

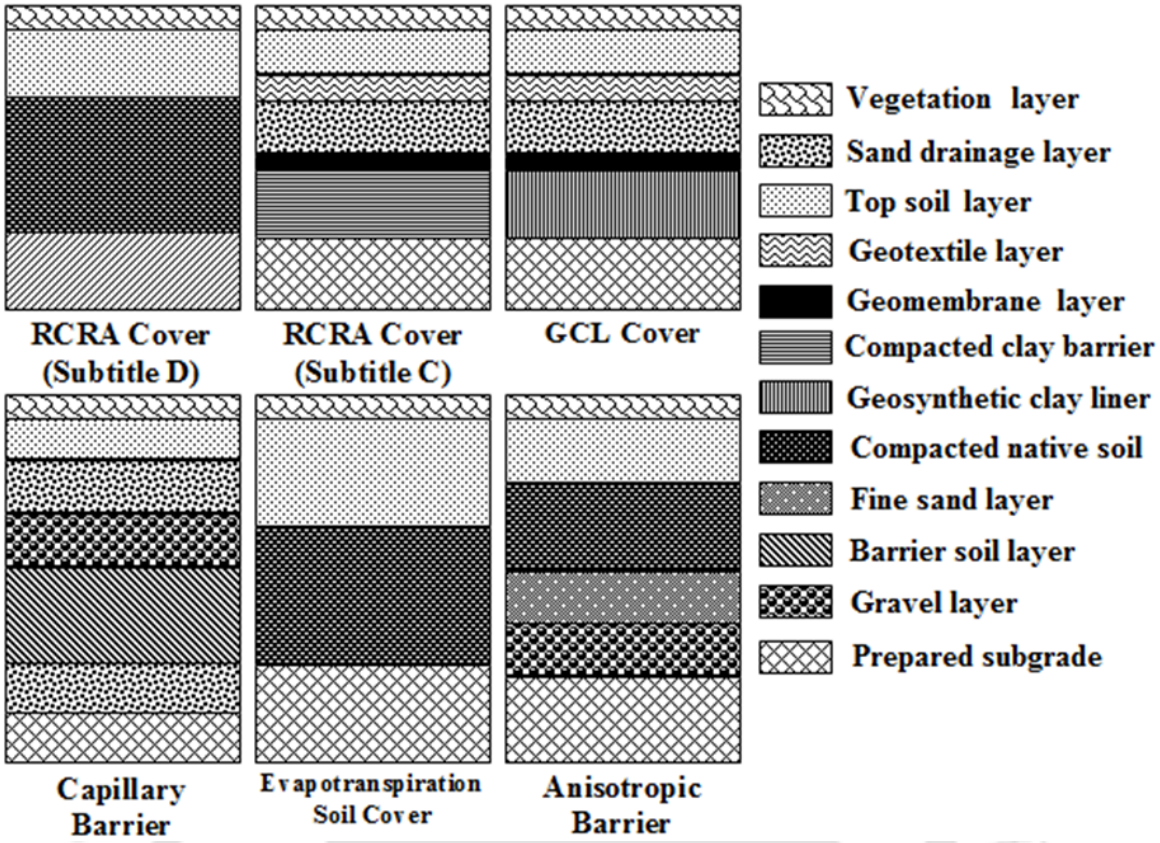

Figure 2.1 Various cover systems installed in ALCD project, DOE, USEPA

Comparing the costs and performance of various cover systems, anisotropic barrier cover and evapotranspiration cover were observed to be more appropriate in arid or semiarid regions. The failure of RCRA subtitle 'D' was attributed to desiccation cracks, while RCRA subtitle 'C' has performed well but the cost of construction was too high. GCL alternative cover was failed due to GCL damage and bentonite extrusion during construction while capillary barrier cover failed due to water build up in fine soil and sudden breakthrough into high permeable layer.

According to Daniel and Wu (1993), desiccation was common in MLC constructed in arid regions. In early study to minimize the desiccation, soil was compacted wet of optimum but it increased the desiccation rate. Later volumetric shrinkage potential was studied and concluded that the desiccation and volumetric shrinkage has one to one correlation. They also found that the cracking was minimal and healing was higher in clay barriers, in case of higher overburden pressure. Reformed clays those, which expand and compress back, cannot have satisfactory properties later. For better performance of cover systems, the following material properties are suggested for a clay barrier:

i) It should have a minimum hydraulic conductivity of 10^{-9} m/s.

ii) The maximum allowable shrinkage should be less than 4% (to avoid desiccation cracks).

iii) The material should have unconfined compressive strength of 200kPa or more (arbitrarily selected after Peck et al. 1974).

The study developed a zone of water content and dry unit weight on compaction curve where the desiccation and hydraulic conductivity will be minimal. For better performance, the cover soil was suggested be compacted dry of optimum at a higher compactive energy. It was also suggested that clayey sand would be a preferable material for the protection layer that would have minimal shrinkage due to low conductivity and compressibility. The study indicated that the desiccation can be completely eradicated if the compacted cover barrier was covered with a geomembrane backfilled by natural soil.

Ho et al. (2001), have discussed the probability of deviation of cover performance in long-term scenario due to increased environmental disaffects and degraded materials in cover system. It was mentioned that the available guidelines has no provision for these deviations, and do not take care of specific site scenario. It was recommended to select appropriate materials and design considerations according to site scenario and future performance deviations. The cover system considered in the study is made of four layers; top surface vegetation layer followed by sand drainage place over compacted clay and geomembrane.

O'Kane et al. (2002) in their manual for design of cover system for mine waste disposal sites described the various measures and controls needed for selecting a site-specific MLC design. The major objectives were to restrict the water and oxygen flow across the barrier system along with minor considerations like rainwater drainage and surface erosion, waste reactivity and corresponding settlements, etc. Utilisation of wet-dry cycles in designing capillary barrier system for arid and semi-arid sites, provision of geomembrane to enhance the performance in alternate cover systems, selection of large thickness protection layer and provision of multiple barriers in complicated cases were dealt in detail. The characteristics and evaluations required for selecting appropriate material for cover system were also discussed.

The methods to evaluate cover systems were explained along with the instruments used for monitoring the performance to achieve long term functioning were mentioned. Three case studies of constructed covers each in different environmental conditions

seasonally humid, semi-arid, and humid locations were explained. In the third case study test, plots consisting four different types of covers were studied for evaluating alternate cover system having better performance. Utilisation of fly ash as cover material was studied in this case study. An individual chapter was dedicated towards the erosion study and its control measures. This signifies the severity of erosion problem in cover systems.

Cooper et al. (2012) have discussed in detail the problems posed by the San Francisco naval shipyard waste and studied five alternatives for its containment. The selected cover design included the provision of underground barrier layer, a conceptual cover consisting of two-foot protection soil layer, gas vents, sloped drainage channels, erosion control measures, storm water management techniques, and proper monitoring and maintenance techniques. The barrier layer was made of compacted clay soil rolled by geomembrane for better performance.

Harshberger et al. (2012) have investigated the problem of Ohio landfill prior to establishment of cover system. The demolition waste along with the mine wastes created enormous pollution in surroundings. The problems identified such as rainfall infiltration, erosion of liquid waste to surroundings, production of hydrogen sulphide, underground fire incidents signifies the importance of constructing engineered cap system. Various stages of cover construction estimation, evaluation, planning, and execution were pictorially explained in detail.

Smith and Christos (2013) have compared the costs and performance of different types of cover systems and suggested that geomembrane or GCL cover systems are best out of all considered. The efficacy of evapo-transpiration covers in arid climates over humid regions was explained in detail. Compacted clay covers and water balance covers are observed to show poor performance in various sites. They study indicated that huge construction costs around $ 3.5 lakh/ha (Koerner, 2000) followed by the failure of traditional covers signifies the importance of design safety and measures to achieve a prolonged low cost cover system.

2.4 Review of cover failures

This section describes the multi-layer cover (MLC) failures reported by various researchers based on the field reconnaissance studies. In most of the past scenario, it was observed that the failure of cover system does not occur solely, but was combined with the failure of waste layer. The common causes of the failure is degradation of waste leading to

differential settlements, geotechnical stability issues, slope stability issues, surface erosion, root penetration, animal intrusion, desiccation of clay layers, clogging of filters and drains, improper sloping and materials used in construction, lack of proper maintenance, unexpected heavy storms, etc. (Siebecker 2005). Further, unnatural and unpredicted causes such as ion-exchange transformation in barriers lead to uncontrolled seepage, aging and expose of radiation deplete the geomembranes and reduce the integrity of cover (Bonaparte et al. 2002) were encountered. In addition, uncontrolled excessive waste intake increases the design slope that further leads to failure for example Kettleman hills hazardous waste landfill in California (Mitchell et al. 1990).

Nandakumaran and Richardson (1999) have identified the major cause for cover or liner failures during construction phase as the weak interface friction characteristics and improper consideration of equipment loads at construction site. The construction involving undesired method of soil placement (heavy movements) will lead to failure of geomembrane, which can be controlled by low volume soil movement under skilled supervision. The failure of drainage layer, due to erosion caused by unexpected precipitation can be prevented by limiting the area of construction of drainage layer in particular stage and sequential planning of further area. The importance of evaluating stability at different phases of construction was clearly explained. The study proposed empirical relations for calculating the design adequacy, surface erosion, and stability factors at various phases of construction.

They have further discussed the causes of the landfill cover failure from the observations of different failure cases and elucidated the design measures to be followed for sustainable design of cover system. A factor of safety equal to eight was proposed for hydraulic drainage design of cover system. The study detailed the procedure for erosion prediction according to RUSLE (Revised Universal Soil Loss Equation) and discussed the improvement of surface soil due to vegetation. Two case histories that failed one in construction phase and the other in service life were explained in detail. The failure in construction phase was observed due to wrinkles formed in geomembrane layer due to over soil movement during drainage soil placement and the tension caused in GCL and geomembrane interface due to excess gas and water pressures generated. Water pressure was generated due to drainage layer failure and gas pressures due to lack of proper gas collection system. The failure in second case was observed due to the drop in transmissivity of drainage layer due to clogging and due to root penetration into geonet drainage layer. In

post analysis, it was also observed that HELP software would overestimate the safety factor in drainage design ignoring complete saturation of cover soil layer that can be prevented by adopting unit gradient design method.

Piet et al. (2005) have described the probable causes for failure of evapo-transpiration cover system and explained the significance of proper planning, designing, monitoring, testing for ease of rehabilitation for long-term performance and economic benefits. The main causes of cover failure identified by the authors were the erosion of surface layer, improper vegetation selection, improper planning, and monitoring, degradation of material and system behaviour with time. The study recommends considering the transient and aging behaviour of materials, failure rate envelop, quality control criteria for safe design. Some important suggestions made in this study include keeping the water losses in bare soil less than the vegetation layer, selecting proper vegetation (as root depth plays important role in infiltration), and evaporation of surface soil (not more than precipitation). Further as infiltration effects the water balance in surface soil in arid areas, it was suggested to provide a surface protection layer of 1 to 2 m. The allowable soil loss rates, process of erosion, working of capillary barrier, Idaho National Engineering and Environmental Laboratory (INEEL) cover, evapotranspiration cover were discussed in detail. Rewetting of clay (swelling) would not completely recover the desiccation cracks.

The most appropriate design suggested by Siebecker (2005) consists of four layers: the bottom low permeable compacted clay liner backed with geomembrane layer just above the waste, which is overlaid by a high permeable geocomposite drain or cohesion less sand layer for draining surface infiltration. The drainage layer was cover by high compacted locally available soil forming top protection layer overlaid by vegetation layer for erosion control. In some cases single layer was used for both protection and vegetation layers.

The preventive measures for cover failure include proper sloping, appropriate material selection having good frictional and interface frictional characteristics with required permeability criteria, high capacity drainage layer and toe drain considering the extensive design period, regular monitoring and maintenance activities.

Sarihan and Stark (2008) have performed back analysis of observed landfill failures. Comparing four cases, the study suggested an average shear strength envelope from which the drained shear characteristics of waste were determined that can be used in

future designs. The causes for all the failures were observed to be due to similar reasons such as improper lining, covering, erosion control, improper compaction, poor drainage facilities and toe designs; non-homogeneity, degradation followed by non-uniform settlements, leachate and gas build-up. .

Richardson et al. (2008) have reported the cause of landfill cover failure that occurred due to lack of landfill gas vent from municipal landfill system. The study recommended construction of levee as a gas collection system and explained the method of establishing it in detail.

Smyth and Smith (2012) have attributed the cap failure to erosion caused due to improper vegetation layer and poor storm-water management systems. As part of remediation process, the waste was accumulated to single place and consolidated prior to cover construction. The cover was constructed from waste materials. 1-inch tire chips having transmissivity 0.3 cm^3/sec was used to construct 6-inch drainage layer that was cover by fill soil over which a vegetation layer was made that was planned to use for a golf course. The gas collection well was also established along with groundwater treatment plant. The treated water was used for agriculture.

Koerner and Koerner (2013) have identified multiple cases of geosynthetic filter failure most of which were located in waste isolation systems. Flow of fines from surface layers clogged the geosynthetic filter that lead buildup of pore pressures in protection layer, leading to failure of cover systems. Hence prior investigation of geotextile-cover soil compatibility through long-term flow tests would an effective way for establishing sustainable filter system.

2.5 Review on surface erosion

Erosion is one of the two major factors that severely affect the performance of surface layer of MLCS. Most of the existing studies dedicated in evaluating hydraulic performance of cover system compared to that of studies involved in interpreting erosion and stability of cover system. Further, very few number of studies involved in field performance evaluation of erosion on surface layers in developing countries like India. This part of literature provides comprehensive insights of various laboratory and field studies involved in evaluating the erosion characteristics of surface soils used in protection layers of MLCS. This section discusses various methods followed by different researchers for evaluating the amount of surface erosion, soil loss and the factors effecting surface erosion. Surface

erosion is assed in different ways in different fields (agriculture, geomorphology, geology, and geotechnology), which are discussed as follows.

D'souza and Morgan (1976) have studied the effect of slope shape and steepness on the amount of erosion on laboratory prepared samples of 2 m x 3 m at rainfall intensity of 53 mm/h. It was found that slope percentage follows a quadratic relation with the amount of erosion that occurs in the field that agreed with the equation proposed by Smith and Wishmeier (1957). Broadly the results indicate an increase in amount of soil loss with increase in slope percentage on all slopes with a relation convex > straight >concave. The amount of soil loss in case of convex slope is comparatively high due to availability of steep sections and is low in case of concave slopes due to deposition. The authors also verified a relation between the flow and the soil loss using Reynolds number, which was observed satisfactory.

Sutherland et al. (1996) have reviewed various causes of surface erosion and found that the rain splash and runoff induced erosion are the main process. The various factors that affect the erosion of a surface layer was found to be water content, aggregate size, bulk density, formation of micro dams and slope. The experimental plot was 0.3m x 0.6m x 0.1 m subjected to rainfall intensity of around 110 mm/h (in 3 h events) with 3.2 mean water drop size. The study observed an increase in runoff with slope and corresponding decrease in infiltration rate, decrease in splash soil in case of thin sediment surface, and variation between rain splash and wash erosion. The study reported the contradictory statement found in literature against their observed trends viz. Poesen, (1987) observed increase in infiltration with slope due to seal formation in sandy soil and El-Swaify, (1980) noted that not all soils were significantly prone to seal development.

Agassi and Bradford (1999) have reviewed the available methods for determining soil erosion and summarized the associated limitations in the methodologies. Erosion is not a single factor based phenomenon rather it is a combination of number of distinct factors rain intensity and runoff, infiltration, soil type and state, soil and water chemistry. Determining erosion under simulated rainfall ideally depends on the simulator characteristics (uniform rainfall intensity, drop size, kinetic energy, and velocity).

Soil loss determined in an experiment depends on its state so the experiment should replicate the insitu conditions, seasonal changes (wetting drying cycles, surface weathering), tillage, chemical effects. Erodability/ soil loss of a soil is comparatively low

in initially stages, which increases progressively. This indicates that variation of shear strength with time need to be verified. The strength of soil drastically changes upon wetting that which needs to be keenly studied.

They observed that soil plot has a crucial role in attaining the net soil loss under given rainfall intensity. Micro plots (0.3m x 0.3m) may overestimate soil loss compared to large plots (1m x1m) with buffer area. Buffer area has a crucial role in case of splash erosion where it helps the splashed soil (that involve in sealing) not to retain over the plot by which net soil loss was controlled. It was suggested that micro plots with no great edges can be tried that can take care of splashed soil which would spill around the sample area. Changing box gradient may cause the non-uniformity in rain characteristics in case of low height simulator. The soil at the edges of the boxes need to be well compacted to take care of edge effects.

Reddi et al. (2000) in the process of comparing the internal and surface erosion processes have discussed various techniques used for evaluating surface erosion of a given soil. The study employed ASTM recommended pin hole test in a sample of dimensions 25mm dia., 50mm length with a hole of 7mm dia. inside it. The samples were made small to decrease the effect of preferential paths, for easy evaluation and compacted on wet of optimum water content, to have a dispersed structure. The change in diameter of hole represents the erodability of soil and the turbidity of sediment solution was correlated to sediment concentration. Simple equations for determining critical shear stress were reported. The study of liquid concentration revealed that with increase in concentration of flowing water the critical shear stress increased.

Hamed et al. (2002) have tried to compare the soil loss results estimated from simulated rainfall experiments with that of observed catchment sediments. The field experimental plot dimensions were 1m x 1m; but the rain was generated over an area of nine m^2 to account for uniformity and runoff. In experimental studies, the runoff was observed to exist with a time lag, deviating from natural scenario. The estimated method and the experimental method ignore the vegetation present over the surface and its growth over the experiment period, which might have an effect on soil loss. The estimation included an upscaling technique which uses Wischmeier and Smith (1978) USLE equation's erosivity factor 'R' as follows

$$SL_{natural}=(R_{natural}/R_{simulated})*SL_{simulated} \quad \textbf{2.1}$$

Where SL represents soil loss and R represents the erosivity of the event.

It was noted that the results obtained from the above equation matched well with the reservoir sedimentation in the three test periods. The proposed equation was found to be valid for rill and sheet erosions.

Romkens et al. (2002) have studied the effects of rainfall regime, intensity, slope, surface roughness, and drainage pressures on the sediment concentration in a flume of 0.6m X 3.75m dimensions under a controlled simulated rainfall. Soil considered here was a silty loam material and the observations were limited to this study. It was noted from this study that Universal Soil Loss Equation (USLE) predictions are limited to US soils, field plot scale and parameters outcome of understanding process. Most of the other parameters like the surface roughness, storm regime, soil suction have been ignored. Detailed discussion on contradictory results of soil loss for insitu moisture content and surface roughness was made. It was noted that initially dry surface has a high soil loss and rate of detachment gradually decreases with progressive wetting. According to the sediment, results at regular intervals of suction increment depicted the decrease in sediment concentration with increasing suction, which was attributed to increase in cohesiveness and low rill formation. The increase in surface roughness resulted in increase in drainage density and it was observed that drainage density has an inverse effect on soil loss.

Leonard and Richard (2004) have reviewed the variation of soil shear strength and critical shear stress proposed by various authors. It was observed that grain shear stress was a better variable to estimate the critical shear stress than the total shear stress. The relationship between grain and critical stresses shows that the grain shear strength is almost 3 times greater than critical shear stress. The authors emphasized this difference was due to the grain shear strength which represents the soil present over a certain depth that is bonded by various forces with surrounding particles while the critical shear stress is because of the freely available particles at the surface.

$$\tau_c = \beta\sigma_s \quad \textbf{2.2}$$

where,

τ_c critical grain shear stress (kPa)

β erosion relation constant

σ_c soil shear strength (kPa)

The study specifies that there is no significant effect of flow (runoff or rainfall), soil texture (clay to sandy loam), and sample length for determining critical shear strength on the proposed relationship. The grain shear strength estimated from hand vane shear was observed to be overestimated compared to that of torvane shear test for which a correction factor of 0.6 was suggested by authors. It was also observed that the surface degradation decreases infiltration and depression storage of a given surface, and particles is eroded due to rolling than lift/drag.

Assouline and Ben-Hur (2006), have studied the effects of slope gradient and rainfall intensity on soil surface sealing and corresponding erosion. Soil layers of 20 mm thickness was placed over 80 mm thick coarse sand layer in a tray of 0.3 m x 0.5 m at a bulk density of 1.26 g/cc. It was reported that the soil erodability is independent of intensity and slope, and depends only on soil type. Moreover, it was found that the effect of rainfall intensity and slope on erosion and runoff was controlled by surface sealing property, which is dependent on soil type. The infiltration rate was found to increase with increase in slopes because at higher slope thin seals of higher permeability were formed due to higher erosion. The effect of slope on erosion increased with increase in rain intensity and was significant at steeper slopes.

Boardman (2006) has reviewed various types of erosion assessments available in fields of geology, agriculture, and engineering from different regions of USA and UK. According to this study, most of the existing models were case specific, results of which were significantly varying case to case for which a multipurpose, multi scale model was required. Existing models does not account field criteria like crusting, gravels, sudden cloudbursts or frequent small-scale rainfall events. For quick estimation, large-scale erosion events can be taken into account that has maximum part in total erosion but this will not take into account runoff induced erosion. Long term monitoring results for 10 years, 28 years will not take into account of future large events relatively important in semi-arid climatic regions where there are predictions of wide variations in rain intensities.

Wide spread Universal Soil Loss Equation (USLE) model (Wischmeier and Smith 1965) does not account for specific / precise erosion data but gives an average soil loss over long period. Purpose of assessment and scale of assessment has significant effect on the erosion prediction. Standard plots 22m x 2m cannot account for a landscape erosion; which results in exaggerated results by a factor of 2 to 10 compared to field, and in some cases, there were contradictory observations. The financial losses incurred by erosion in agriculture and geology, demand for an optimum model for appropriate erosion assessment.

Arnaez et al. (2007) have tried to evaluate amount of erosion in vineyards and compared the observed soil loss rates with that of Modified Universal Soil Loss Equation (USLE-M) model, and developed a model for the observed soil loss rates. Rainfall intensities of 2 to 127 year return periods were produced on 0.45 m diameter circular plots using portable rain simulator on a slope of 3.8°. Drop diameters and kinetic energies of different intensities were calculated using flour technique and energy correlations respectively. Results portray an increase in rainfall energy, soil loss, runoff, and wetting front with increase in rain intensity. The amount of soil loss calculated from the proposed equation was observed to be less than that predicted by USLE-M, which was attributed to the presence of gravel cover and lack of Length-Slope (LS) factor in proposed equation. The overestimation of soil losses at low intensities was due to the lack of consideration of water absorption. The high amount of soil loss at initial stages of rainfall was due to high availability of sediments and upon progressive rainfall the availability of loose and free soil decreases. The negative value in soil loss equations for intensity variation indicated the infiltration induced decrements in runoff and soil loss.

Briaud (2008) has explained the fundamental principles behind the erosion process from geotechnical perspective. According to this study, soil type, water flow, and geometry of sample were the three main factors that control erosion process. It was reported that particle drag, reduction in normal stress over particle and fluctuation in boundary forces around particle takes place during erosion due to buoyancy of flowing water. It was also stated that soil under suction has an apparent cohesion that can resist erosion action. Complete erosion including the turbulent action of water was formulated as a function to represent erodability of soil and an experimental device was developed to evaluate erodability. This study has classified the behaviour of soil from highly erodible to non-erodible based on the erodability of the soil with respect to their particle size and the velocity of water flowing over its surface.

Thoman and Niezgoda (2008) have tried to determine the critical shear strength, erodability and cohesive soil properties of river or channel bed that effect erodability, so that allowable discharge that can resist erosion can be assessed for a given in situ condition. Jet erosion test was conducted to determine the erodability and critical shear parameters. According to the attained data, a model was proposed correlating the properties of soil, to predict critical shear stress and was further validated from the experimental data. The weightage given to water content effect was observed to be low and contradicting the literature and the model has ignored the effect of dry density. The deviation of predicted and observed results might be due to the same reasons. An increase in critical shear stress was observed with increase in vegetation there by decreasing erodability.

Zhu et al. (2008) have reviewed the available techniques for determining surface erosion of cohesive soils that occur due to flowing water. Most of the available experimental techniques can only determine surface erosion but not the mass (gully) erosion. The factors effecting erosion was listed as shear strength, salinity of pore liquid, specific surface area, clay mineral, organic content, sodium absorption ratio, compressibility, particle gradation, temperature, density and pH In case of cohesive soils chemical properties plays a vital role in erodability along with physical properties while the latter is more influential for cohesion less soils.

Lei et al. (2008) have proposed a rational method for estimating erodibility and critical shear stress of eroding rill and the proposed method was validated through small-scale detachment tests conducted in the lab. The observed that for high resisting soils changes in soil erodibility with change in slope angle is inconsiderable and for accurate erodibility determination, they suggest to use samples of small dimensions. In this study critical shear stress is determined from sediment concentration while the water shear stress inside a rill is determined using the product of water density, slope and the flow depth. The proposed equation represents the dependency of erodibility on sediment volume and flow rate. Soil erodibility of water erosion prediction project (WEPP) was ten time less than the erodibility values determined by them.

Ekwue and Harrilal (2010) have studied the effects of soil type, peat content, compaction effort, and slope on the erosion of surface soil. It was noted that increase in peat content decreased infiltration contributing to high runoff and erosion. With increase in

compactive effort, infiltration decreases and runoff increases but erosion decreases. Increase in slope decreased infiltration there by increasing runoff and erosion.

Gaucher et al. (2010) have studied the effect of compaction on erosion of cohesive soil. Three types of soils were compacted at Proctor optimum in rectangular dimension 39cm x 26cm x 11cm on a flume bed. The compacted samples were subjected to the shear stress of flowing water. As expected, it was found that at Proctor optimum and near optimum, the amount of erosion occurring in the soil was minimum. The soil loss at optimum was two times less than that observed at 92% optimum compaction. It was reported that presence of entrapped air could accelerate the erosion of compacted soils.

Joshi and Tambe (2010) have conducted field erosion experiments on six different plots of 2m x 2m in Pravara basin, India to study the effect of slope and vegetation on the erosion under simulated rainfall. The observations found in six plots were reported as:

Plot 1: Runoff initiated after 40 min. that represents the grass induced higher infiltration. High infiltration, low runoff, and erosion were reported from this plot representing the efficacy of grass over slope.

Plot 2: As the surface soil in this plot was loose, a steady increase in runoff and sediment yield was observed in initial stages. Once the top soil was eroded, a crust was formed and then sediment yield dropped marginally.

Plot 3: Due to the organic matter (crop residue) in this plot, high infiltration and low runoff were observed in the first 30 min. The final sediment was also observed to be relatively low, representing the efficacy of organic matter resisting erosion.

Plot 4: The steep gradient and dry bare surface resulted in higher erosion and runoff in this plot. Out of all six plots, high amount of erosion was reported for this plot.

Plot 5: Moderate slope with higher gravels on this surface produced sharp decrease in infiltration rates at initial stages. The sediment amount was reported high but no much fines were transported.

Plot 6: The infiltration was observed high in this plot even with a steep slope due to higher grass content. The high infiltration, low runoff, and erosion represented the efficacy of grass in minimizing erosion.

Bagarello et al. (2011) have tried to establish the relation between amount of soil loss versus length and width of agricultural plot. Comparing the results from 2 x 11 m^2, 4 x 11 m^2, 8 x 22 m^2 and 2 x22 m^2, 8 x 22m^2 it was concluded that the effects of width and

length on soil loss were event based. In case of low and medium erosive events, the effect was significant and in case of highly erosive events, it was insignificant.

Defersha and Melesse (2012) have studied the effects of intensity, slope, and antecedent moisture content on the sediment concentration. Three types of soils were considered in this study with three rain intensities, three slopes, and two moisture conditions (air-dry and prewetted soil). The tests were conducted in a 320mm x 450mm pan under a rotating disk rain simulator (Foster, 1996) on a sample of thickness 60mm overlaid on 90mm gravel layer in the pan. The highest sediment yield was observed for air-dried soil at highest rainfall (120mm/h) and steeper slope (45%) while the highest runoff was observed for prewetted soil at same conditions. It was opined that high splash occur on dry surface, on wet surface sealing occurs which results in decrease in infiltration, and hence increase in runoff. The sediment concentration had no significant relationship with any of the factors. It was concluded that the effects of slope and intensity on sediment ratio, sediment yield, runoff coefficient and sediment enrichment ratio were dependent on soil type and moisture content.

Most of the existing erosion models USLE, RUSLE, MMF, EUROSEM, GUEST, etc. have been applied for predicting the soil loss from agricultural field so far to identify the highly eroded area so that suitable remedial measures can be adopted in order to preserve the fertility and productivity of the soil. Use of these models in geotechnical field is very limited. Mondal et al. (2016) has estimated the soil loss in Narmada river basin using USLE, RUSLE, and MMF alongside experimental evaluations. Further, comparing the results from different methods it is found that RUSLE was more effective with respect to other estimation methods.

2.6 Review on slope stability analysis

Stability of earthen embankments is a major issue in most parts of the world. Geotechnical structures involving layers of different materials similar to MLCS are majorly prone to translational failure where the interface between different materials is a weak medium highly prone to fail. Other comprehensive issues causing the failure of these systems include use of inappropriate materials, improper stability analysis, limitations of numerical models, unexpected high rainfall conditions. The following are some of the literature that identify the concerns with past slope stability analysis of various earthen systems.

Anderson et al. (2000) have reported the causes for the reactivation of latent earth flow under a roadway in Colorado. The site was composed of stratified soft soil (silt over clay) over a soft clay rock. The failure was initiated in the shear zone at the contact of clay rock and soft clay above it, where there was a high built up of pore pressure for long duration due to high precipitation in 1997. This was further aggravated by increased width of an unlined irrigation ditch located adjacent to the highway. The removal of soil from ditch to highway depression decreased global stability.

David and stark (2000) have explained the importance of 3D slope stability analysis over conventional 2D analysis. Conventional 2D analysis or available 3D analysis ignores the resistance on vertical sides on the sliding mass, which results in uncertain factor of safety (FoS) mainly in case of complicated topography, complex pore pressure condition, special variation in strength and presence of different materials. This problem was resolved by application of calculated amount of resistance at the centroid of sliding mass. The variation of FoS was significant in case of 3H: 1V (Slope horizontal: vertical) and W/H<4 (Width / Height ratio). The effect of variation of soil was also studied by varying the strength of lower layer and not disturbing surface layer. A significant variation in FoS was observed for 5H: 1V and W/H <4, where the former increased with decreasing W/H ratio.

Beikae (2000) has proposed a new method to analyse the stability of a slope unlike the conventional limit equilibrium method. The finite difference program DSLOPE used by the author takes the dead weight of the sliding slope, saturated and unsaturated shear strengths, shear modulus, bulk modulus and the direction of movement as input with no initial movement. From these input, it calculates the local FoS of individual slices and the deformation at the toe. The results of DSLOPE were compared with that of conventional closed form solutions and the anomaly in results was attributed to the difference in assumptions.

Bouazza and Michel (2000) have explained the complexities in assessment of stability of domestic waste slope in Poland where the uncertainty was due to the drastic variation in the characteristics of the waste, high void ratio resulting in high compressibility, variation of properties with degradation, unexpected changes in leachate or groundwater table with seasonal change. The landfill was not engineered and it was formed from about 3 centuries that lead to increase in the discrepancies in the material properties during stability analysis. Stability of the waste slope was analysed using

TALREN 97 by varying the material properties over a broad range and varying the leachate or groundwater table. The study suggested installation of a drainage path as a remedy to stabilise the existing slope.

Raymond and Tang (2000) have proposed a new calibration technique to find the true reliability of slope failure using notional reliability factor and Bayesian approach. Conventionally assessed reliability factor based on lab and field experiments, failure criteria, and model studies was a notional probability factor that cannot be used for decision-making. In this study, authors proposed a calibration technique using this old probability method and comparing it with the probabilities of failed and unfailed slopes of similar soil in Hong Kong according to Bayes theorem. It was observed that calibrated curve shows lower probability factor than the notional probability factor, which was not similar for all cases, i.e., calibrated curve might sometimes lead to higher failure probability according to site conditions. A sensitivity analysis was also done to specify the importance of notional probability determined from conventional reliability techniques.

Tami et al. (2004) have tried to evaluate the efficiency of sloped capillary barrier system both numerically and experimentally with an intention to apply capillary barriers in stabilising rain induced steep landslides. Various types of materials (both fine sand and gravel layers) were tested in capillary barriers of different dimensions both numerically and experimentally in wetting and drying conditions. The variations in pore pressures were monitored numerically using SEEP-W and SV flux and were compared with the experimental results monitored using tensiometer and TDR probes.

With increase in precipitation, the pressure heads in the top layer was observed to increase without any change in gravel layer representing efficiency of barrier. Boundary effect on pressure head profiles was observed up to 0.2 m on both ends. The pore-pressure head results in both numerical and experimental analysis were found to be same. It was concluded that the simulation in drying and wetting processes could predict outflow and inflow quite accurately.

However, Geostudio SLOPE/W is good in considering the transient seepage analysis results from SEEP/W module of Geostudio, in analyzing the rain-induced stability, the translational stability analysis in Geostudio has the following limitations for which it was not used to evaluate the stability of MLCS at prior. (Geostudio 2007). The limitations of translational stability analysis in Geostudio include:

1) Intuitive manner of defining interface shear characteristics. In Geostudio the interface shear characteristics are defined by incorporating a thin layer of new material with representative properties.
2) Numerous problems associated with fully specified and block specified (special parallel form) slip surface method of analysis (in Geostudio SLOPE/W) used to define the probable failure surfaces prone to failure. Some of the major issues include:
   (i) Different FoS for force and moment equilibrium (diverged percentage of interslice force function),
   (ii) Slip surface not intersecting the ground surface line and slip surface enter or exit beyond the slip surface limit (which happens due to numerical confusion in computing intersection point when multiple interfaces were simultaneously analyzed).
   (iii) Slip surface does not have a converged solution while analyzing extreme conditions of multiple interfaces with layers of minimal thickness.
3) Huge amounts of time and effort involved in drawing different geometries (in studying the effect of slope angle and slope length), repetitive process of defining material properties, and multiple runs of analysis for analyzing multiple interfaces of MLCS.

Koerner and Soong (2005) have extended existing translational stability analysis of uniformly laid cover soil over geomembrane layer proposed by Koerner and Hwu (1991) by incorporating numerous factors that influence the stability of cover system. The study included various destabilizing cases such as movement of construction equipment, rain induced submergence, seismic forces encountered in earthquake events. Improvement measures such as construction of toe berm, geosynthetic reinforcements, and use of tapered cover layers were analyzed. Design curves for all the analysis were proposed in this study.

Singh et al. (2009) have described design charts to estimate the probable horizontal displacement studying the behaviour of municipal waste using non-linear elastic hyperbolic model (NLEH) and SIGMA/W module. Procedure to estimate the input parameters of SIGMA/W using NLEH was clearly explained. The charts clearly explain the effects of slope angle, height of slope and properties of waste material on the lateral displacement of the landfill. The results of these charts were validated from monitoring Brock west landfill 2004.

Rahimi et al. (2010) have evaluated the stability of soil slopes made of low and high permeable soils under the influence of different rain intensities. From this study, it is understood that the high permeable soil slopes fail under high intensity rainfall that were a fraction of the saturated hydraulic conductivity of the in-situ soils. While the low permeable soils were found to fail under low rainfall intensities, which were greater than the saturated hydraulic conductivity of the in-situ soils. Further, the stability of low permeable soil slopes was observed to have significant influence due to variation in SWCC parameters in comparison to the high permeable soil slopes.

Rahardjo et al. (2013) has studied the effect of flux boundary condition on pore-pressure variations in a sloped model using Geostudio Vadose/w and validated the analytical results with those of field monitoring residual soil slope at Yishunusing, Singapore. They systematically brought forward the importance of evaporation conditions alongside infiltration in evaluating the pore-pressure variations. The evaporation was estimated by two different methods using the available climatic data and found that Penman's method of estimation is superior and suggestable for further studies. The variation of amount of infiltration for different events of rainfall has shown an average of 40 to 50% rainfall is infiltrated in the soil and even more for events less than 50 mm/hr.

Koerner and Koerner (2013) identified numerous translation failures that initiate along the geotextile reinforcements. Clogging induced pore-pressure increments along with weak interface friction characteristics have lead to such failures. Improper analysis, excessive loading, long-term degradation, improper fill materials, poor placement, and compaction, non-existing water control systems, clogged drains were other factors that influence the stability of these systems. Statistical analysis of failed slopes indicated that 69% of failures were due to improper design while 29% were due to improper execution.

Qian and Koerner (2015) have used the modified translational stability analysis to evaluate the stability of numerous interfaces of multi-layered liner systems. The influence of waste depth, properties of waste on stability of different critical interfaces is brought forth. The study identifies the probability of weakest plane formed by the combination of alternate interfaces in base and back slope. The depth and location of weakest plane is influenced by the geometry of the waste mass that include depth, top width, front slope and back slope.

2.7 Critical appraisal of the reviewed literature

The reviewed literature brings out the significance of cover systems in isolating the waste components from atmospheric interaction. The literature also identifies the major concerns that challenge the existence of cover systems. As identified by numerous researchers the major function of cover system is to minimize the downward rainfall seepage into the waste and protect the components of landfill system from atmospheric variants. Use of multiple materials having proper interaction is therefore necessary for performing different tasks encountered in appropriate functioning of cover system. The design of cover system, the configuration of cover layers, the material selection, are subjected to the climatic conditions and the type of waste isolated in landfill system.

Surface layer of cover system plays major role in protecting the different components of landfill system, which is frequently influenced by rainfall and temperature variations in atmosphere. The surface layer soil is hence subjected to erosion, infiltration, and desiccation that require a multi-disciplinary approach in designing it. The poor design of filter and drainage layers in cover systems lead to clogging of flow paths that induce abrupt increase in pore-pressures, finagling causing whole cover or landfill system to fail. Use of in-appropriate materials, insufficient thickness, non-consideration of shear strength criteria, lack of long-term compatibility, etc have majorly influenced the performance of filter and drainage layers in cover systems.

There are very few documentations on the performance evaluation of field pilot multi-layered cover systems. Not many researchers focused on such studies, as most of the landfills were active until recent times and have not reached their capacity. However, such studies are required to evaluate the performance and longevity all layers of cover system by exposing the pilot field system to varying climatic conditions (natural or simulated). Further, understanding the limitation of field or laboratory studies in evaluating the true performance for long design periods some researchers have focused in estimating the future performance through analytical and numerical studies.

Many studies identified the uncertainty in stability of multi-layered cover system caused by the weak interaction of different layers present in it. Translational failure is of major concern and no method in literature was fully capable in evaluating the stability of multiple layers of cover system under different conditions encountered in real field. Review of commonly used numerical models have indicated the limitations of the methodologies

such as inappropriate assumptions, diverged numerical equations, geometric incompatibility, convergence issues in translational studies, unconventional definition for interface shear characteristics. Analytical methods proposed by some of the researchers were found to be relatively superior, which however necessitate certain modifications for evaluating stability of multi-layered cover systems.

To summarize the integrity and stable performance of multi-layered cover systems can only be established both by having appropriate individual components of cover systems and by having proper coordination at their interfaces. Performance of surface layer and translational stability are major concerns. Field studies under varying climatic conditions are essential in confirming the reliability and suitability of cover configuration. There is immense need to revisit existing design criteria and adopt necessary modifications with appropriate laboratory, field, analytical and numerical studies in systematic manner.

Chapter 3

Evaluation of surface soil and its compaction state for MLCS

3.1 General

Surface layer of multi-layered cover systems (MLCS) play a significant role in the serviceability of landfill system. The role of surface soil in protecting other layers of multi-layered cover system (MLCS) for different landfill facilities is very well recognized and attempts were made to understand the performance of surface soil under different atmospheric variants (Forman and Anderson 2005; Rahardjo et al. 2015). It protects the remaining layers of MLCS from adverse effects such as heavy rainfall, high temperatures, animal intrusions, roots of vegetation, etc. Failure of surface soil would lead to degradation of complete MLCS and hence the landfill facility (Suter et al. 1993; Daniel and Wu 1993; Koerner and Daniel 1997). The role of surface layers has higher concern in Indian sub-continent with extremely contrasting climatic conditions (cycles of arid to semiarid and higher precipitation with change in seasons). i.e., it should resist both desiccation and erosion, controlling infiltration. The only available guideline for selecting surface soil in cover system is that its permeability should be less than 1E-07 m/s (USEPA1989; 40CFR 258.60 2002). Past literatures identified erosion (Piet et al. 2005), desiccation/ shrinkage (Daniel and Wu 1993), infiltration (Benson et al. 2001) and lack of strength (Daniel and Wu 1993) as the major factors inhibiting the performance of surface soil. However, these performance markers were not considered explicitly for evolving criteria for the selection and design of surface soil layer in MLCS.

Earlier researchers (Daniel and Wu 1993) have suggested preferable criteria for liner systems considering strength, shrinkage index and seepage potential of given soil. However, considering the importance of erosion in cover systems an attempt is made in this study to evolve suitable guidelines for surface layer by introducing erosion indices. Soil type and compaction state are the primary parameters that govern the performance of surface soil in MLCS (Suter et al. 1993; Daniel and Wu 1993; Benson et al. 1994; Koerner and Daniel 1997). This study investigates the role of primary parameters on the erosion, desiccation, infiltration, and strength characteristics (performance markers) of five soils considered as potential surface layer of MLCS. The results of the above-mentioned performance markers were used to assess soil suitability as surface layer in MLCS. The

flow chart describing the experimental sequence followed in this part of study is detailed in Figure 3.1.

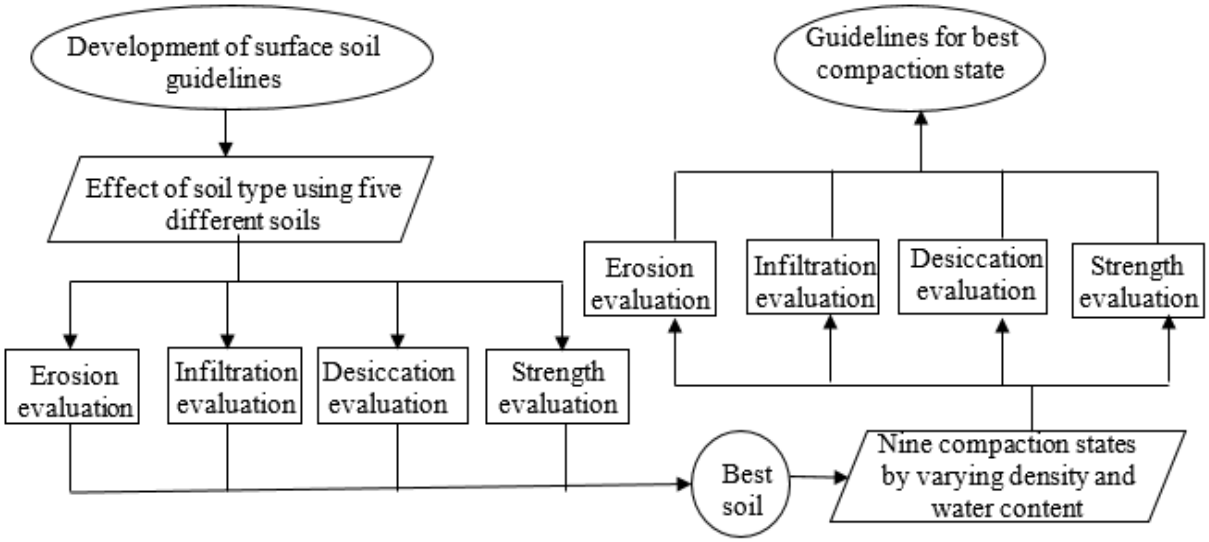

Figure 3.1 Experimental program to evaluate surface soil and its compaction state for MLCS

A set of five soils (S1, S2, S3, S4, and S5) from different sources around Guwahati region of India having low to medium plasticity, were selected for this study. Selected soils were characterized for their geotechnical properties, following the recommendations of American Society for Testing and Materials (ASTM D854-14, ASTMD6913-04, ASTM D7928-16, ASTM D4318-10, ASTM D2487-11, and ASTM D698-12). The obtained results are summarized in Table 3.1.

After preliminary characterization, all the soils are subjected to various index tests for evaluating effect of soil type on performance of surface soil. However, there are different methods available for understanding each of the erosion, infiltration, desiccation and strength characteristics of surface soil, methods followed by numerous researchers that provide a reliable understanding of soil behavior are selected for this study. For understanding erosion index of soil, pin hole test was adopted as recommended by Reddi et al. (2000). Desiccation potential of the soil has great correlation with shrinkage potential of the soil (Kleppe and Olson 1985) and hence volumetric shrinkage index of cylindrical soil samples was investigated to understand desiccation potential similar to Daniel and Wu (1993). For evaluating infiltration potential, ‘mini disk infiltrometer’ was employed, a robust device commonly used in recent times (Angulo-Jaramillo et al. 2000). To understand the strength potential the regularly adopted geotechnical method ‘unconfined compression

strength test' is conducted (ASTM D2166/D2166M-16). Soils satisfying the specific recommendations for each of the performance markers are identified individually and finally the type of soil that achieved all of the preferential criteria is selected as best performing surface soil.

Table 3.1 Summary of basic geotechnical properties of selected soils

Property		Soils				
Designation		S1	S2	S3	S4	S5
Specific gravity		2.68	2.65	2.69	2.64	2.64
Particle size distribution	% Coarse sand	2	6	0	4	10
	% Medium sand	26	30	6	18	8
	% Fine Sand	23	27	19	22	23
	% Silt	34	22	49	40	33
	% Clay	15	15	26	16	25
Atterberg limits	Liquid limit %	28	33	40	51	60
	Plastic limit %	12	16	22	26	34
	Plasticity index %	16	17	18	25	26
Unified soil classification system		SM	SM	ML	MH	MH
Optimum moisture content %		11	15	17	22	29
Maximum dry density (g/cc)		1.6	1.56	1.7	1.63	1.39

Further, nine compaction states of best performing surface soil were selected to evaluate the effect of compaction state on performance of surface soil. Nine different compaction states were selected by varying density between 0.95 and 1.05 times maximum dry density (MDD) and water content between ±5% optimum moisture content (OMC) as shown in Figure 3.2. However, 1.05MDD-OMC+5% is not practically achievable as it is beyond 100% saturation and hence is controlled to a lower water content as shown in the figure. The errors in density are maintained well below 0.02 gm/cc and water content 0.05% during experimentation. Acceptable zone of compaction for every property is identified as per recommendations made by different researchers. Finally, by superimposing individual acceptable zones of compaction, an overall acceptable zone satisfying guidelines of all properties is evolved.

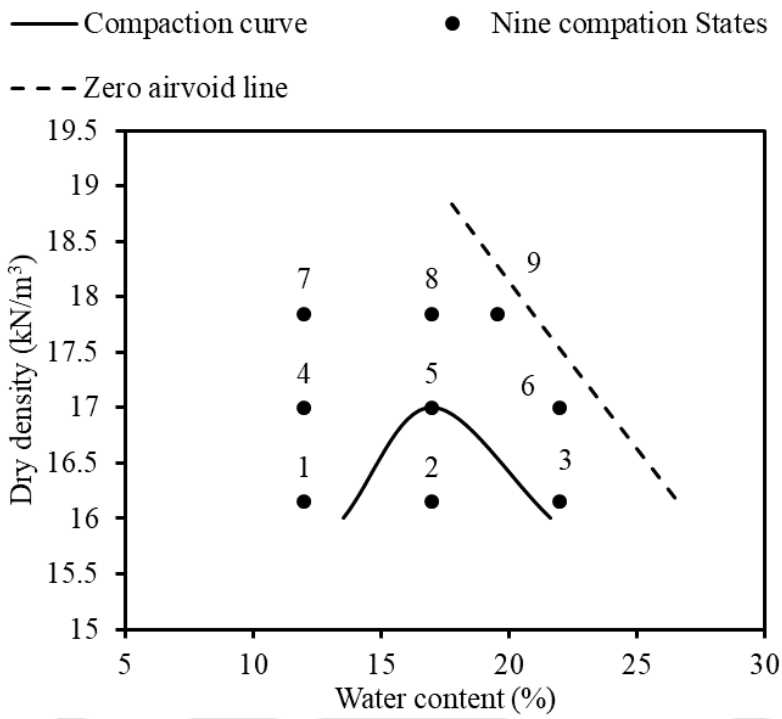

Figure 3.2 Selected compactions states around compaction curve of best performing soil

3.2 Pin hole test

3.2.1 Pin hole method

Pin hole test is one amongst the most commonly adopted index tests to evaluate the erosion sensitivity of the soil by various researchers (Sherard et al. 1976; Reddi et al. 2000; Wan and Fell 2004). Figure 3.3 shows the line diagram of pin hole testing setup with cylindrical sample of 25mm diameter and 50mm length. Required amount of soil, calculated as per target density has been transferred in to the pin hole sampler in three layers with uniform compaction as shown in Figure 3.4. A hole of 7mm diameter is induced in the sample using a fixed solid rod with sharp edge as shown in Figure 3.5. The sample thus prepared has been installed in an in-house fabricated pin hole testing apparatus and different flow rates were applied as depicted in Figure 3.6.

To have a practical relevance the flow rates having energy same as different rainfall intensities were selected. Table 3.2 depicts the kinetic energy corresponding to different rainfall condition (Sanchez-Moreno 2012). Three forms of rainfall, which include heavy, excessive and cloud burst that are prone to significant erosion (Boardman 2006) were selected for this study. Corresponding pin flow rates 115 ml/min., 164 ml/min., and 235 ml/min. are obtained using Eq. 3.1.

$$\text{Discharge}(Q) = \left(\frac{2E}{\rho_w}\right)^{1/3} \times \frac{\pi d^2}{4} \qquad \textbf{3.1}$$

where,

E = Energy of rainfall ; ρ_w = Density of water; d = Diameter of pin hole

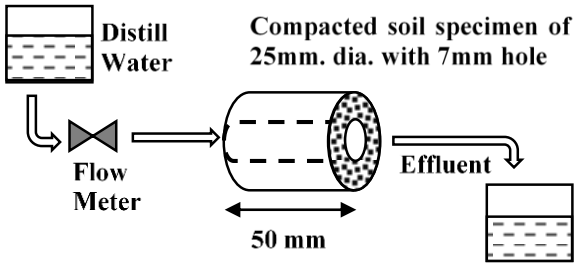

Figure 3.3 Schematic representation of pin hole setup

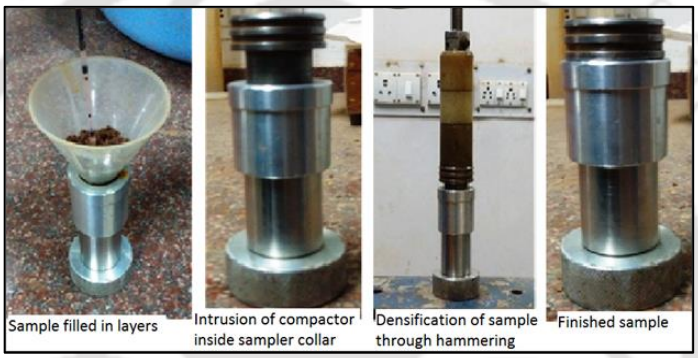

Figure 3.4 Compaction procedure of pin hole sample

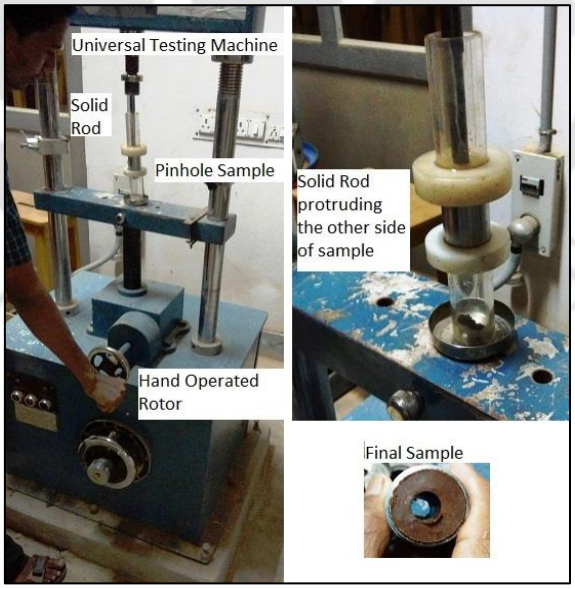

Figure 3.5 Provision of hole inside pin hole sample

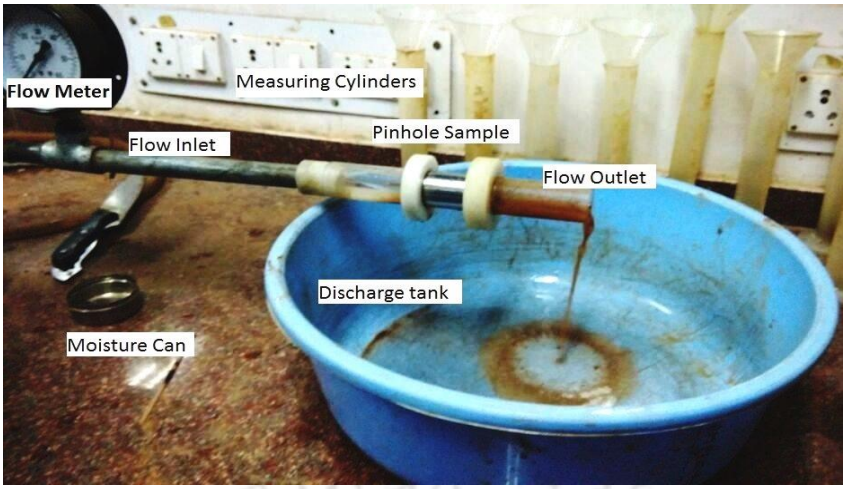

Figure 3.6 Image of in-house fabricated pin hole testing apparatus

Table 3.2 Energy and flow rates corresponding to various rainfall forms

Rainfall form	Intensity (mm/hr)	Kinetic energy ($J/m^2/hr$)	Flow rate (ml/min)
Drizzle	< 1	2	20
Light	1	10	35
Moderate	4	50	60
Heavy	15	350	**115**
Excessive	40	1000	**164**
Cloudburst	100	3000	**235**

The flow is maintained by controlling a ball valve and monitored using a flow meter attached in the circuit as shown in Figure 3.6. Output flow is verified before and after every test, to eliminate any anomalies. The sediment solution is collected and filtered (Figure 3.7) at regular intervals of time. The sediment mass attained at various flow rates helps in evaluating the erosion indices of given soil sample. The soil loss was further used to determine shear stress (τ) and erosion rate (ε) using Eq. 3.2-3.4 (Reddi et al. 2000).

Figure 3.7 Figure depicting the filtration of sediment solutions

$$\varepsilon = \frac{M}{At} \qquad \textbf{3.2}$$

$$\frac{\Delta P}{L} = \frac{q}{A} \times \frac{8\eta}{n} \quad \textbf{3.3}$$

$$\tau = \frac{\Delta P}{L} \times \frac{R}{2} \quad \textbf{3.4}$$

where,

ε Erosion rate (kg/m^{2}s)

A Surface area of eroded sample (m^2)

t elapsed time (s)

M Cumulative mass of soil eroded (kg)

τ Shear stress (Pa)

L Length of the sample (m or mm)

$\frac{\Delta P}{L}$ Pressure gradient

q Discharge rate (m^3/s or ml/s)

η Dynamic Viscosity of water (Pa-s)

R Radius of hole in the soil sample (m or mm)

The variation of erosion rate with shear stress for three flow rates, are numerically fitted to the standard erosion equation as shown in Eq. 3.5 (Reddi et al. 2000). Corresponding outcomes, the critical shear stress (τ_c) and erodibility coefficient (k) are the generalized parameters used for analysis of erosion. Soil erosion rate index (SEI) for pin hole erosion test was evaluated as described in Eq. 3.6, to classify the erodibility similar to Wan and Fell (2004). SEI has a magnitude of 0 to 6, which represents extremely rapid to extremely slow erosion rates as listed in

Table 3.3.

$$\varepsilon = k.(\tau - \tau_c) \quad \textbf{3.5}$$

where,

ε= erosion rate (kg/m^{2}s)

k=erodibility coefficient (s/m)

τ= shear stress (Pa)

τ_c=critical shear stress (Pa)

$$SEI = -\ln(k) \quad \textbf{3.6}$$

Table 3.3 Classification of erosion based on soil erosion rate index (Wan and Fell 2004)

Group number	Soil erosion rate index (SEI)	Classification
1	SEI <2	Extremely Rapid
2	2<SEI<3	Very Rapid
3	3<SEI<4	Moderately Rapid
4	4<SEI<5	Moderately slow
5	5<SEI<6	Very slow
6	6< SEI	Extremely slow

3.2.2 Pin hole characteristics

3.2.2.1 Effect of soil type

The pin hole erosion test results of various soils are discussed in this section. The tests were performed at their standard compaction state. The variation of shear stress with erosion rate of different soil types is depicted in Figure 3.8. This variation is numerically fitted to a linear regression equation to evaluate the critical shear stress (τ_c) and erodibility coefficient (k), the generalized parameters used in numerical analysis for various erosion studies. (Wan and Fell 2004) The critical shear stress represents the minimum amount of stress required for initiation of erosion process. The pin hole erosion characteristics of selected soils are listed in Table 3.4.

From Table 3.4, it is found that the erodibility (k) of soil is decreased with increase in plasticity of the soil. On other hand, the shear stress (τ_c) is observed to increase simultaneously. This could be mainly attributed to the additional cohesion due to increase in fine contents of high plastic soil. Similar findings were reported for internal erosion studies of hydraulic earthen dams by Wan and Fell 2004; Haghighi et al. 2013).

Table 3.4 Pin hole characteristics of various soil types

Soil	k (kg/N-s)	τ_c (Pa)	SEI (-ln k)
S1	0.064	0.0002	2.76
S2	0.028	0.0028	3.57
S3	0.014	0.0074	4.30
S4	0.011	0.0091	4.51
S5	0.017	0.0061	4.10

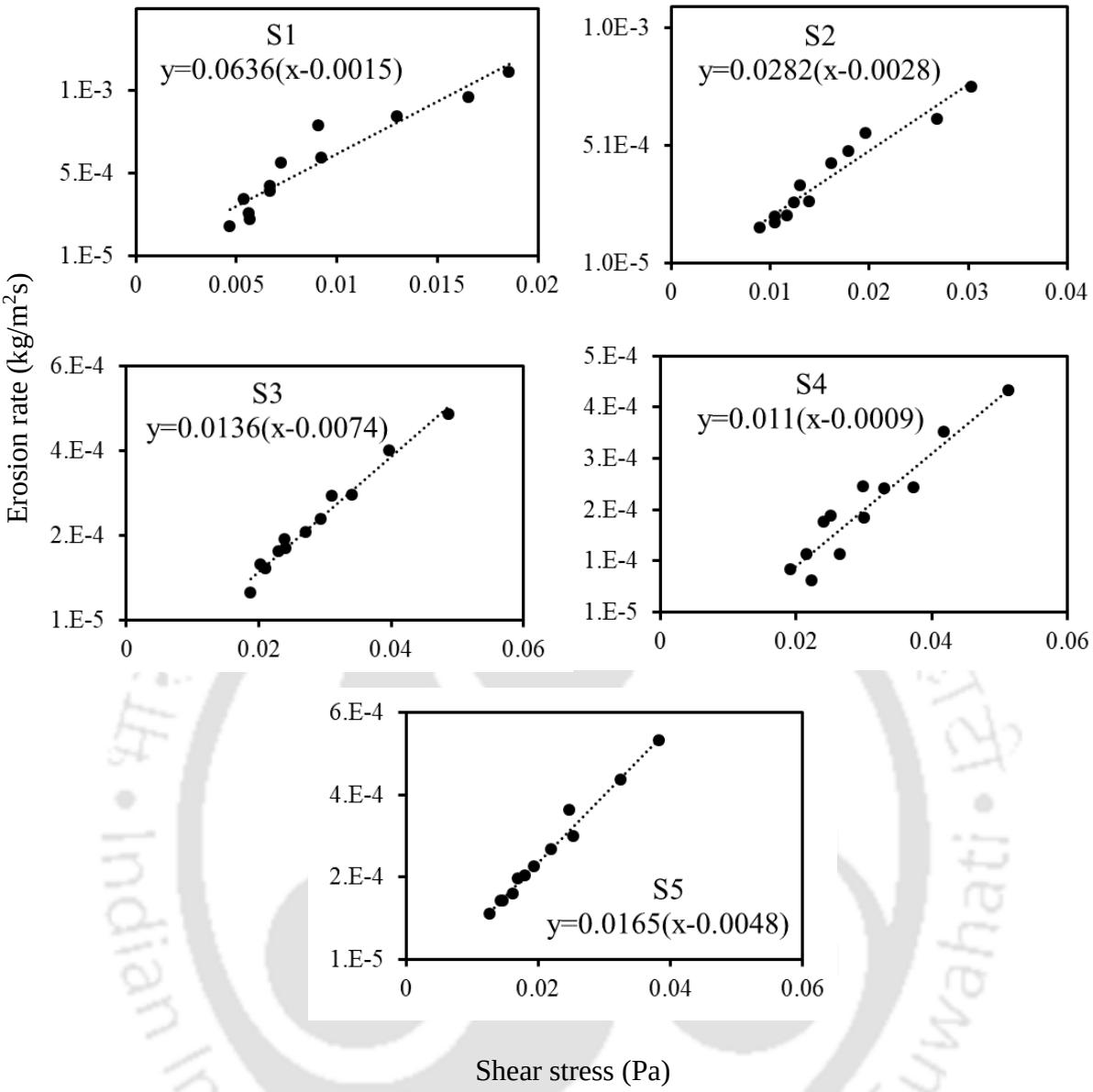

Figure 3.8 Shear stress versus erosion rate variation of different soil types

3.2.2.2 Effect of compaction state

The variation of erosion rate with shear stress for three flow rates considered in this study, are presented in Figure 3.9 individually for all the compaction states. The variation in erosion rate and shear stress is numerically fitted to standard erosion equation, as shown inside figure to evaluate critical shear stress and erodibility. Figure 3.10 summarizes the variation of critical shear stress (τ_c) with change in water content corresponding to different dry densities. The figure indicates that the τ_c increases with increase in water content at a given dry density. The increase in soil resistance with increasing molding water content can be due to dispersed particle structure at higher water contents (Lambe 1958). The

phenomenon can be broadly understood from illustrations described in Figure 3.11. Figure explains that the flowing water can easily erode the flocculated particles in dry sample, as there is end to face interaction, while in case of dispersed particles the flow happens along the particle surface and hence produces relatively less drag. While for a given water content, critical shear stress increases with increasing density. The dense soil samples generally possess higher shear strength. This additional strength at higher dry densities could have resisted flow induced stresses, thereby enhancing erosion resistance. This means it requires more amount of flow (i.e. rainfall) to cause erosion at higher densities and water contents. It may be further noted that the sensitivity of dry density on critical shear stress is reduced for water contents close to plastic limit of the soil.

Figure 3.12 summarizes the variation of erodibility with change in water content and density. The figure shows that the erodibility decreases with increase in water content for a given dry density. Also with increase in dry density for a given water content. As in the case of critical shear stress, the sensitivity of dry density on erodibility also becomes minimal at higher water contents close to plastic limit. The observations ascertain that compacting the soil at higher densities and water content close to plastic limit would reduce erosion of surface soil of MLCS.

For classifying the potential erodibility of different soil states, Soil erosion index (SEI) defined by Wan and Fell (2004) is used. Figure 3.13 depicts the value of SEI indicated against different compaction states considered in this study. The soil states with SEI > 4 represents very slow erosion prone zone. Based on the SEI values, a zone was identified for SEI ≥ 4, which can be considered as relatively stable zone of compaction, for the soil considered in this study. The unknown density and water content corresponding to SEI value of 4, on the boundary of selected zone were attained through interpolation of known SEI values for used compaction states. It is believed that the surface soil with compaction within this prescribed zone would exhibit minimal surface erosion.

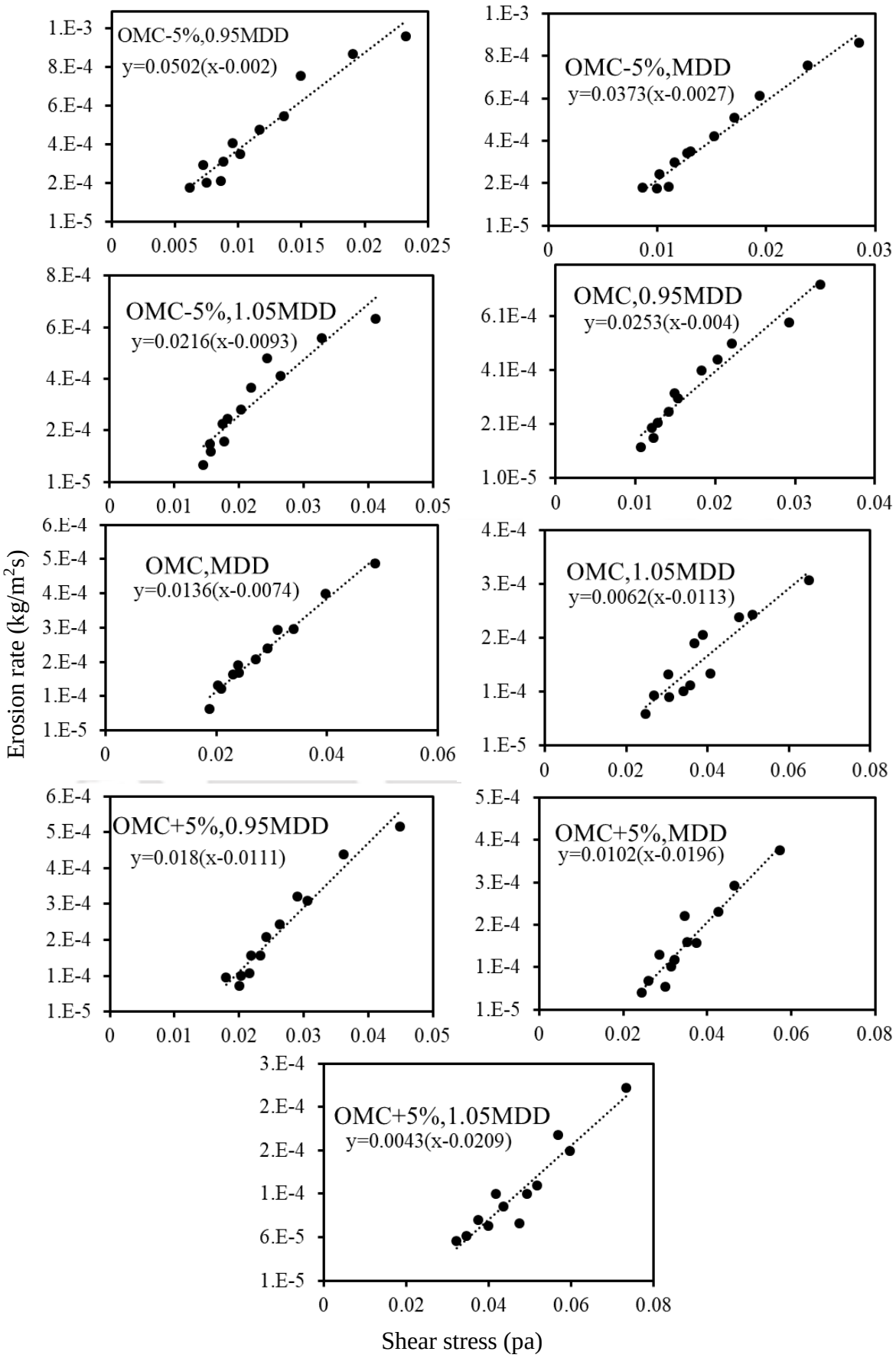

Figure 3.9 Variation of erosion rate with shear stress for different compaction states

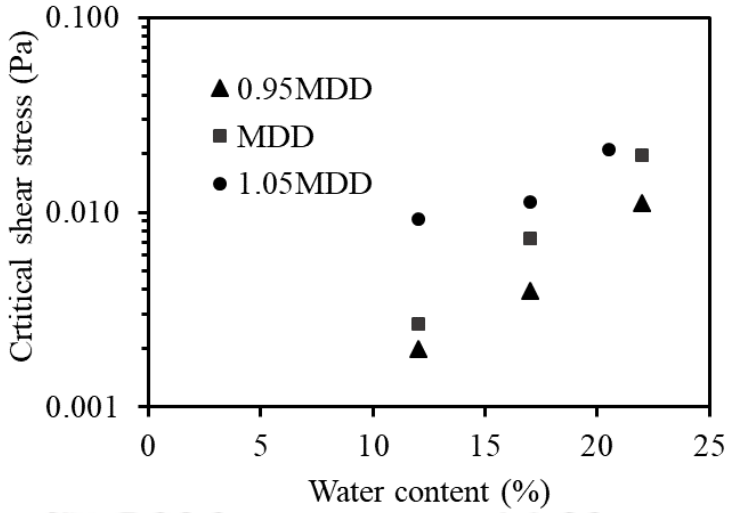

Figure 3.10 Variation of critical shear stress against water content at different densities

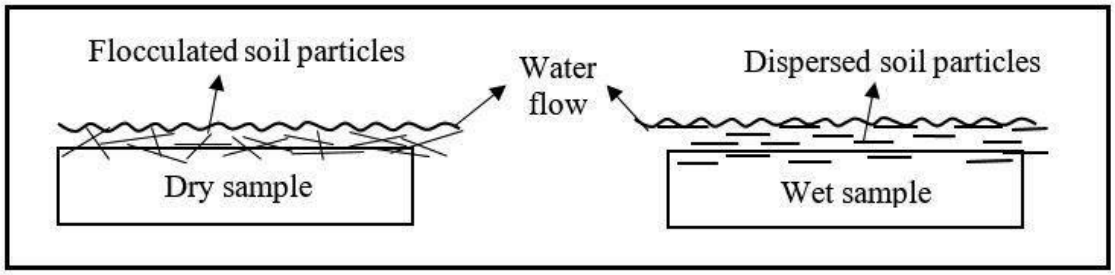

Figure 3.11 Conceptual illustration of erosion phenomenon at different water contents

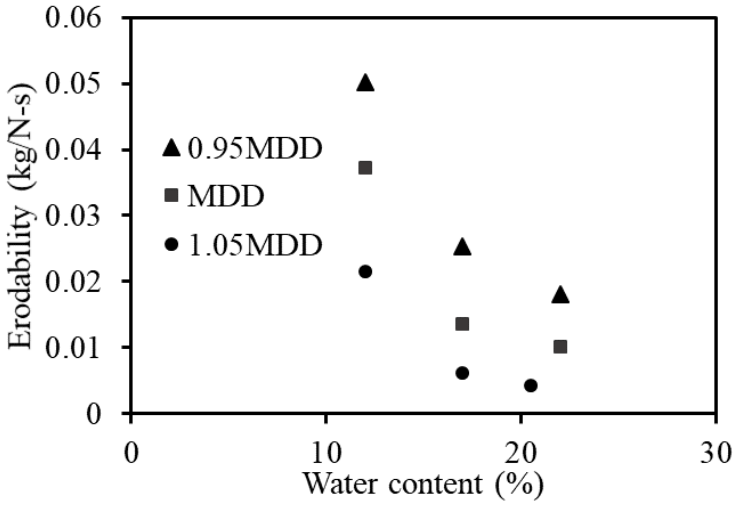

Figure 3.12 Variation of erodibility against water content for different densities

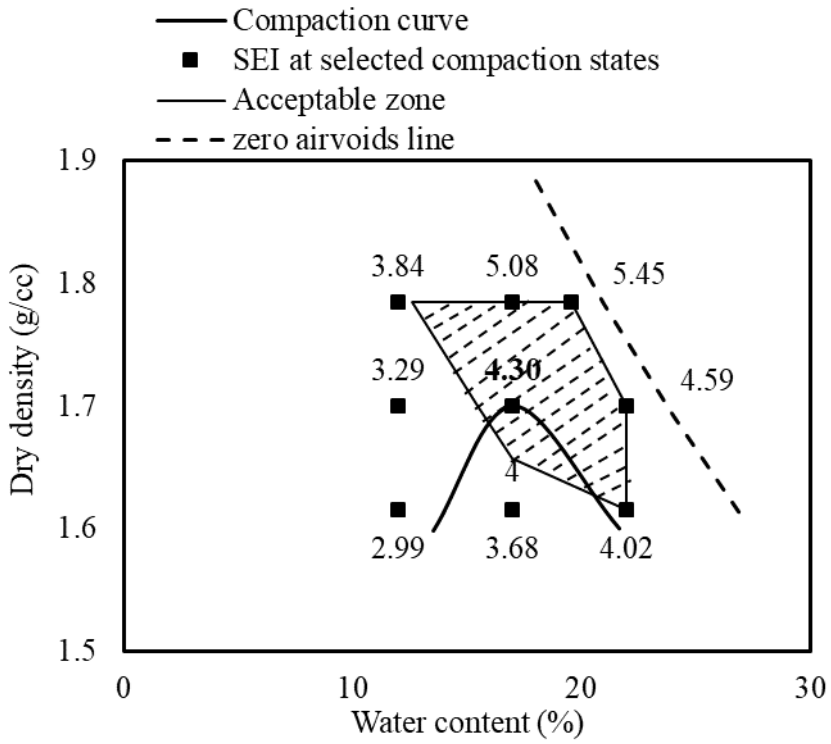

Figure 3.13 Erosion indices for different compaction states

3.3 Jet erosion test

The jet erosion test is to develop an understanding on the erosion resistance of surface soil towards impact of raindrop. The conventional jet erosion test designed by Hanson (1990) and mentioned in ASTM D 5852-00 was mainly used for soil under submerged condition for studying the erosion caused by flowing water. The same test procedure has been modified by removing the submergence condition of the soil sample and modifying the jet properties to represent rain induced erosion on surface soil. The conceptual illustration of modified jet erosion test is depicted in Figure 3.14.

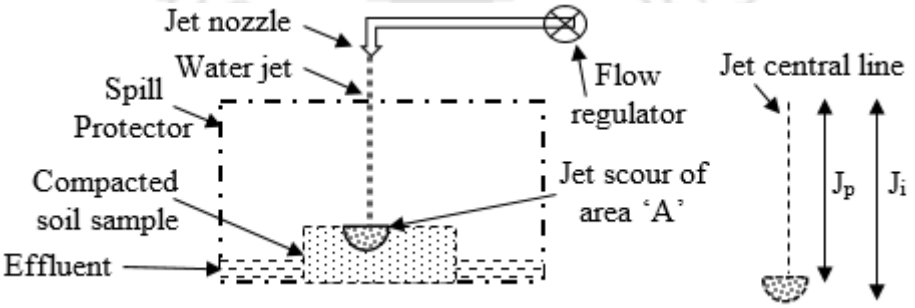

Figure 3.14 Conceptual figure describing jet erosion test

The modified jet has the nozzle diameter of 2.4 mm simulating closely the average raindrop size. The soil sample of desired water content and density was prepared similar to the procedure adopted for pin hole erosion test. The required amount of soil was compacted into the jet erosion sampler in three layers with proper compaction as shown in Figure 3.15. The prepared sample was transferred to the testing platform and covered using a solid metal plate until the discharge of the jet gets adjusted. The distance between the sample surface and the jet nozzle was maintained 22cm, similar to the existing submerged jet devices.

Figure 3.15 Figure depicting the sample preparation for jet erosion test

The intensity of the jet was varied by adjusting the flow rates to simulate energy corresponding to different rainfall conditions as shown in Table 3.5. (Sanchez-Moreno 2012). Three forms of rainfall, which include heavy, excessive and cloud burst that can cause significant soil erosion (Boardman 2006) were selected for this study. Corresponding jet flow rates 35 ml/min., 50 ml/min., and 70 ml/min. are obtained using Eq. 3.1. The flow regulator as shown in the Figure 3.14 was used to achieve the required rainfall energy based on the calibration relationship developed between flow rate and rainfall intensity. Once the stable jet flow intensity was achieved, the sample surface was exposed to jet impact as shown in Figure 3.16 and the effluent was collected at regular intervals of time. The effluent was filtered and oven dried as discussed for pin hole test. The oven dried soil mass was used to determine erosion characteristics.

Table 3.5 Energy and flow rates corresponding to various rainfall forms

Rainfall form	Intensity (mm/hr)	Kinetic energy (J/m^2-hr)	Flow rate (ml/min)
Drizzle	< 1	2	5
Light	1	10	10
Moderate	4	50	15
Heavy	15	350	**35**
Excessive	40	1000	**50**
Cloudburst	100	3000	**70**

Figure 3.16 Jet impact on the soil surface

The amount of soil loss corresponding to a particular flow rate was used to determine erosion rate and shear stress using the Eq. 3.7- 3.9 (Hanson and Cook 2004).

$$\varepsilon = \frac{M}{\rho A t} \quad \textbf{3.7}$$

$$\tau = \tau_o \times \left(\frac{J_p}{J_i} \right)^2 \quad \textbf{3.8}$$

$$\tau_o = C_f \rho_w U_o^2 \quad \textbf{3.9}$$

where,

ε= erosion rate (m/s)

A = surface area of eroded portion (m^2) as shown in Figure 3.14

t = elapsed time (s)

M = cumulative mass of soil eroded (kg)

ρ = dry density of soil sample (kg/m^3)

τ = boundary shear stress (Pa)

τ_o = the maximum stress due to the jet velocity at the nozzle (Pa)

J_p = the potential core length (m) as shown in Figure 3.14

J_i = the jet orifice height at any instant 'i' (m) as shown in Figure 3.14

C_f = the coefficient of friction = 0.00416

ρ_w = the fluid density (kg/m^3)

U_o = the velocity at the jet nozzle (m/s)

The variation of erosion rate with shear stress for three flow rates considered in this study were used to determine critical shear stress (τ_c) and erodibility coefficient (k) by fitting Eq. 3.10 to the experimental data by least square regression.

$$\varepsilon = k.(\tau - \tau_c) \quad \textbf{3.10}$$

where,

k=erodibility coefficient (m^3/N-s)

τ_c=critical shear stress (Pa)

Observing the variation of τ_c' and 'k' for broad range of soils, Hanson and Simon (2001) have proposed a chart for classifying the erosion resistance of soil as shown in Figure 3.18. As shown in the figure, the soils are classified as very resistant (VR) to very erodible (VE).

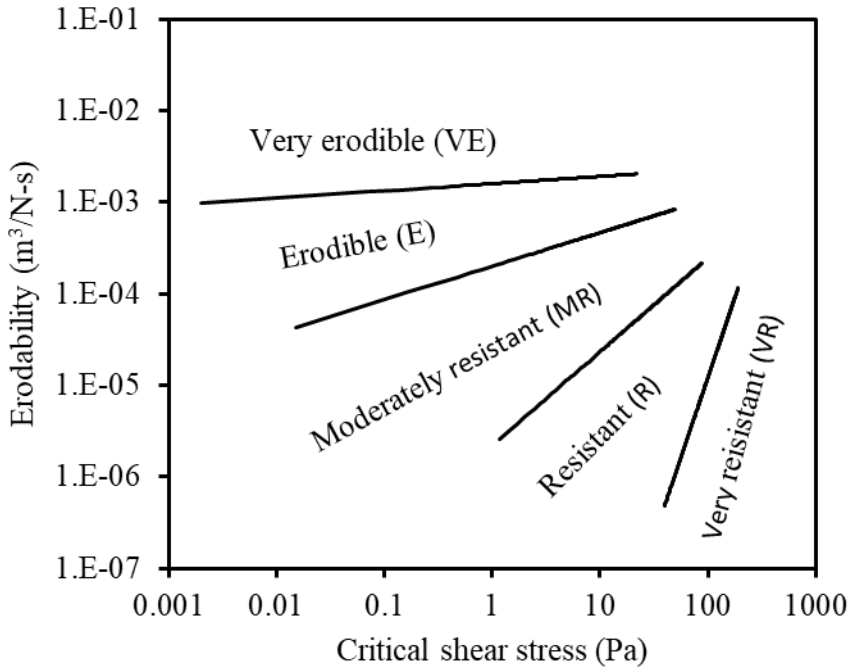

Figure 3.17 Classification chart for jet erosion test (Hanson and Simon 2001)

3.3.1 Jet erosion characteristics

3.3.1.1 Effect of soil type

Jet erosion characteristics (JEC) represent the splash type of erosion, which is the dislodgement of particles from compacted soil surface essentially during rainfall or irrigation. Soil loss measured for various flow rates was converted to shear stress (τ) and erodibility (k) as described in the previous section. The erosion rate versus shear stress variation of different soils compacted at optimum standard Proctor compaction for jet erosion test (JET) is depicted in Figure 3.18.

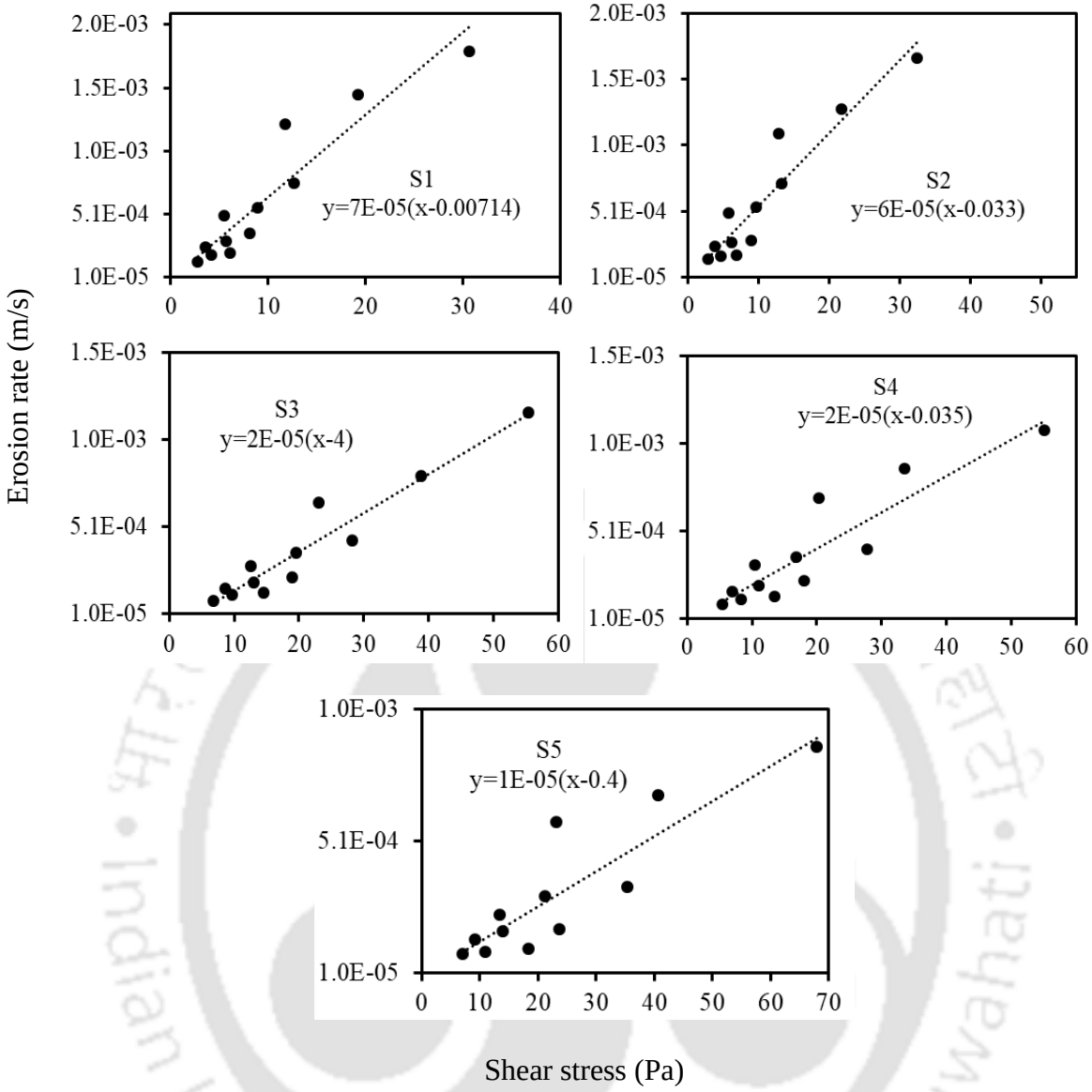

Figure 3.18 Variation in jet erosion rate with shear stress for different soil types

It can be noted that the results are similar to the pin hole test. Based on these results, the erosion characteristics 'τ_c' and 'k', classification based on erosion resistance are summarized in Table 3.6 and the same are overlaid on chart proposed by Hanson and Simon (2001) as shown in Figure 3.19.

Table 3.6 Jet erosion characteristics of various soil types

Soil	k (m^2/N-s)	τ_c (Pa)	JEC
S1	7.0E-05	0.01	E
S2	6.0E-05	0.03	E
S3	2.0E-05	4.00	MR
S4	2.0E-05	0.35	MR
S5	1.0E-05	0.40	MR

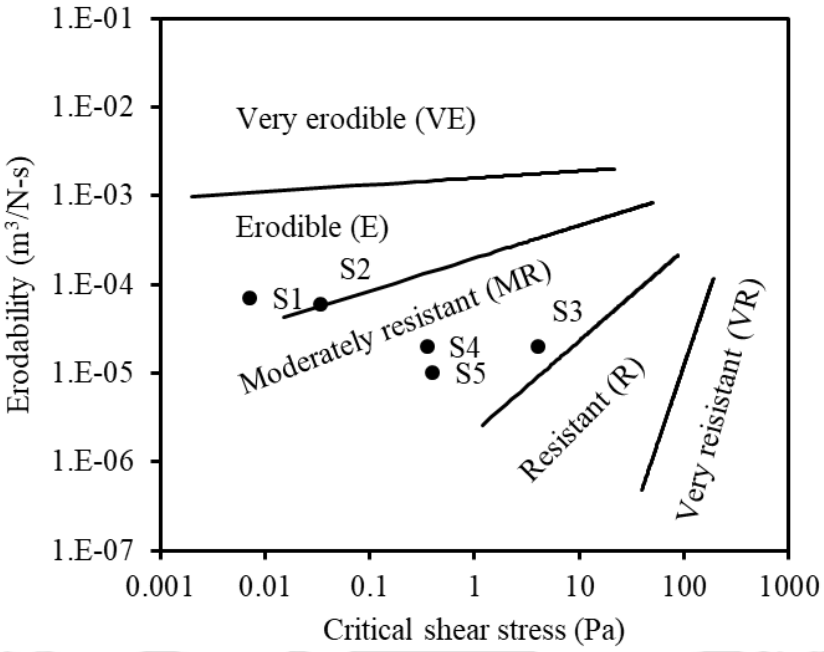

Figure 3.19 Jet erosion characteristics of different soils

From Figure 3.19, it can be noted that soils S1 and S2 are identified as erodible (E) type and S3, S4 and S5 are identified as moderately resistive (MR). The amount of fines has shown greater influence the jet erosion characteristics of given soil. Similar observations were reported by USBR-DSO (2008) in evaluating erosion characteristics of earthen dams. Further, it can be noted that S3 exhibit higher τ_c, as compared to S4 and S5. At the same time, S3 to S5 have comparable erodibility. Based on this observation, it can be ascertained that S3 has better erosion resistance as compared to other soils. The same soil has been considered further for studying the influence of compaction state. It is interesting to note that both the pin hole test and jet erosion test identified S3 as the soil having better erosion resistance.

From Figure 3.19, it can be noted that soils S1 and S2 are identified as erodible (E) type and S3, S4 and S5 are identified as moderately resistive (MR). The amount of fines has shown greater influence the jet erosion characteristics of given soil. Similar observations were reported by USBR-DSO (2008) in evaluating erosion characteristics of earthen dams. Further, it can be noted that S3 exhibit higher τ_c, as compared to S4 and S5. At the same time, S3 to S5 have comparable erodibility. Based on this observation, it can be ascertained that S3 has better erosion resistance as compared to other soils. The same soil has been considered further for studying the influence of compaction state. It is

interesting to note that both the pin hole test and jet erosion test identified S3 as the soil having better erosion resistance.

3.3.1.2 Effect of compaction state

The shear stress versus erosion rate variation for different compaction states (in Figure 3.2) of soil S3 is shown in Figure 3.20. The critical shear stress and erodibility of soil are determined by fitting a linear regression equation (in Eq. 3.10) to the data points as shown in Figure 3.20. The equation obtained through fitting are indicated on the respective figures along with its regression coefficient. The 'τ_c' and 'k' values for different compaction states are represented on jet erosion characterization chart (JEC) proposed by Hanson and Simon (2001), as illustrated in Figure 3.21. From figure, it can be ascertained that compaction states 1 to 5 (in Figure 3.2) are observed to be moderately resistant while 6 to 9 (in Figure 3.2) are resistant to erosion. These points along with jet erosion classification are shown in Figure 3.22.

From Figure 3.22 it can be noted that higher compaction around OMC is a suitable zone of compaction for S3 that exhibits better erosion resistance. However, all the compaction states of S3 have relatively good erosion resistance not less than moderately resistant as noted from the figure. Compacting soil within the identified zone of compaction ensures higher erosion resistance. However, the workability range is quite high based on the jet erosion index test as compared to pin hole results since all the compaction state has sufficient resistance greater than or equal to moderately resistant.

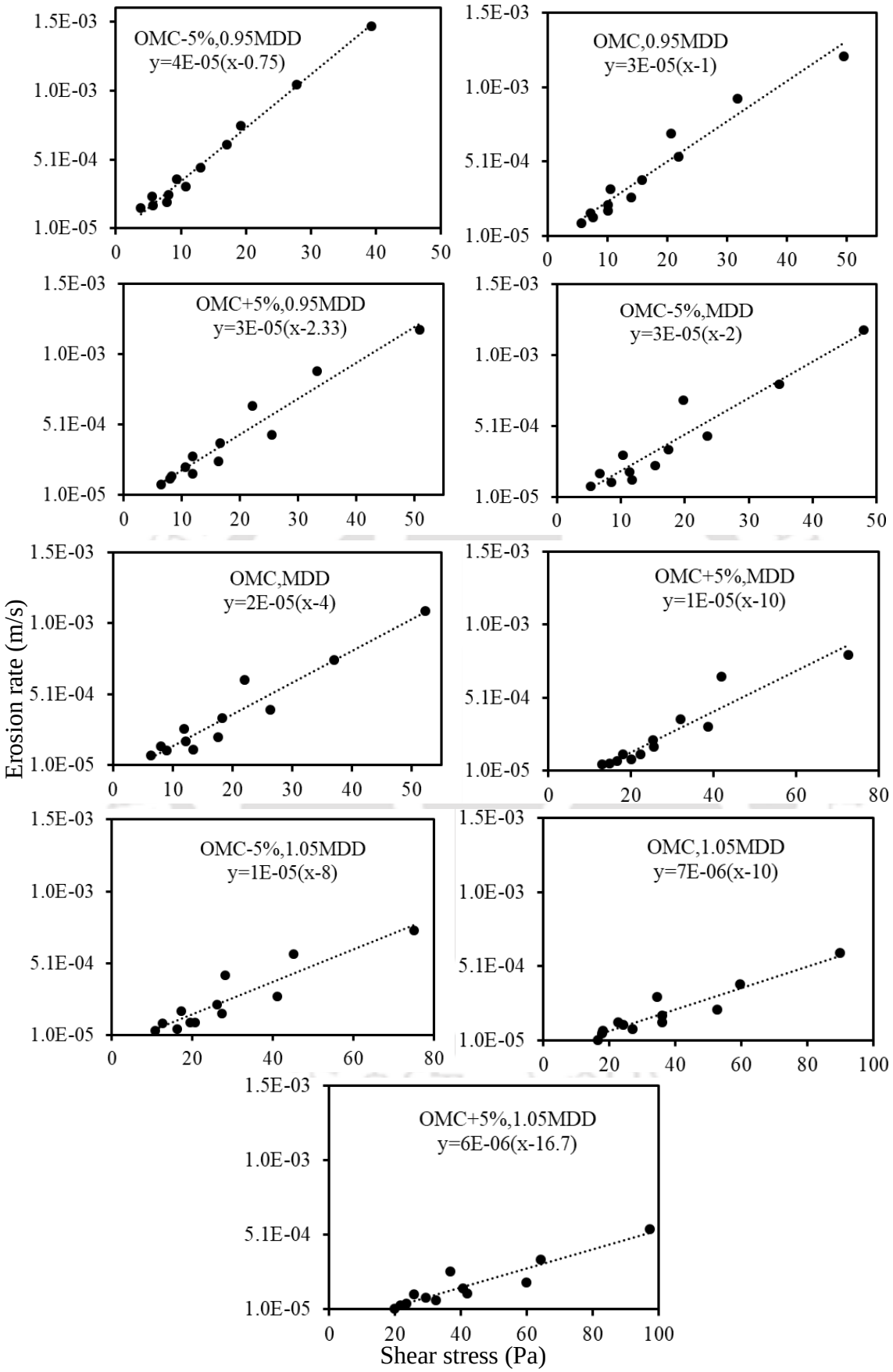

Figure 3.20 Variation in jet erosion rate with shear stress for different compaction states

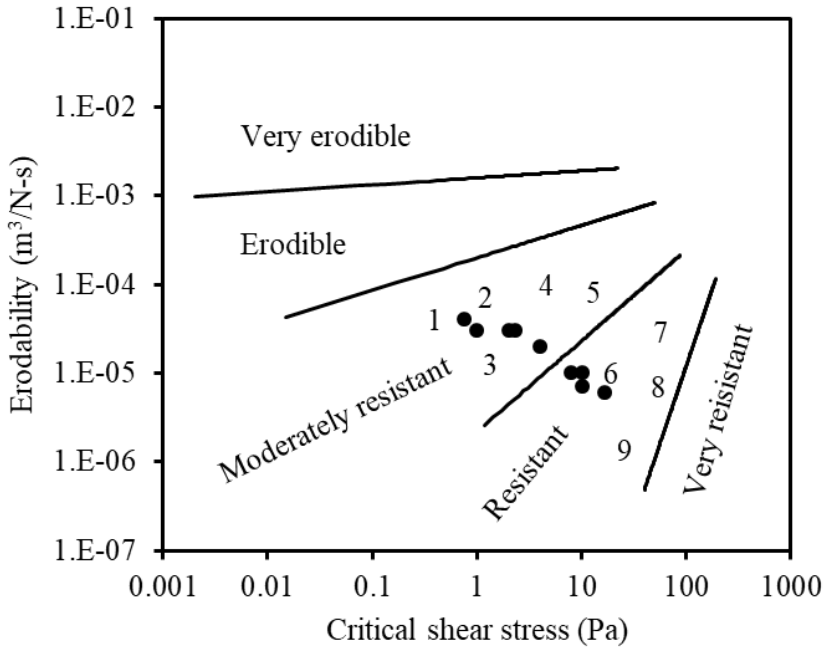

Figure 3.21 Classification of jet erosion characteristics for different compaction states

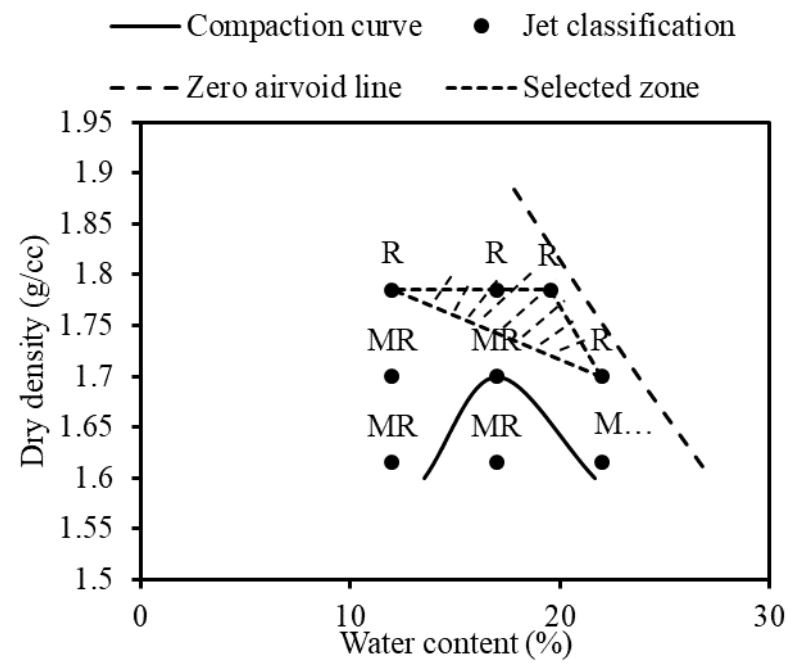

Figure 3.22 Compaction recommendations using jet erosion classification

3.4 Mini disk infiltration test

Infiltration potential of given soil plays a vital role in assessing the stability of surface layer in MLCS. Infiltration also has an inverse relation with erosion potential of given soil (Mannering and Meyer 1963). Mini disk infiltrometer (MDI) is a robust devise used to evaluate the potential infiltration of given soil (Decagon devices 2007), both in lab and

field (Dohnal et al. 2010). The infiltrometer depicted in Figure 3.23 is placed over sample surface and the flow rate is measured until it attains an equilibrium. However, there are no specific guidelines for sample dimensions in laboratory evaluation. Hence, initially the test was conducted on cylindrical samples of different diameters as shown in Figure 3.24 through which a standard diameter is evolved beyond which there is no dimensional dependence. The soil mixed with target water content and bulk mass measured to specific density is compacted in a rigid cylindrical mold of standard diameter.

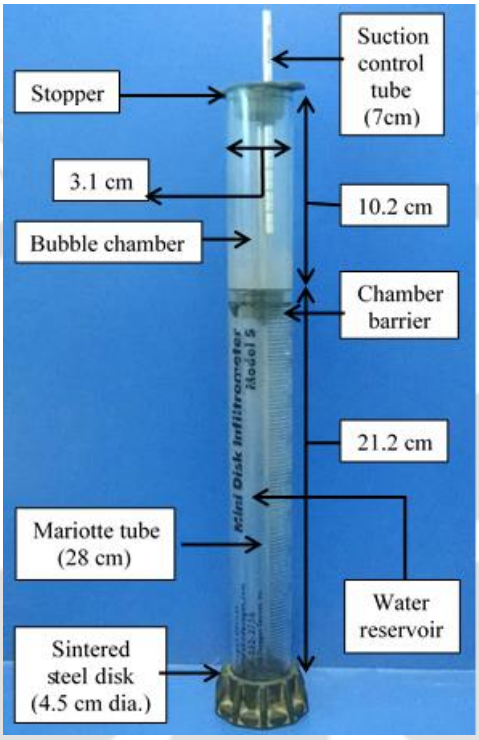

Figure 3.23 Pictorial representation of mini disk infiltrometer

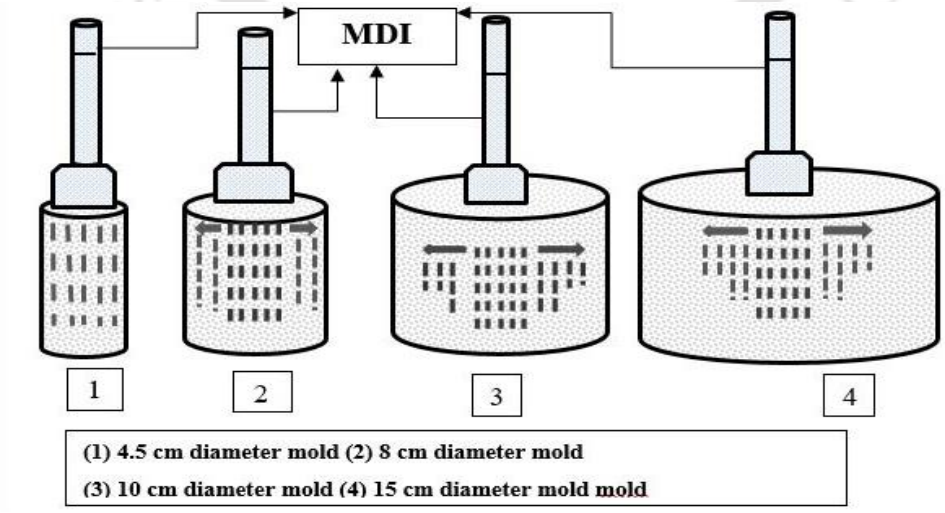

Figure 3.24 Schematic representation of infiltration on samples of different diameter

The variation in cumulative infiltration through MDI with respect to the square root time is fitted to a quadratic equation as shown in Eq. 3.11. The rate of infiltration or near saturated hydraulic conductivity of soil samples (k) is then calculated according to Eq. 3.12 defined by Zhang (1997a, b).

$$I=C_1\, t+ C_2\, \sqrt{t} \qquad \textbf{3.11}$$

where,

C_1, C_2 = fitting constants

t = time

$$k=C_1/A \qquad \textbf{3.12}$$

where,

$$A=\frac{11.65(n^{0.1}-1)\exp\left[2.92(n-1.9)\alpha\, h_o\right]}{(\alpha r_o)^{0.91}} \quad \text{For } n>1.9$$

$$A=\frac{11.65(n^{0.1}-1)\exp\left[7.5(n-1.9)\alpha\, h_o\right]}{(\alpha r_o)^{0.91}} \quad \text{For } n<1.9 \qquad \textbf{3.13}$$

The parameter "A" is dependent on vanGenuchten (vG) soil water characteristic curve (SWCC) parameters of selected soil, tension applied on disk (h_o) and radius of disk (r_0) as represented by Eq. **3.13**. The typical vG parameters '*n*' and 'α' for different soil textures are listed in Carsel and Parrish (1988), for MDI the value of radius (r_0) 2.25 cm. For more accuracy, lab determined SWCC parameter was used to evaluate *k*. According to 40CFR 258.60 (2002) guidelines, the surface soil should have a hydraulic conductivity less than 1E-07 m/s. The appropriateness of given soil and its compaction conditions is further assessed according to this.

3.4.1 Infiltration characteristics

3.4.1.1 Effect of soil type

Table 3.7 summarizes the infiltration test results of different soils, evaluated at Proctor's standard compaction state. Results indicate that as plasticity of soil increases, the infiltration of soil reduced. Similar observations were made by (Younus and Sreedeep 2012) in hydraulic conductivity studies of soil-bentonite mixes. As per recommendations of 40CFR258.60 (2002), the surface soil in cover system should have a hydraulic

conductivity less than 1E-07 m/s. It is found that all the three soils S3, S4, and S5 satisfy the set limit, while the S1 and S2 are found marginally on higher side of the recommendation. Though S4 and S5 have significant difference in their compaction states, have resulted in minimal change in infiltration rate, which can be attributed to the difference in amount of fines present in soils.

Table 3.7 Summary of overall performance markers of various soils

Soil	SEI ($-\ln K_d$)	JEC	Infiltration rate (m/s)	Change in volume %	UCS (kPa)	Remarks
Acceptable limits	4 (Wan and Fell 2004)	(Hanson and Simon 2001)	1E-07 (40CFR258 .60 2002)	4% (Kleppe and Olson 1985)	200 (Daniel and Wu 1993)	
S1	2.76	E	1.43E-06	3.2	161.63	
S2	3.57	E	2.50E-07	3.6	177.82	
S3	4.30	MR	2.87E-08	3.9	258.83	Acceptable
S4	4.51	MR	7.92E-09	4.3	227.89	
S5	4.10	MR	3.39E-09	5.1	207.12	

3.4.1.2 Effect of compaction state

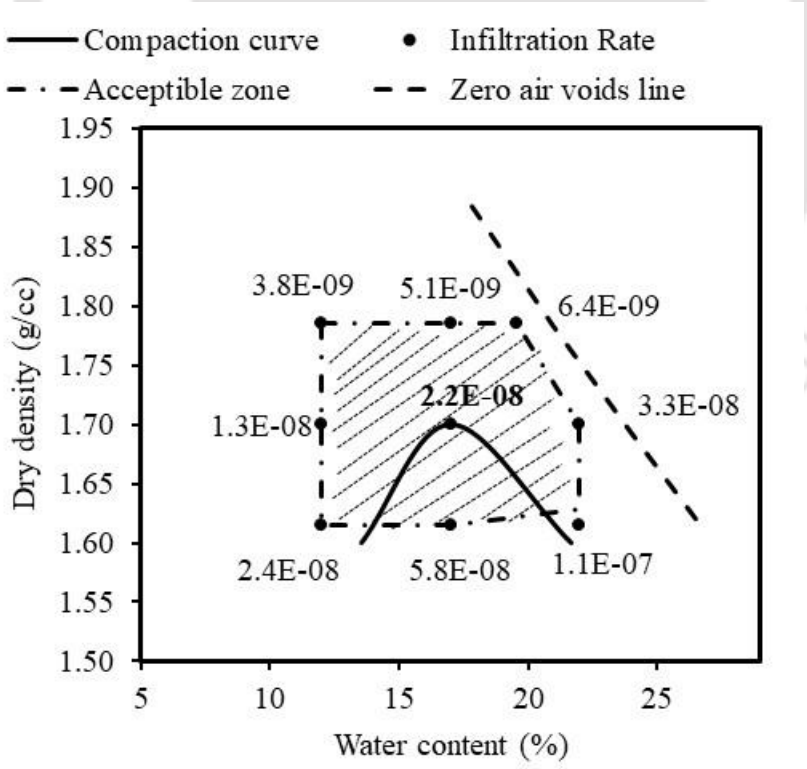

Figure 3.25 Variation of infiltration rates at different compaction states

The infiltration results evaluated using mini disk infiltrometer for different compaction states were evaluated as explained earlier and are summarized in Figure 3.25. As can be

seen from the figure, the amount of infiltration is observed to increase with increase in molding water content. Though particles are dispersed in nature, increase in saturation levels likely would have resulted in this marginal increase in infiltration flow. Similar trends are observed by Akram and Kemper (1979). On other hand, the infiltration was observed to decrease with increase in density at any given water content. This is obvious, as increased density would decrease the available pore space for flow of water through it. 40CFR258.60 (2002) has suggested that surface soils in MLCS should have conductivity less than 1E-7 m/s and hence compaction zone satisfying this recommendation is identified as preferable zone as shown in Figure 3.25. Compacting soil within this zone would exhibit relatively better performance.

3.5 Volumetric shrinkage test

Desiccation is a phenomenon by which moist soil undergoes reduction in volume with increase in temperature and hence form cracked surface. Kodikara et al. (2000) have studied the cracks initiated in slurry soil slabs of different dimensions varying base constraints. The study observed that the crack initiation moisture is desiccation rate dependent, controlled by boundary constraints. Desiccation of compacted soils cannot be understood using these methods. In addition, slurry soil samples are not encountered in general except in agricultural fields. Oren et al. (2006), Tang et al. (2011) have performed image analysis for understanding the crack behavior of clay soils, which requires expensive cameras and complex computing tools. Tay et al. (2001) have studied the desiccation of compacted soil samples, which is close to field circumstances. However, samples exhibited considerable volume change upon drying as shown in Figure 3.26, no visible desiccation cracks were observed except for some instants with micro cracks of thickness less than 1mm.

The volumetric shrinkage test appears to be most suitable to understand the effect of soil state on desiccation potential of a given soil (Kleppe and Olson 1985; Daniel and Wu 1993; Albrecht and Benson 2001; Osinubi and Nwaiwu 2008). The samples were made similar to unconfined compressive test as shown in Figure 3.27 and then left for air-drying for about seven days to eliminate micro cracks. The samples were then dried in oven at 105ºC for complete drying for a period of 24 hours. The change in volume both on its circumference and height were measured at five different locations to evaluate maximum allowable shrinkage of a given soil state.

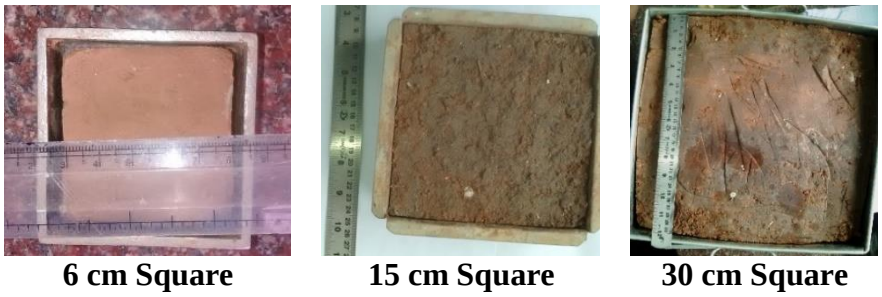

6 cm Square **15 cm Square** **30 cm Square**

10 cm diameter **15 cm diameter** **30 cm diameter**

Figure 3.26 Shrinkage test of lab scale rectangular and circular compacted specimens

Figure 3.27 Figure depicting oven dried soil samples

The amount of shrinkage the soil undergoes in this process is calculated as given in Eq. 3.14, indirectly represents the desiccation potential. The higher the volume changes the more susceptible to cracking in field. Kleppe and Olson (1985) correlating field desiccation with laboratory shrinkage, have suggested that soils with shrinkage less than 4% would relatively show minimal desiccation in field.

$$\text{Change in volume}(\%) = \frac{\text{Initial volume-Final volume}}{\text{Initial volume}} \times 100 \qquad \textbf{3.14}$$

3.5.1 Volumetric shrinkage characteristics

3.5.1.1 Effect of soil type

Table 3.7 also presents the results of volumetric shrinkage test for different soil types used in this study. It is observed that the change in volume increases with increase in plasticity

of the soil, similar to the findings of Amadi and Eberemu (2013) in landfill barrier studies of soil-bentonite mixes. With increase in plasticity from 16 to 26, the percentage change in volume varied from 3.2 to 5.1 respectively. More likely, the increased optimum water content with increased plasticity could be a reason for increased shrinkage. Klepee and Olson (1985) observed that increase in laboratory volumetric shrinkage would result in increased field desiccation. From this, it can be understood that soils with higher plasticity are expected to crack severely if used in construction of surface layers in cover system.

3.5.1.2 Effect of compaction state

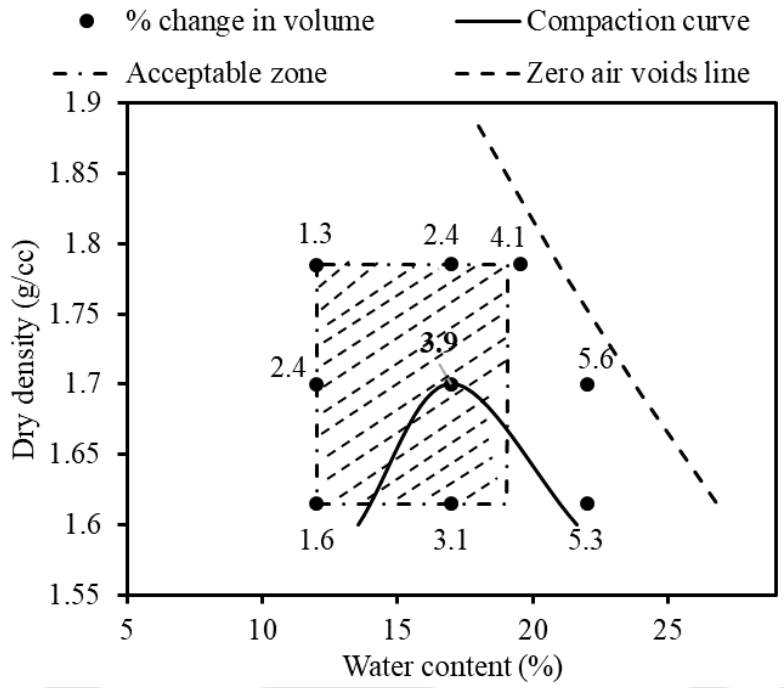

Figure 3.28 Variation of volumetric shrinkage test at different compaction states

The change in volumetric shrinkage behavior of S3 with change in water content and density are portrayed in Figure 3.28. The results revealed an increase in shrinkage behavior with increase in water content for any given density. The effect of water content is an obvious phenomenon as reported in literature (Daniel and Wu 1993; Osinubi and Nwaiwu 2008). Loss of increased water contents would induce higher shrinkage energy, resulting in increased shrinkage. The effect of density on shrinkage behavior is minimal. The percentage shrinkage was found to be marginally higher for MDD as compared to 0.95 and1.05MDD. Similar variations were reported by Osinubi and Nwaiwu (2008). The effect of density can be attributed to low void volume available to shrinkage at highest densities, while at low densities it could be due to low energy associated with easy escape of water

from large voids. The region of acceptance for limiting desiccation is recognized based on the 4% shrinkage volume suggested by Klepee and Olson (1985), as shown in the figure. From figure, it can be understood that irrespective of density in concern constructing surface earthen systems at higher molding water contents is not suitable, as it may lead to significant desiccation.

3.6 Unconfined compressive strength test

Figure 3.29 Unconfined compression test sample preparation and extraction

Unconfined compressive strength test (UCS) is one of the most commonly used geotechnical index testing to evaluate the strength potential of given soil. The simple test starts with preparation of cylindrical soil samples of 38 mm diameter and 76 mm height. The soil mixed with target water content and bulk mass measured to specific density were transferred into cylindrical mold with compacting screw setup on either edges as shown in Figure 3.29. The compacted samples were extracted from cylindrical molds using a controlled sample extractor and the final density, water content was verified. These samples were then compressed under constant rate loading frame assembled with proving ring and strain gauge for measuring compressive load and displacement. The observed compressive load (P) is converted to compressive stress (σ) using Eq. 3.15, considering the changes in area according to Eq. 3.16, where the strain (ε) is calculated according to Eq. 3.17. Daniel and Wu (1993) suggested a minimum required unconfined compressive strength of a cover soil as 200 kPa.

$$\sigma = \frac{P}{A_c} \quad \textbf{3.15}$$

$$A_c = \frac{A_o}{(1-\varepsilon)} \quad \textbf{3.16}$$

$$\varepsilon = \frac{\Delta l}{l_o} \quad \textbf{3.17}$$

where,

σ Unconfined compressive stress (kPa)

P Compressive load (kN)

A_c Corrected area (m^2)

A_o Initial area of the sample (m^2)

ε Strain of the soil sample %

Δl Change in length of the soil sample (mm)

l Initial length of the soil sample (mm)

3.6.1 Unconfined compressive strength characteristics

Unconfined compressive strength (UCS) results for various soil types are presented in Table 3.7. There is no linear relationship between soil type and strength of the soil. With increase in plasticity, the strength is observed to increase initially and then has shown a decreasing performance. The low plastic soil having higher coarse contents has relatively low bonding and hence would have resulted in less strength. While higher contents of water in high plastic soils might be the reason for the low strength. Continuous increase in percentage strain at failure can be attributed to the increase in plasticity of the soil itself.

3.6.1.1 Effect of compaction state

The variation of unconfined compressive strength and strain at failure with change in water content and density of S3 were evaluated using UCS testing. The strength results of nine compaction states are represented alongside compaction curve as depicted in Figure 3.30. It is observed that the strength of the soil reduces both with decrease in density and with increase in water content, while the strain at failure-behaved contrast as shown in Figure 3.31. However, the strain at failure increased with increase in water content, the relative increase in percentage strain is significant on wet side of OMC than on dry side. This is likely because of increase in the plasticity (ductile behaviour) of soil at higher water contents. Similar observations were reported by Bordoloi et al. (2015). The acceptable zone of compaction is selected based on the minimum criteria of 200 kPa suggested by Daniel and Wu (1993). Though the strength is higher on the dry side of optimum water content, it could not help in resisting erosion as can be seen in Figure 3.13 while it helped in resisting volumetric shrinkage as detailed in Figure 3.28. This signifies the need for combining overall results for more reliable performance.

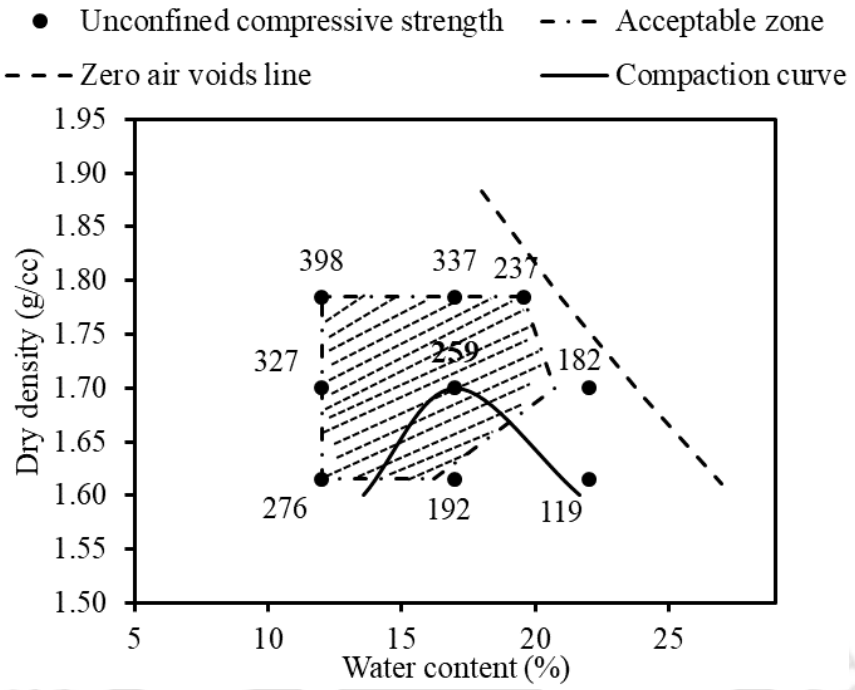

Figure 3.30 Variation of unconfined compressive strength at different compaction states

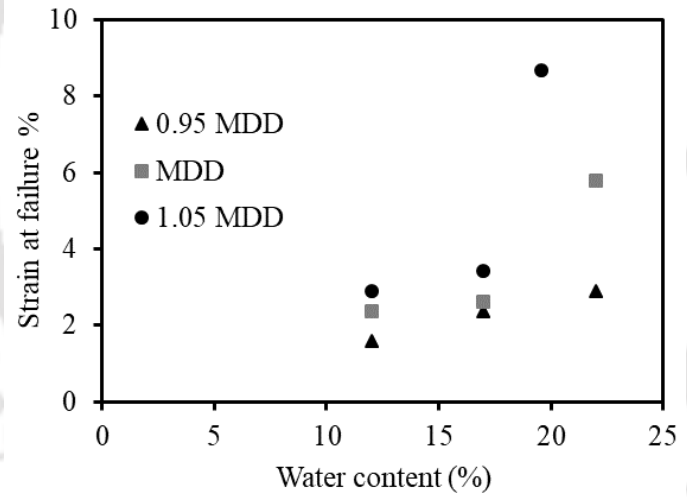

Figure 3.31 Variation in failure strain at different compaction states

3.7 Suitability of soil as surface layer of MLCS

Table 3.7 summarizes the results of all performance markers for different soils considered in this study. Different researchers have suggested preferential criteria for each of the performance markers. Considering the suggestions, the best soil satisfying the requirements of all performance markers is selected in this part of the study. Wan and Fell (2004) have suggested that soils with SEI>4 would have relatively low amount of erosion. While according to 40CFR258.60 (2002) the hydraulic conductivity of surface soil has to be lower

than 1E-7 m/s. From Table 3, it can be observed that S1 and S2 do not satisfy both of these criteria. Klepee and Olson (1985) have suggested that soils with volumetric shrinkage less than 4% would relatively exhibit a lesser amount of desiccation cracking. In continuation, from results it can be ascertained that S4 and S5 deficient in performance against desiccation. On other hand, Daniel and Wu (1993) have suggested that surface soils should have a minimum of 200 kPa UCS strength. S1 and S2 are observed to lack in strength characteristics too. The documented interpretations specify that the S3 is the only soil that satisfies multiple requirements of surface soil used in MLCS. Based on the results, it is apparent that a low plastic soil would be highly prone to erosion (less cohesion, (Wan and Fell 2004; Haghighi et al. 2013)) and exhibit high infiltration. A high plastic soil have tendency of excessive shrinkage and desiccation. Therefore, soils with medium range of plasticity which falls under ML classification can be considered as a suitable surface soil. However, a detailed study is needed for evolving a guideline based on plasticity for surface soils. Suitability of soil compaction state

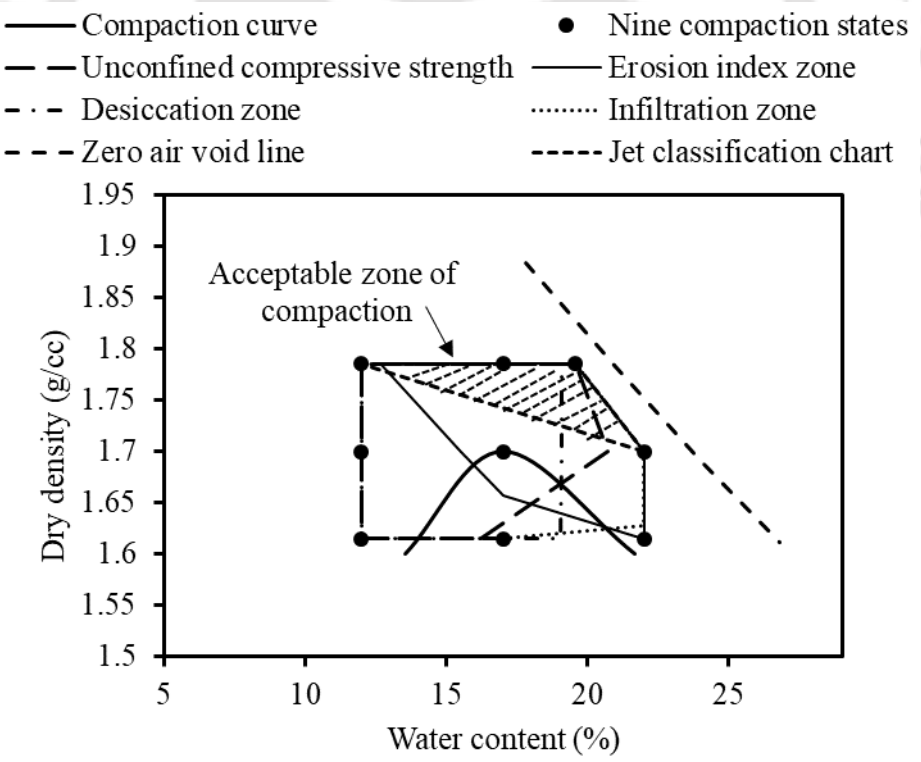

Figure 3.32 Final zone of acceptance based on overall performance markers

Final zone of acceptance satisfying all the performance markers viz. erosion, infiltration, desiccation induced volumetric shrinkage, and unconfined compressive strength is evolved by intersecting all the individual acceptable zones as depicted in Figure 3.32. Figure shows

that only one out of nine selected compaction states are satisfying all the performance markers. The acceptable zone here is restricted by erosion index on dry side of optimum water content while by desiccation induced shrinkage zone on wet side of optimum. The density on lower side is restricted by the jet erosion. Adding together, the final acceptance zone suggests constructing the surface layer of cover system at moderate water content near OMC to higher densities for attaining a better performance.

3.8 Summary

This study attempts to propose a new set of performance markers for evaluating the suitability of surface soil and its compaction state for multi-layered cover system (MLCS). With an understanding that the performance of surface soil is influenced by various soil-atmosphere interactions, four performance markers viz., erosion, infiltration, desiccation, and strength were used to develop a new criterion for its evaluation. Inclusion of erosion as one of the important characteristics for evaluating surface soils for MLCS is a new approach adopted in this study. Based on the results and discussion, the following conclusions were drawn.

1) Low plastic soils are observed to have low strength and are prone to severe erosion, further susceptible to significant infiltration therefore are not suitable for use in surface layers of MLCS. On other hand, high plastic soils are observed to shrink heavily and prone to desiccation. Based on this study, it is recommended to use soils with moderate plasticity in surface layers of MLCS due to its low amount of erosion, infiltration, and desiccation besides possessing adequate strength.
2) Soil compacted at lower water contents are observed to erode severely. While soil compacted at higher water contents are observed to shrink heavily and prone to desiccation, further susceptible to significant infiltration. Accordingly, it is suggested to compact the soils at moderate water contents near OMC for satisfactory performance as indicated by all performance markers.
3) Soils compacted to lower densities are observed to have low strength, prone to erosion and susceptible to higher infiltration. Therefore, it is recommended to compact the soils to higher densities for superior performance in surface layers of MLCS as observed from all index evaluations.

Chapter 4

Hydraulic performance of filter and drainage layers

4.1 General

Most of the designs of geotextile filters and/or drains were based on hydraulic conductivity/transmissivity or pore size criterion. However, for geotextiles used in multi-layered cover system (MLCS) it is important to study the long-term hydraulic performance and compatibility with adjacent materials. In this study, the long-term flow characteristics of soil-geotextile combination are evaluated to understand the adequacy of geotextile filter/ drainage layer used in MLCS. The effects of soil type, gradation, and geotextile on long-term performance of filter is established. One of the disadvantages of long-term flow test is the time duration required for equilibrium, which is approximately close to one month. Effort was made in this study to explore the possibility of using a geotechnical centrifuge for studying the long-term flow characteristics of soil-geotextile combination in relatively less time.

Application of coarse aggregates as drainage layers in landfill is a well-known practice (Rowe and Yu 2012). Lack of combined strength and hydraulic design criteria for materials used in drainage layers has resulted in failure of MLCS. Accordingly, attempt was made in this study to evaluate the performance of aggregates used in drainage layer of MLCS based on both shear and seepage characteristics. The effect of particle size and relative density on performance of the drainage layer was assessed.

4.2 Hydraulic performance of geotextile filter layer

Evaluation of hydraulic performance of geotextiles is vital for its use as filter or drainage layers in MLCS. Geotextiles are fastly replacing or substituting the conventional materials due to its versatility, cost-effectiveness, durability, and quick and controlled installation procedure. While the short-term benefits of geotextiles are beyond doubt, their long-term performance still needs systematic assessment. There are several accelerated-aging laboratory studies, field studies, and numerical simulations for understanding the long-term performance of geotextiles (Koerner et al. 1998; Faure et al. 1999; Giroud et al. 2000; Aydilek 2006; Wu et al. 2008). In addition, various researchers have explored the degradation in mechanical characteristics of geotextiles with time (Faure et al. 1999; Hsuan et al. 2008; Take et al. 2015). In spite of extensive research, there are numerous instances of hydraulic failure of geotextile filters attributed to the lack of compatibility of the soil-

geotextile interface (Rowe 1998; Koerner and Koerner 2013). The major factor governing the compatibility of the soil-geotextile combination is the dislodgement and clogging of soil particles in the pores of geotextiles. Clogging would decrease the efficiency of the geotextiles used as filters and drainage layers in MLCS (Sansone and Koerner 1992). Earlier studies attempted to evaluate the performance of geotextiles based on the opening size and permeability of geotextiles alone, which could not ensure the long-term filtration performance of the soil-geotextile combination (Carrol 1983; Giroud 2005).

To evaluate the worst possible field performance, long-term flow tests have to be carried out for determining its long-term compatibility (Almeida et al. 1995; Bergado et al. 1996). Hence, the main objective of the present study is to determine the long-term permeability of different soil-geotextile combinations used in MLCS. The experimental program to study long-term hydraulic performance of soil-geotextile combinations is described in Figure 4.1. The effect of soil and geotextile type on soil-geotextile compatibility was studied based on long-term permeability and clogging characteristics. The present study explored the possibility of using geotechnical centrifuge for studying long-term permeability characteristics in short interval of time. Such methodologies are essential for the selection of appropriate soil-geotextile combinations as drainage or filter layer in MLCS.

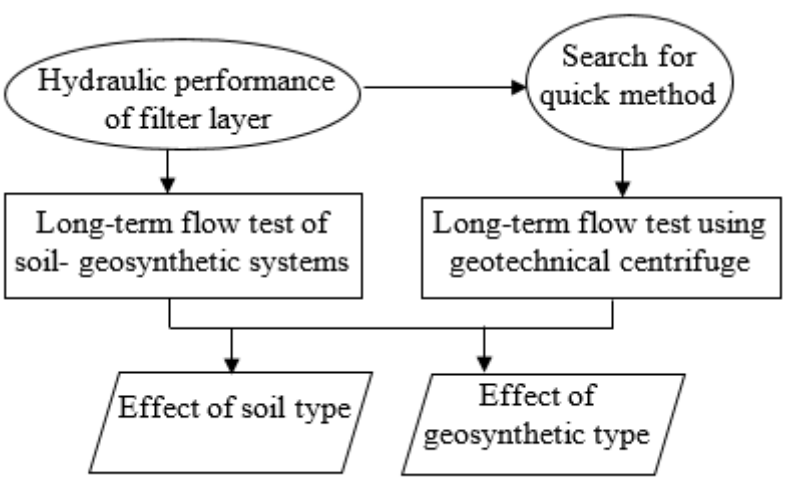

Figure 4.1 Experimental program to evaluate performance of geotextile filter

The efficacy of geotextiles as filters was ascertained based on: (1) permeability improvement factor (I_{pf}), which is the ratio of the equilibrium permeability (k_{eq}) of the soil-geotextile combination to the saturated permeability of the soil, and (2) stabilization time

(t_{eq}), defined as the time required by the soil-geotextile combination to achieve hydraulic equilibrium.

Three types of soils S2, S3, and S4 were selected for this study based on their optimal performance as surface soil in MLCS as stated in section 3.7. Five types of geotextiles designated as G1, G2, G3, G4, and G5 were selected to study the influence of its type. G1 and G2 are woven geotextiles, G3 and G4 are non-woven geotextiles, and G5 is a composite geotextile made of woven and non-woven faces. The basic properties of selected geotextiles are summarized in Table 4.1. The geotextiles were characterized according to the recommendations reported in the literature (ASTM D5199-01, ASTM D5261-10, ASTM D4491 - 99a, ASTM D6574 - 00, ASTM D4632 - 08). Apparent opening size (O_{95}) was determined by analyzing the images of geotextiles obtained from field emission scanning electron microscope (FESEM) (Bhatia and Smith 1996; Fisher et al. 1996). The pictorial and FESEM images of geotextiles used in this study are shown in Figure 4.2.

Table 4.1 Summary of basic properties of selected geotextiles

Property	Geotextiles				
Designation	G1	G2	G3	G4	G5
Thickness (mm)	0.01	2.5	3.87	1.44	0.3
Mass per unit area (kg/m^2)	0.17	1.03	0.79	0.43	0.78
O_{95} (mm)	0.157	0.623	0.110	<0.075	0.133
Permeability (m/s)	1.27E-5	2.371E-4	1.44E-4	9.60E-5	1.57E-4
Transmissivity (m^2/s)	5.27E-5	2.19E-6	3.95E-5	9.29E-6	1.85E-6
Grab tensile load (kN/m)	2.98	38.13	27.45	25.91	20.70

4.2.1 Long-term flow test

Long-term flow test is useful to evaluate the hydraulic compatibility of soil-geotextile combination (Rollin and Lombard 1988; Williams and Abouzakhm 1989; Koerner and Koerner 1992). The major advantage of this method is the simplicity in measurements and direct conclusions that can be drawn from the observed trends. The long time span for flow-equilibrium and possibility of biological growth in the system is a major drawback of this test (Sasone and Koerner 1992). However, the use of distilled and de-aired water as permeant minimizes biological growth (Fannin et al. 1994). Six numbers of long-term permeability setup were fabricated in-house, according to the standard specifications available in the literature (Almeida et al. 1995). Figure 4.3 (a) and (b) depicts the photograph and conceptual figure of long-term permeability setup comprising three

sections: the top section acts as water reservoir, the middle section is the specimen holder for preparing compacted sample, and the bottom section is the receiver for collecting effluent water.

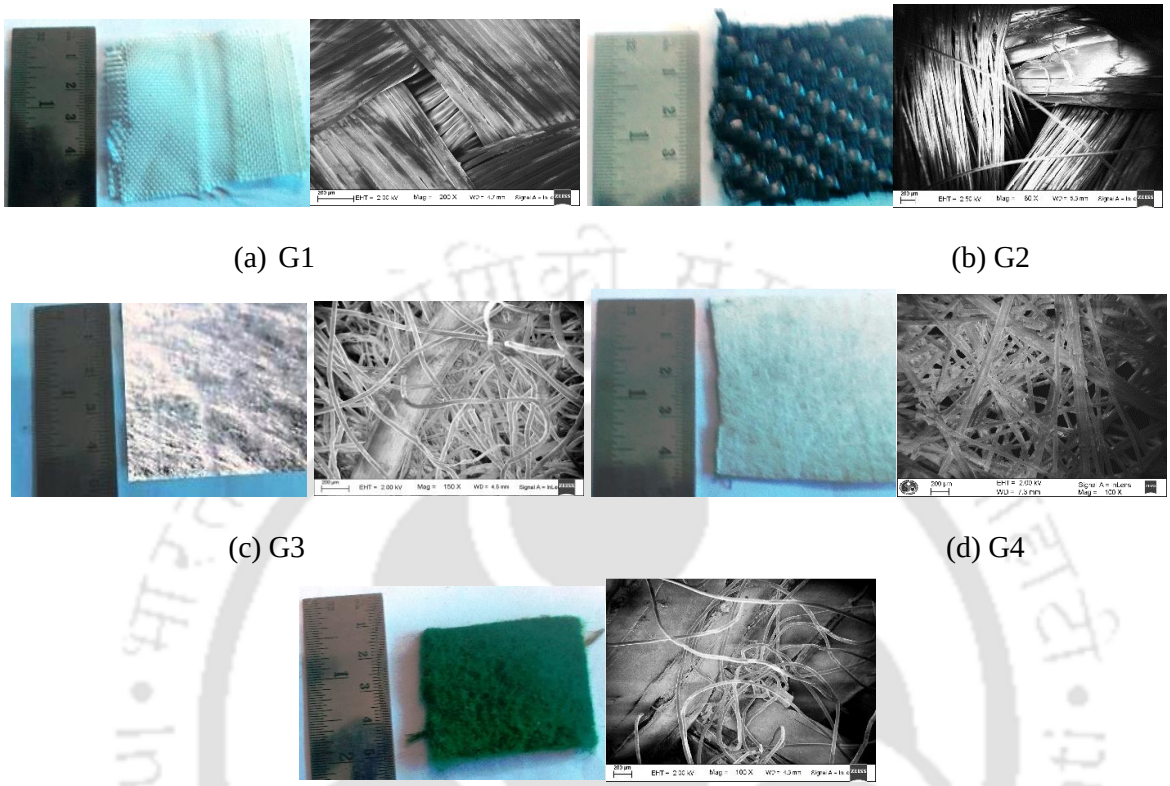

(a) G1 (b) G2

(c) G3 (d) G4

(e) G5

Figure 4.2 Pictorial and microscopic representations of various geotextile samples

The geotextile was cut into circular specimen of 10 cm diameter and soaked in water for 24 hours for saturation prior to the experiment. The soil was compacted in three layers at standard Proctor maximum dry density and optimum moisture content. The saturated geotextile was placed beneath the soil at the interface between the mold and receiver, identical to the sequence in which it is placed in the field. Initially, the bottom outlet was connected to a water tank with constant head arrangement for upward flow and saturation of the soil sample. This was confirmed by the steady-state discharge of water from the soil-geotextile combination measured with respect to time. After saturation, the direction of flow is reversed from top to bottom by connecting the inlet to constant headwater tank. In this test, the soil lying above the geotextile plays a major role in the permeability characteristics initially. With passage of time, the geotextile also starts contributing to

permeability, until equilibrium permeability is achieved (Rao et al. 1992; Mlynarek et al. 1991).

In the initial stage of the long-term permeability (k) test, the outlet was opened and the water flow rate was measured for every 24-hour interval for a total duration of 30 days. The hydraulic gradient equal to 10 was maintained according to ASTM D 5567-94, which is the maximum hydraulic gradient used for the soils with hydraulic conductivity varying between 1×10^{-7} m/s and 1×10^{-8} m/s. The test was performed by changing the soil type, gradation of soil, and geotextile type. Normally, granular soils take 10 hours and fine-grained soils take 200 hours to achieve equilibrium conditions (Koerner 1998). For a saturated soil, the varying trend of k is governed by the progressive piping and clogging which is dependent on soil type, type and pore structure of geotextiles, particle size distribution, and flow characteristics. Negative slope after the transition phase (time varying response of k) indicate excessive clogging where as positive slope represents excessive piping, which denotes incompatibility of the soil-geotextile combination (Rao et al. 1992; ASTM D 5567-1994). If the system permeability (k) versus time (t) response follows a zero slope after the transition phase, it represents an equilibrium condition.

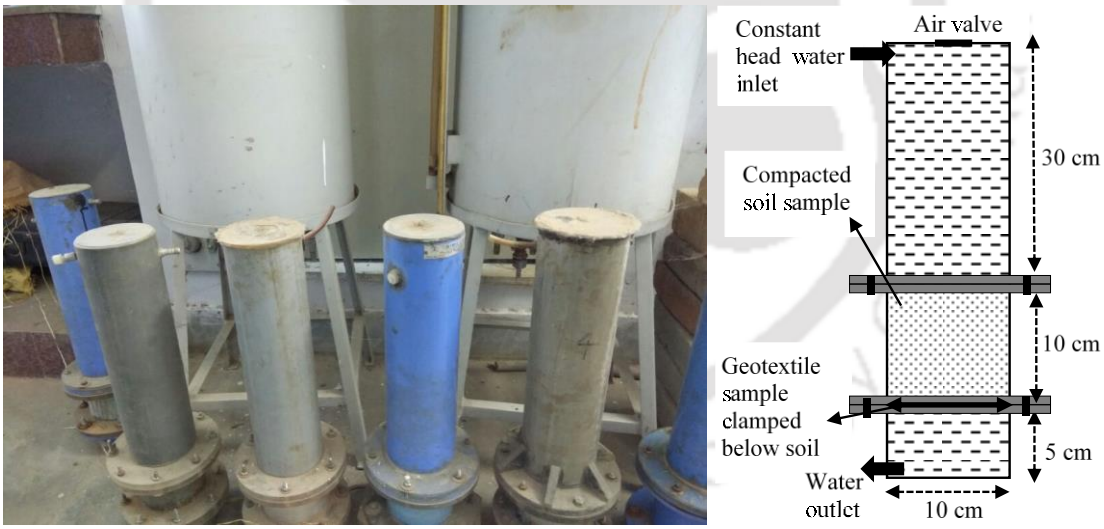

Figure 4.3 (a) Pictorial and **(b)** schematic representation of long-term permeability setup

4.2.2 Geotechnical centrifuge modelling of long-term permeability test

The experiments done for long-term permeability for different soil-geotextile combination under 1-g laboratory conditions were repeated in geotechnical centrifuge. Centrifuge

modelling is an effective tool for simulating flow of water and contaminants in soil column in a short interval of time (Singh and Gupta 2000). Centrifugation is the process of rotating soil model at high angular velocity to induce enhanced gravitational acceleration (centripetal force), which result in higher inertia that in turn result in enhanced hydraulic gradients (Zornberg and McCartney 2010). Geotechnical centrifuge was earlier used by researchers to reduce the testing time of steady-state flow process in different soil systems (Butterfield 2000; Singh and Gupta 2000; Taylor 2003) and transient flow behaviour in variably saturated soil systems (Cargill and Ko 1983; Singh and Kuriyan 2002; Rao and Singh 2012). Motivated from these studies, an attempt was made in this study to explore the utility of geotechnical centrifuge for long-term hydraulic flow behaviour of soil-geotextile system using the concepts of centrifuge modelling (Kumar 2007).

Figure 4.4 Small-scale geotechnical centrifuge facility installed at IIT Guwahati

Figure 4.4 presents the fabricated small-scale geotechnical centrifuge facility installed at Indian Institute of Technology (IIT) Guwahati with a beam diameter of 1 m. The buckets at the end of the centrifuge beam facilitate a space of 0.15 m x 0.15 m x 0.15 m for placing soil model. The geotechnical centrifuge with effective radius 'R_e' rotating at an angular velocity 'ω' induce a centripetal acceleration of $R_e\omega^2$. The equivalent enhancement (N times) in acceleration due to gravity 'g' on scaled soil model is evaluated according to Eq. 4.1. The technical details of geotechnical centrifuge installed at IIT Guwahati are detailed in Table 4.2.

$$Ng = R_e\omega^2 \qquad \textbf{4.1}$$

where,

N Number of times the acceleration due to gravity 'g' is enhanced

R_e effective radius of centrifugal beam (m)

ω angular velocity (radians per second)

Table 4.2 Details of centrifuge

Type of centrifuge	Beam centrifuge with swinging bucket on both sides of the arm
Beam diameter	1m
Centrifugation range	150-700 rotations per minute
Maximum acceleration	270g

Figure 4.5 depicts the test set up used for evaluating long-term performance of soil-geotextile system in a geotechnical centrifuge. The dimensions of the set up were decided according to the capability of centrifuge, without violating the physical laws of flow (Darcy's law). Darcy's law is valid for fluid flow in soil with Reynolds number less than 1 (Bear 1972). For example at maximum acceleration of 270g for a centrifugal fluid velocity of 270 x 10^{-7}m/s (which represent the 1 x 10^{-7}m/s (1g) the USEPA limitation for surface layer soil), the Reynolds number is 6.06 x 10^{-5} (<1) affirming the validity of Darcy's law. As depicted in the Figure 4.5, the centrifuge test set up consist of a collection chamber of 2cm height, soil sample with thickness of 3cm (>6 times the maximum particle size), water column of 4 cm, and constant head water supply chamber of 4cm with a rubber stopper. The overall height of the mold was 15 cm (available space) and the hydraulic gradient achieved in the centrifuge model was 3. The rubber stopper facilitates easy refilling of supply chamber. The outward flow from collection chamber enters into the centrifugal bucket, which is emptied during every refill of supply chamber.

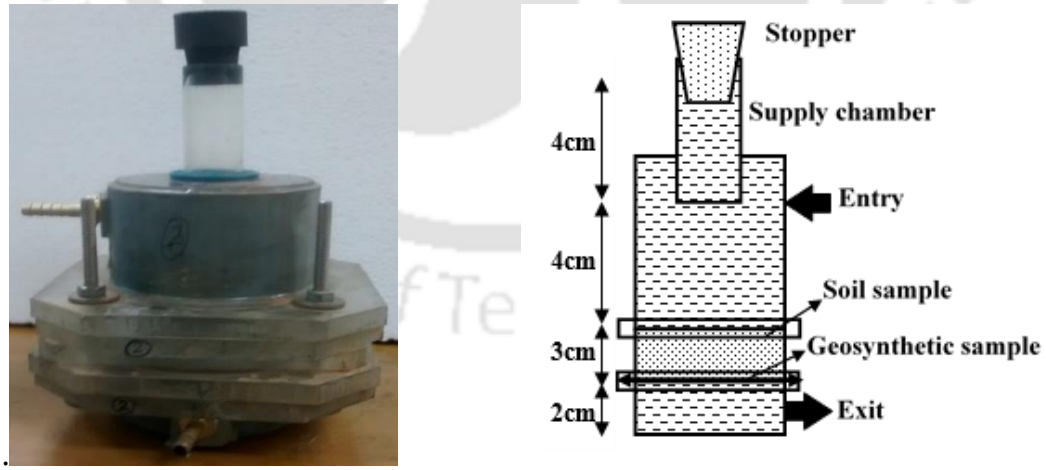

(a) **(b)**

Figure 4.5 (a) Pictorial and **(b)** Schematic depiction of centrifugal long-term permeability setup

4.2.2.1 Derivation of scaling laws

The scaling laws for different parameters used in centrifuge modelling are derived as follows:

Considering the effect of stress on material properties to be same, stresses must be similar in the model and the prototype and hence the scaling law for stress (SL_σ) can be written as:

$$\frac{\sigma_m}{\sigma_p} = SL_\sigma = 1 \qquad \textbf{4.2}$$

where, σ_m and σ_p are the stresses in the prototype and centrifuge model.

When same material is used in model and prototype, the density of the material remains same and hence the scaling law for density (SL_ρ) would be 1.

$$\text{i.e. } \frac{\rho_m}{\rho_p} = SL_\rho = 1 \qquad \textbf{4.3}$$

where, ρ_m and ρ_p are the densities of the material in the model and prototype.

Combining Eq. 4.2 and Eq. 4.3, the scaling law for length (SL_l) can be computed as:

$$\frac{\sigma_m}{\sigma_p} \times \frac{\rho_p}{\rho_m} = \frac{m_m g_m A_p}{A_m m_p g_p} \times \frac{m_p V_m}{m_m V_p} = \frac{Ng}{g} \times \frac{l_m}{l_p} = 1$$
$$SL_l = \frac{l_m}{l_p} = \frac{1}{N} \qquad \textbf{4.4}$$

where, m_m and m_p are the masses of the material in the model and prototype;

A_m and A_p are the area of the samples in the model and prototype;

V_m and V_p are the volume of the material in the model and prototype;

g_m and g_p are the acceleration acting on the material in the model and prototype;

g is the acceleration due to gravity and

N is the number of times gravity is enhanced in centrifuge model (Eq. 4.1).

Similarly, the scaling law for permeability (SL_k) can be derived as:

$$SL_k = \frac{k_m}{k_p} = \frac{K_m \rho_m g_m \mu_p}{\mu_m K_m \rho_p g_p} = \frac{Ng}{g} = N \qquad \textbf{4.5}$$

where, K_m and K_p are the intrinsic permeability of material in the model and prototype (which are same); μ_m and μ_p are the viscosity of the fluid passing in the model and prototype (which are same).

In case of geometric similitude, where Eq. 4.4 is valid, the scaling law for hydraulic gradient (SL_i) is computed as:

$$SL_i = \frac{i_m}{i_p} = \frac{h_m l_p}{l_m h_p} = \frac{N}{1} \times \frac{1}{N} = 1 \qquad \textbf{4.6}$$

where, i_m and i_p are the hydraulic gradients on the in the model and prototype;

h_m and h_p are the hydraulic heads applied in the model and prototype.

However, as the geometric similitude is not maintained in the present case (if centrifuge model is compared with the 1-g model) the SL_i is calculated as:

$$SL_i = \frac{i_m}{i_p} = \frac{h_m l_p}{l_m h_p} = \frac{9}{3} \times \frac{10}{100} = 0.3 \qquad \textbf{4.7}$$

Similarly, SL_l is calculated as:

$$SL_l = \frac{l_m}{l_p} = \frac{3}{10} = 0.3 \qquad \textbf{4.8}$$

Accordingly, scaling law for interstitial velocity (SL_v) is computed as:

$$SL_v = \frac{k_m i_m \eta_p}{k_p i_p \eta_m} = SL_k \times SL_m \times 1 = 0.3N \qquad \textbf{4.9}$$

where, η_m and η_p are the porosity of the material in the model and prototype (which are same for the same compaction state). Finally, the scaling law for seepage time (SL_t) can be derived as:

$$SL_t = \frac{L_m v_p}{L_p v_m} = \frac{SL_l}{SL_v} = \frac{0.3}{0.3N} = \frac{1}{N} \qquad \textbf{4.10}$$

Accordingly, to simulate flow of 1-day (1440 minutes) in 1-g to happen within 20 minutes, the N value is calculated as:

$$SL_t = \frac{t_m}{t_p} = \frac{20}{1440} = \frac{1}{72} = \frac{1}{N} \qquad \textbf{4.11}$$

Hence, the centrifuge model in this study is rotated at 350 rotations per minute to attain 72 times gravity enhancement in the acceleration acting on it, i.e. 72g.

4.3 Long-term flow behaviour at 1-g condition

4.3.1 Effect of soil type

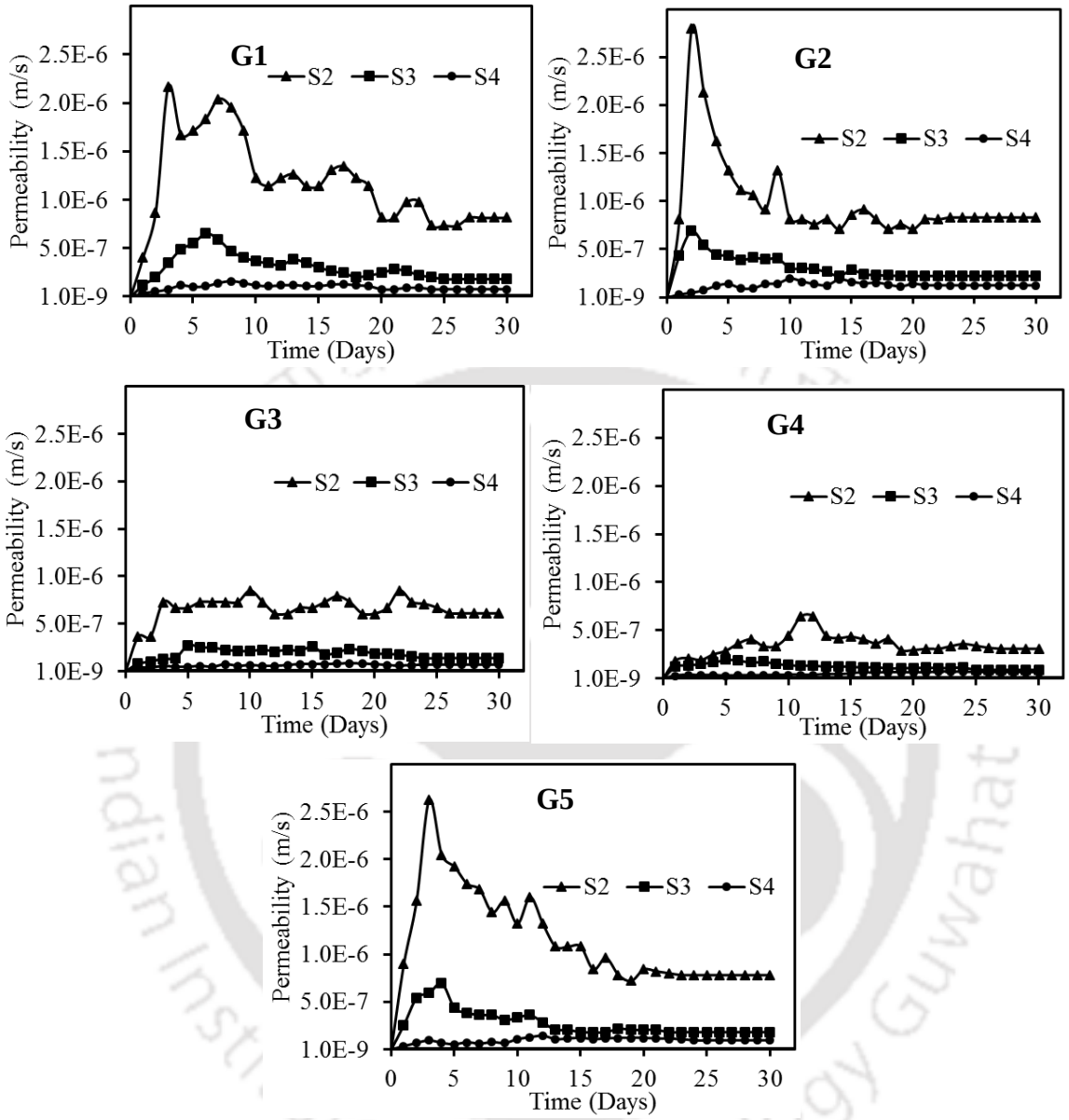

Figure 4.6 Effect of soil type on long-term permeability of different soil-geotextile combinations at 1-g condition

The effect of soil on permeability (k) variation with time of different soil-geotextile combinations tested in long-term apparatus at 1-g condition is shown in Figure 4.6. It can be noted that, for all soils, there is an initial increase in k followed by a sudden decrease. The fluctuations in k are, in general, soil dependent and attributed to piping and clogging phenomena. The trend in which there is initial increase and decrease in flow rate followed by constant value (k_{eq}) (equilibrium) is similar to those expected for a long-term flow test

as reported in Rao et al. (1992). The trends are consistent for all the geotextiles considered in this study. In the case of S2 and S3, there was a high rate of cyclic piping, clogging, and dislodgement of particles deposited at the geotextile pore space, causing high fluctuations during the initial flow process. The spike in k value was found to be less for S3 and the least for S4. The initial permeability of S2 was higher than that of S3 due to higher dislodged particles compared to the S3. Higher fines content along with coarse-grained particles results in denser, stable soil structure (Rao et al. 1992). Although the trends were similar for all soils, the extent of fluctuation was relatively less in S3, least in S4 as compared to S2. This difference is likely due to the increased fine content of S3 and S4. The final equilibrium permeability (k_{eq}) was found to be marginally higher than the initial permeability ($k_{initial}$) for all the soil- geotextile combinations, as reported in Table 4.3.

For S4, the initial rate of piping-clogging readjustment was less and marginally increased to its stable equilibrium value. These trends were verified repeatedly and found to be consistent. For the sake of brevity, not all the repeatability studies are presented here. For S4, there was meager piping initially, due to immediate dislodgement of fine particles from the geotextile pore space, resulting in marginal increase in k_{eq}. With time, the dislodged fine particles deposited at the soil-geotextile interface causes progressive piping until an equilibrium is attained. This was confirmed by the turbid water collected in the beginning, which progressively became clear, indicating the stabilization by clogging. Similar dislodgement behavior of fine particles was observed by Narejo et al. (2013). The variation of equilibrium permeability (k_{eq}) for all the three soils is consistent with all the geotextiles and follows the order S2>S3>S4. It is clear that the soil type has a significant effect on the k variation with time. Similar behavior was observed in Rao et al. (1992).

4.3.2 Effect of geotextile type

Figure 4.7 presents the temporal variation of k of S2, S3, and S4 in conjunction with different geotextiles considered in this study. A series of fluctuations in k was observed for all geotextiles, irrespective of soil type considered, which progressively stabilizes to an equilibrium k value. The overall flow rate showed a decreasing trend until it achieved the k_{eq} for all the geotextiles except for S4. Though the slope and the manner of fluctuations of k vary marginally for all the geotextiles, the trends were quite consistent for both S2 and S3. However, the trend of permeability of geotextiles in S4 was different from that of S2 and S3, with k progressively increasing to k_{eq}. G2 has shown higher k_{eq} for all soils likely

due to higher AOS as compared to other geotextiles (Table 4.1). Similar observations were made by Fannin et al. (1994) and Maheshwari and Gunjagi (2008) for geotextiles with higher AOS.

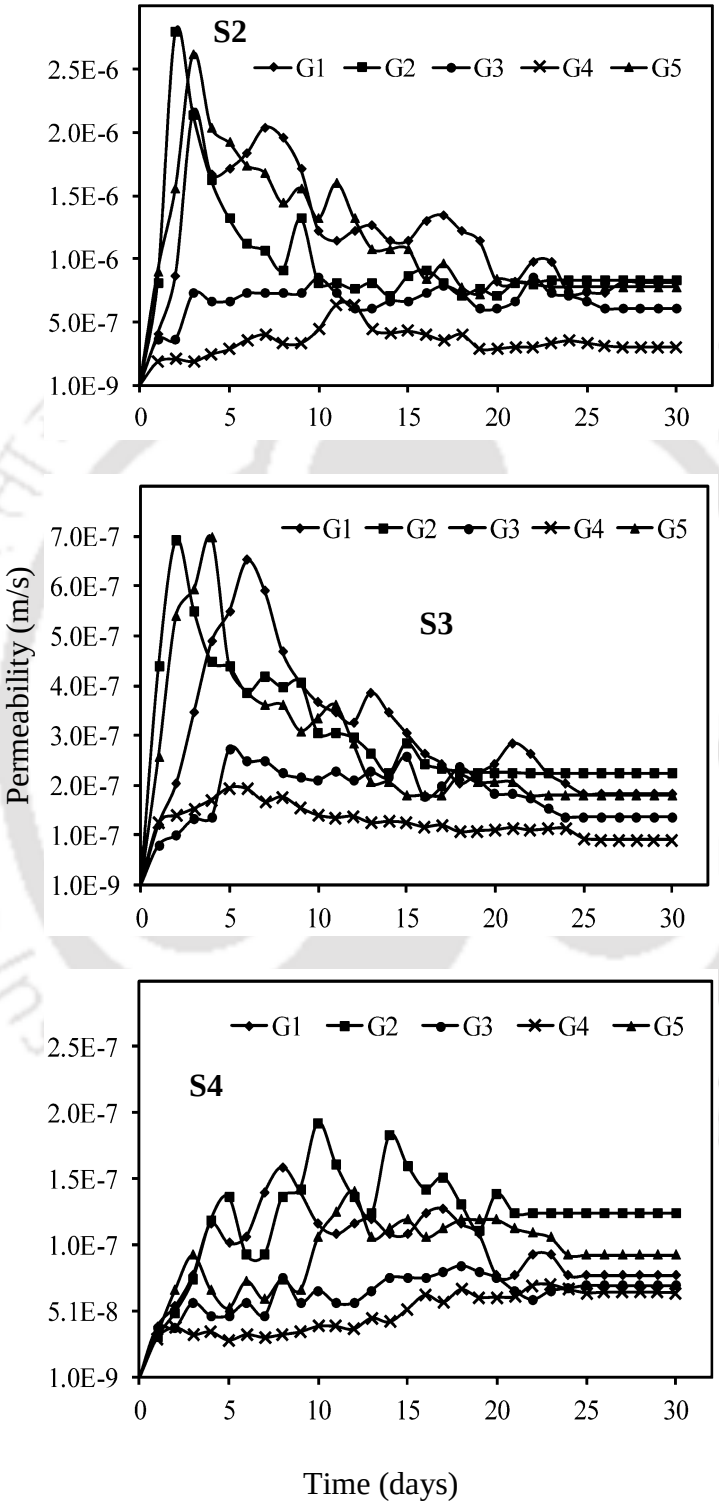

Figure 4.7 Effect of geotextile type on long-term permeability of different soil-geotextile combinations

Figure 4.7 further indicates that all the soil-geotextile combinations considered in this study achieved equilibrium within 30 days. In spite of initial fluctuations attributed to cyclic clogging and piping, it is noted that k_{eq} is close to initial permeability ($k_{initial}$) for all the soil-geotextile combinations, as listed in Table 4.3.

Table 4.3 Summary of long-term permeability characteristics of different soil-geotextile combinations at 1-g condition

Geotextile type	Soil type	System permeability		Stabilization time (t_{eq})	Permeability improvement factor (I_{pf})
		$k_{initial}$	k_{eq}		
G1	S2	4.1E-07	8.2E-07	27	1.2
	S3	1.2E-07	1.8E-07	25	4.8
	S4	3.9E-08	7.8E-08	24	1.4
G2	S2	8.1E-07	8.3E-07	23	1.2
	S3	4.4E-07	2.2E-07	22	5.9
	S4	3.1E-08	1.2E-07	21	2.2
G3	S2	3.6E-07	6.1E-07	26	0.9
	S3	8.0E-08	1.4E-07	24	3.6
	S4	3.8E-08	7.0E-08	25	1.3
G4	S2	1.9E-07	3.1E-07	27	0.5
	S3	1.3E-07	9.2E-08	26	2.4
	S4	3.0E-08	6.5E-08	25	1.2
G5	S2	9.0E-07	7.8E-07	23	1.2
	S3	2.6E-07	1.8E-07	22	4.8
	S4	3.3E-08	9.4E-08	24	1.7

From Table 4.3, it can be understood that all the three soil types selected in this study attain stable *k* value. The time taken to attain k_{eq} for all soil-geotextile combinations are also listed in Table 4.3. In general, stabilization time (t_{eq}) increased with an increase in fines content of the soil, which is similar to the trend reported by William and Abouzakhm (1989). In terms of t_{eq}, G2 showed the least value. Permeability of a severely clogged geotextile for a fine soil fraction in the range of silt or clay particle is less than 1×10^{-9} m/s (Sasone and Koerner 1992). From Table 4.3, it can be noted that the stabilized permeability values of all soil-geotextile combinations was higher than 1×10^{-9} m/s. This indicates that none of the selected geotextiles was severely clogged and hence can be used as filters in landfills. The stabilization time in the present study was found to be relatively low, which is attributed to the high compaction condition of the sample and the relatively high hydraulic gradient used during testing (Denkler et al. 2000). Higher compaction leads to low flow

rates with relatively less variability and high hydraulic gradients help in more pore volumes of flow in less time, achieving quick stabilization.

The basic requirement of the geotextile to behave as a good filter is that its permeability should be higher than the permeability of the soil sample (Carroll 1983; Christopher and Holtz 1985). Table 4.3 further depicts the permeability improvement factor of different soil-geotextile combinations. Permeability improvement factor (I_{pf}) is defined as the ratio of equilibrium coefficient of permeability of the soil-geotextile (k_{eq}) combination to the coefficient of permeability of soil alone $(k_{eq})_s$, as shown in Eq. 4.12. The factor I_{pf} indicates the improvement in filter capabilities of the soil-geotextile combination. This factor was originally defined for horizontal drainage flow by Raisinghani and Viswanadham (2010), but in this study, it is used to understand the vertical flow. The I_{pf} is observed to vary from 0.5 to 5.9 for the soil-geotextile combinations considered in this study. The G2 showed highest improvement for all the soil types while G4 showed the least improvement. Further S2 has shown low improvement with all geotextile owing to its high permeability. With its high tensile strength (refer Table 4.1) and high permeability improvement factor (refer Table 4.3), the geotextile G2 becomes the best candidate geotextile that can be used for filter application.

$$I_{pf} = k_{eq} / (k_{eq})_s \qquad \textbf{4.12}$$

where,

I_{pf} Permeability improvement factor

k_{eq} Equilibrium permeability of a soil-geotextile system

$(k_{eq})_s$ Saturated permeability of a soil

4.4 Centrifuge modeling of long-term flow test

4.4.1 Long-term flow results corresponding to 72-g

Figure 4.8 presents the temporal variation of k for long-term flow test of different soil-geotextile combinations conducted in centrifuge at enhanced gravity of 72-g. However, the relative magnitude of variation is low it is interesting to note that the trend of permeability fluctuations in centrifuge matches are similar to those observed in 1-g condition. Further, it can be observed that all the soil-geotextiles tested in centrifuge reached equilibrium within 600 minutes, which would otherwise need about 30 days (see section 4.3). This clearly portrays the competence of centrifuge in reducing the testing time in evaluating long-term flow behaviour of different soil-geotextiles. Nevertheless, the efficiency of

centrifuge in exact replication of 1-g results can only be understood by evaluating scale factors for permeability at equilibrium.

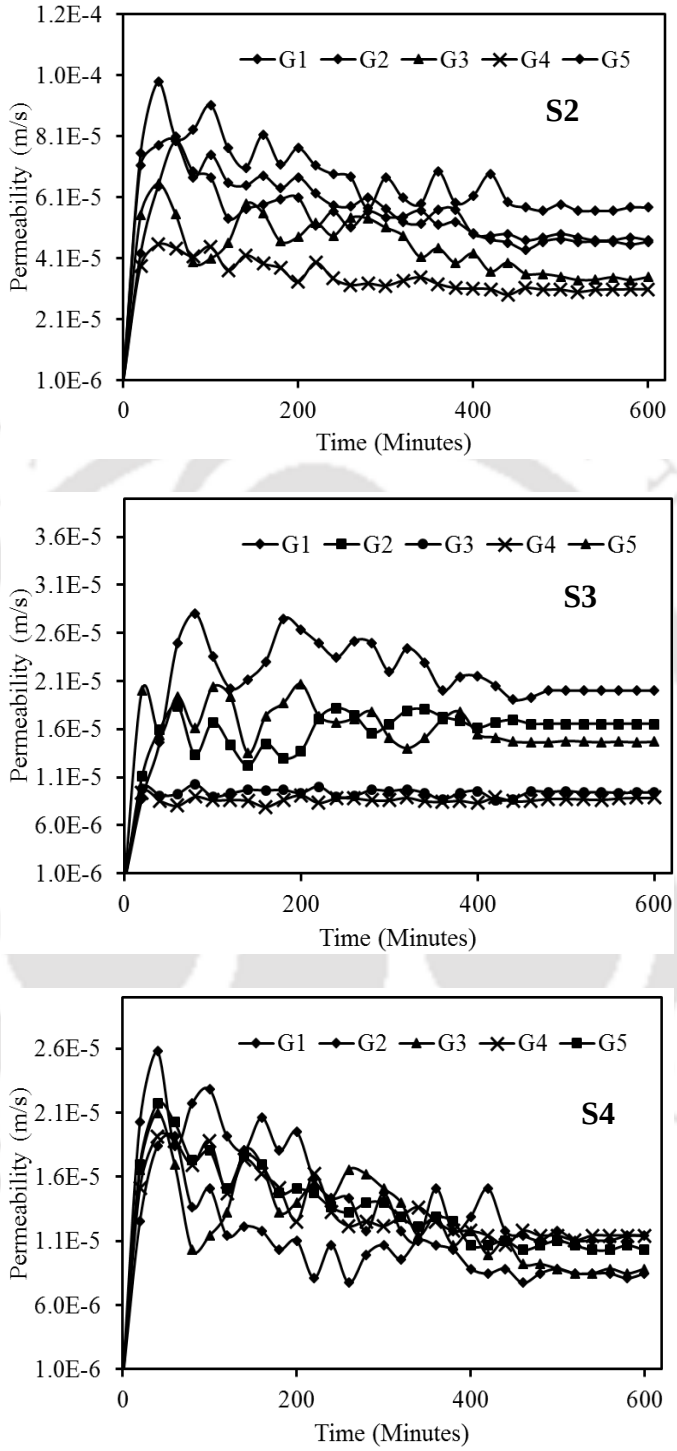

Figure 4.8 Temporal variation of long-term permeability of different soil-geotextile combinations tested at 72-g centrifugation

4.4.2 Scale factors for permeability at equilibrium

The scale factor represents the sensitivity of results obtained through centrifugation with respect to that of conventional testing. Hence, the scale factors of centrifugal modeling for equivalent permeability (SF_k) of different soil-geotextile combinations were evaluated respectively using Eq. 4.5 and Eq. 4.13 (Singh and Gupta 2000; Kumar 2007).

$$SF_k = \ln(k_{eq-m} / k_{eq-p}) / \ln(N) \qquad \textbf{4.13}$$

where,

SF_k Permeability scale factor

k_{eq-p} Equilibrium permeability of a soil-geotextile system in 1-g condition

k_{eq-m} Equilibrium permeability of a soil-geotextile system in N-g condition (centrifuge model)

N Level of acceleration due to gravity

Table 4.4 Summary of scale factors

Soil type	Geotextile type	Equilibrium permeability (m/s)		Permeability factor (SF_k)
		1-g	72-g	
S2	G1	8.2E-07	4.6E-05	0.94
	G2	8.3E-07	5.8E-05	0.99
	G3	6.1E-07	3.5E-05	0.95
	G4	3.1E-07	3.1E-05	1.08
	G5	7.8E-07	4.7E-05	0.96
S3	G1	1.8E-07	2.0E-05	1.10
	G2	2.2E-07	1.6E-05	1.01
	G3	1.4E-07	9.4E-06	0.99
	G4	9.2E-08	8.8E-06	1.07
	G5	1.8E-07	1.4E-05	1.03
S4	G1	7.8E-08	1.2E-07	1.10
	G2	1.2E-07	1.6E-07	1.06
	G3	7.0E-08	1.2E-07	1.13
	G4	6.5E-08	1.6E-07	1.21
	G5	9.4E-08	1.4E-07	1.10

Table 4.4 summarizes the centrifuge scale factors for different soil-geotextile combinations used in this study, evaluated according to Eq. 4.13. From table it can be understood that the scale factor for equivalent permeability varied from 0.95 to 1.21 for different soil-geotextile

combinations, which are much close to 1 (theoretical value, refer Eq.3.6). Therefore, centrifuge can be satisfactorily used for quick evaluation of long-term performance of different soil-geotextile combinations, even in the absence of geometric similitude. Singh and Gupta (2000) observed similar outcome, in case of permeability scale factors evaluated for centrifugation of silty soils.

4.5 Hydraulic-mechanical performance of drainage layer

Drainage layer in MLCS intercepts infiltrating water and diverts it to drainage collection system where it is pumped out. This decreases the hydraulic head over the barrier layer present underneath (Koerner and Daniel 1997) thereby reducing the possibility of seepage considerably. In general, locally available aggregates or coarse sand are used for drainage layer construction (Jesionek and Dunn 1995). By-products like shredded tires (Reddy et al. 2009), crushed concrete chips (Forrester 2001), alternate materials such as geonets (Tedder 2005) and composite geotextiles (Ramsey and Narejo 2005) are also used. Even though geotextiles offer constructional ease and better quality control, there are relatively a few data on its long-term performance in NSDF. The behavioral degradation of these geotextiles under severe leaching and clogging conditions is under investigation (Zornberg et al. 2004; Rowe 2005; Koerner et al. 2005). Hence, natural aggregates depending upon its availability are still preferred as drainage layer in spite of the issues related to quality control and constructional difficulties.

Improper design of the aggregate drainage layer may lead to failure of MLCS as a whole (ITRC 2003). The shear strength and seepage characteristics of drainage layers, which are part of sloped cover, have considerable influence on the overall stability of the structure (Koerner and Daniel 1997; USEPA 2015). Not many studies account for both shear strength and seepage characteristics in evaluating the effectiveness of coarse aggregates used in drainage layers (Tao et al. 2008). It was found that the particle size distribution of aggregates and relative density affects its permeability and plays a vital role in drainage design (Cedergren 1989; DOE 2000). According to USEPA (1989), the recommended aggregate particle size is 6.3–12.7 mm for filter or drainage layer of hazardous waste landfill. The minimum permeability recommendations for drainage layers are 10^{-5} m/s and 10^{-3} m/s for hazardous landfills and municipal landfills, respectively. In most of the existing MLCS, materials used in drainage layer were selected based on seepage

and particle size (Rowe 2005; Aydilek et al. 2006) without much attention to the shear strength characteristics.

Landfill reconnaissance studies indicate that the failure of most cover systems and landfill systems are due to improper material characterization, insufficient capacity, and poor performance of drainage layer (Koerner and Daniel 1997; Merry et al. 2005). Therefore, this study attempts to understand the effect of particle size and relative density of selected aggregates on its shear strength and seepage characteristics. The observations from this study were used to suggest a criterion for selecting drainage layer aggregates based on combined shear strength and seepage characteristics. The detailed experimental plan for achieving the optimum drainage criteria is detailed in Figure 4.9. The basic properties of aggregates selected for this study is detailed in Table 4.5. The particle size is evaluated as per ASTMD6913-04 and index densities are evaluated according to ASTM D4254-16.

Table 4.5 Summary of basic properties of aggregates selected for drainage layer in MLCS

Aggregate type	Particle size (mm)	Minimum density (ρ_{min})	Maximum density (ρ_{max})
A	12.5–10	1.341	1.486
B	10–8	1.290	1.443
C	8–6.3	1.266	1.412

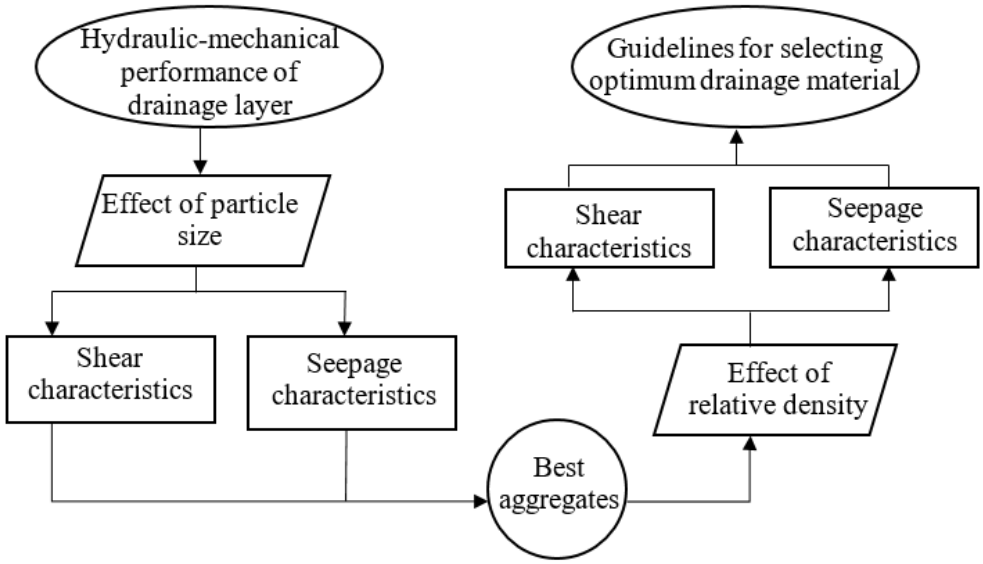

Figure 4.9 Experimental program to evaluate guidelines for optimum drainage material

The particle size range was selected based on the recommendations of USEPA (1989) as discussed above. The uniformly sized particles were selected as they have higher permeability as compared to that of well-graded aggregates (Stormont 1995). The shear strength of selected aggregates was determined using a large direct shear test box according to guidelines stated in IS 2720 part 39 (1977) and ASTM D 3080-11. The selected aggregate is placed in a shear box of dimensions 300 mm x 300 mm x 150 mm to a target relative density. The compaction was done using a thin rod of 10 mm in diameter and 300 mm long. Due care was taken to ensure better packing and non-breakage of particles. The compacted aggregate layer was allowed to saturate with tap water for 2 hours under desired normal stress and submerged condition. The sample was placed between two high permeable brass porous plates, which help in imparting double drainage condition. In general, displacement rate plays a vital role in results of drained direct shear test. However, it was reported that the displacement rate has insignificant effect on shear strength characteristics of cohesion-less materials (Skempton and Bishop 1950; Tatsuoka et al. 2006). Skempton and Bishop (1950) has concluded this based on the experimental investigation of cohesion-less sands but with a benefit of doubt with respect to coarse aggregates generally used in subgrade (Casagrande and Shannon 1948). Therefore, efforts are made in this study to affirm the effect of displacement rate on shear strength of aggregates. The saturated hydraulic permeability of the aggregates was determined using constant head rigid wall permeameter based on ASTM D2434-06. Permeability studies were conducted in a 0.1 m diameter permeameter mould IS 11209 (1985) and the hydraulic gradient was chosen according to ASTM D5567-94 recommendations.

4.5.1 Effect of displacement rate on shear characteristics

Aggregate ‘B’ passing 10 mm sieve and retained on 8 mm sieve was selected to study the effect of displacement rate (% of sample width traversed in unit time) on the shear characteristics of the aggregate. The selected aggregate was uniformly compacted to 80% relative density and were sheared at three different displacement rates of 0.336, 1.065, and 3.336%/min, under a constant normal stress of 59 kPa. The selected displacement rate represents relatively slow, moderate, and quick loading conditions (Ishihara 1996). When there is no perfect peak observed in stress–displacement curve, IS 2720 part-13 (1986) recommends the stress corresponding to displacement at 20% of sample width as the failure stress while ASTM D 3080-11 recommends stress corresponding to displacement at 10% of sample width. It can be observed from Figure 4.10 that there is negligible variation in

the stresses at 10 and 20% displacements and hence a displacement level of 10% is selected in this study. From the results illustrated in Figure 4.10, it can be observed that there is only a marginal effect of displacement rate (about 10 to 15%) on failure shear stress of aggregates. The aggregates being highly permeable result in quick dissipation of excess pore pressure generated during shearing. Therefore, shear characteristics are not significantly influenced by the range of displacement rate considered in this study. As there is minimal effect of displacement rate on shear characteristics of aggregate, a moderate displacement rate of 1.065%/min was selected. The insignificant/minimal effect of displacement rate is limited to uniformly graded aggregates with high permeability only. The effect of displacement rate on shear strength of well-graded aggregates of moderate permeability and fine grained soils with relatively low permeability need to be studied in detail.

Since the aggregate was well compacted to 80% relative density, significant amount of dilation was expected during shearing (Li and Dafalias 2000). However, no significant dilation and peak was observed for the results reported in this study. The results were repeated thrice to ensure the trends, and were found to be consistent. The mechanism involved in the development of dilation and post peak reduction is due to the non-homogenous deformation zones such as shear bands, which might not have developed in the case of coarse aggregates. The probable reason for this can be attributed to the crushing of particles during shearing which predominates the rolling of particles over one another there by suppressing dilation effect. Similar observations were reported by Arslan et al. (2009) in case of direct shear testing of manufactured granular material and Indraratna et al. (2014) in case of triaxial testing of rock ballast. This breakage of particles might have occurred due to the continuous rearrangement of particles associated with shearing. This was confirmed by the particle breakage noise during shearing due to crushing at the interface. After every test, the material was dried and sieved with its lower size sieve (for e.g. 10 mm sieve in the case of aggregate A), which resulted in 4–8% of material passing through the sieve. This confirms the particle breakage that occurred during shearing. Similar particle breakage behaviour during shearing was observed by Hardin (1985). The breakage of particles was observed to increase with increase in displacement rate, which is evident from the number of readjustments in stress during shearing as shown in Figure 4.10.

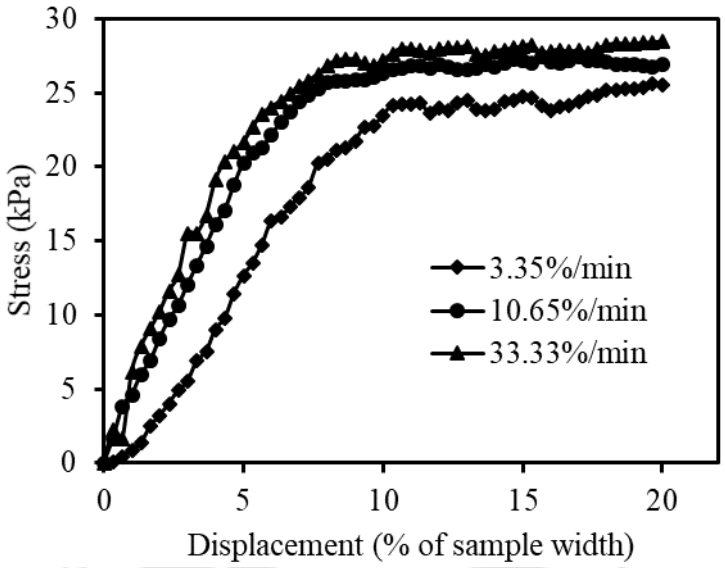

Figure 4.10 Variation of shear stress against displacement for different displacement rates

4.5.2 Effect of particle size and relative density on shear characteristics

The three sets of uniformly graded aggregates: A, B and C were compacted at 80% relative density and sheared at moderate displacement rate of 1.065%/min under three normal stresses of 59, 108, 157 kPa. The stresses considered here are well in the range of stresses encountered in NSDFs of 10–15 m depth. As mentioned before, no peak stress was observed and hence the shear stress corresponding to a displacement at 10% of sample width was considered as the failure stress according to ASTM D3080 (2011). Shear stress versus normal stress variation for different particle sizes is shown in Figure 4.11. Results portray an increase in shear resistance of aggregates for higher particle size compared to that of lower sized particles. Similar observation was made by Islam et al. (2011) for sandy soils. This may be due to the increased interlocking of large size aggregates. Observing the high shear resistance of large size particles, the same set of aggregates were selected to study the effect of relative density on the shear characteristics of aggregates.

The selected set of large size aggregate ‘‘A’’ were uniformly compacted at three different relative densities 40, 60 and 80% and were sheared under three different normal pressures of 59, 108, and 157 kPa. The results of failure shear stress versus normal stress variation for different relative densities are shown in Figure 4.12. It can be observed that the angle of shearing resistance increases with increase in relative density, which may be attributed to the dense packing and interlocking.

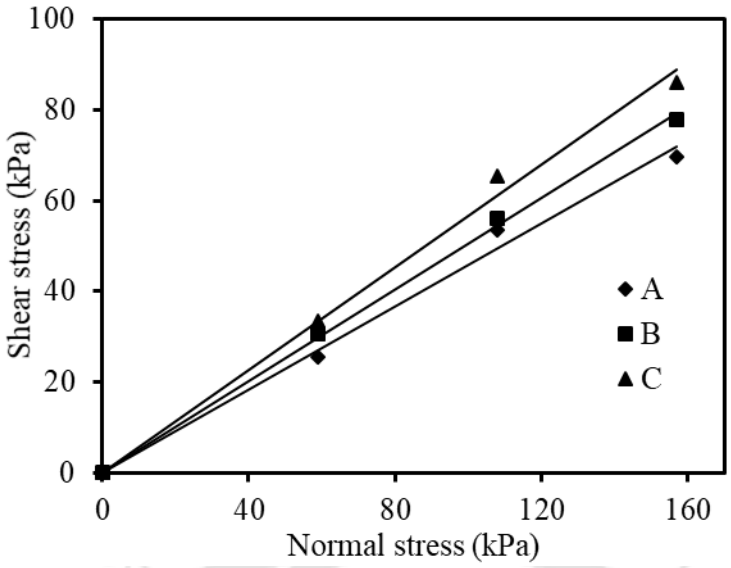

Figure 4.11 Variation of shear stress against normal stress for different size aggregates

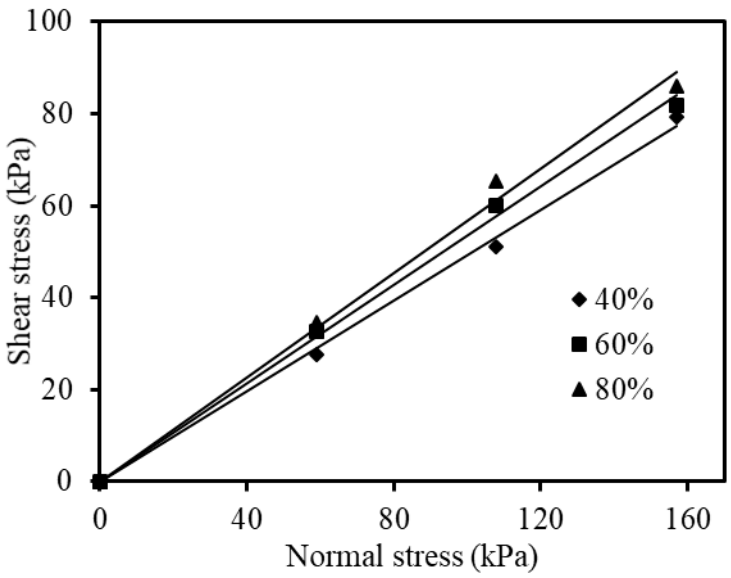

Figure 4.12 Variation of shear stress against normal stress for different relative densities

4.5.3 Effect of particle size and relative density on seepage characteristics

The saturated hydraulic conductivity of selected aggregates was determined at 80% relative density compaction condition under a constant hydraulic gradient of 5. The results of hydraulic permeability with variation in particle size are summarized in Table 4.6. The permeability values observed in this study satisfy the recommendations of USEPA (1989) for hazardous waste disposal facility. The hydraulic conductivity was noted to increase with increase in particle size of aggregates due to the increase in void distribution and its interconnectivity. Similar observations were reported by Yu and Rowe (2012). Observing

the better shear strength and hydraulic conductivity of aggregates of higher particle size, the same set of aggregates 'A' was selected to study the effect of relative density on seepage characteristics.

Table 4.6 Permeability values of various particle sized aggregates

Particle size	Permeability (m/s)
A (12.5-10 mm)	$1.47E^{-04}$
B (10-8 mm)	$1.35E^{-04}$
C (8 -6.3 mm)	$1.06E^{-04}$

Similar to previous sections, three relative densities of 40, 60, and 80% were selected to study the effect of relative density on seepage criteria. The variation of permeability with different relative densities of aggregates is summarized in Table 4.7. A marginal decrease in permeability was observed with increasing relative density. This decrease in permeability could be due to the decrease in void space and inter connectivity at higher relative density.

Table 4.7 Variation of permeability values with relative density of aggregates

Relative density	Permeability m/s
80%	$1.47E^{-04}$
60%	$1.66E^{-04}$
40%	$1.76E^{-04}$

4.5.4 Combined variation of shear strength and seepage characteristics

The combined variation of angle of frictional resistance and saturated permeability of aggregate with change in particle size are shown in Figure 4.13. It may be noted that both the shear strength and permeability increases with an increase in particle size for a particular relative density. Based on this, the study recommends the use of higher size particles, for having better performance in the drainage layer of MLCS.

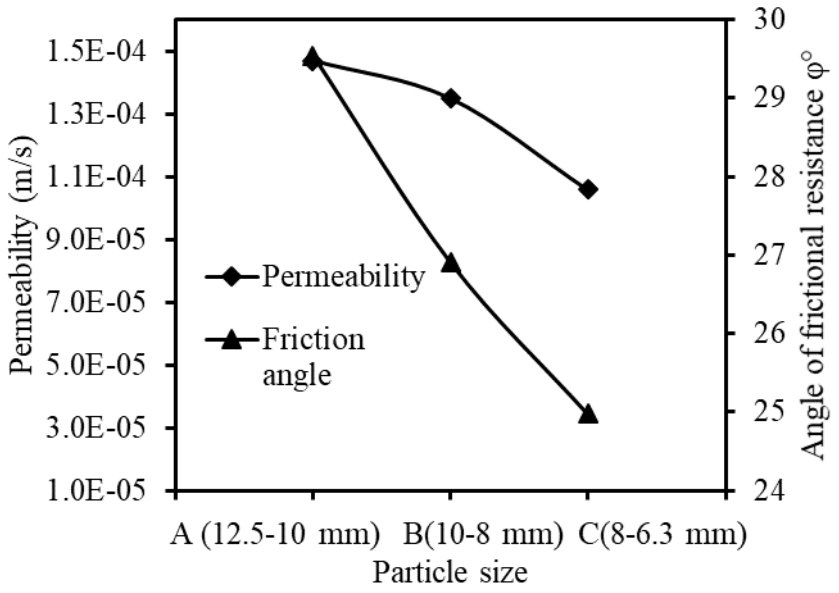

Figure 4.13 Variation of permeability and angle of shear resistance for varying particle size

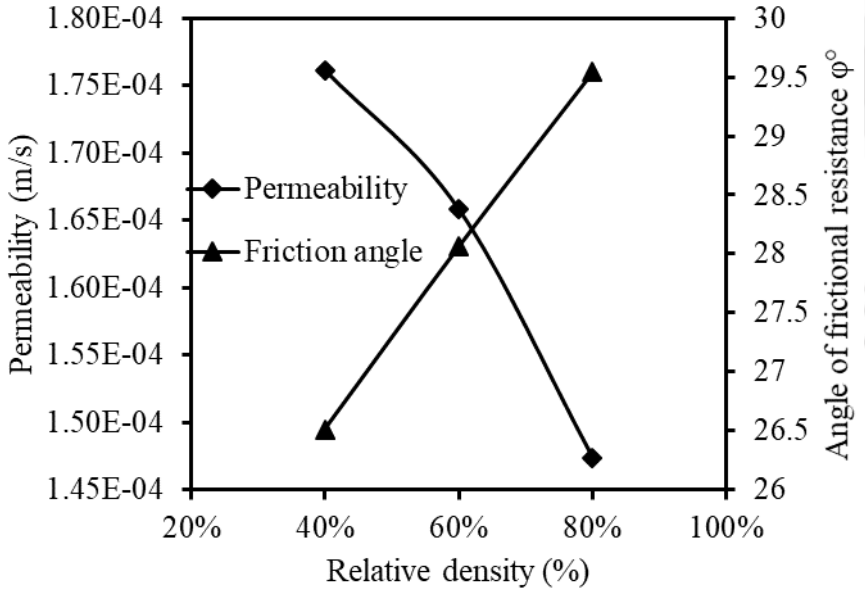

Figure 4.14 Variation of permeability and angle of shear resistance for varying relative density

The combined variation of angle of frictional resistance and permeability of coarse aggregate, with change in relative density for aggregate 'A' are shown in Figure 4.14. It can be observed that the permeability of aggregates decreased and angle of frictional resistance increased with increase in relative density. Based on the result, it can be noted

that an optimal relative density is 63.5% where the permeability variation curve meets with the friction angle variation. The results from this study indicate that higher size aggregate ‘‘A’’ compacted at relative density of around 60% can be used as drainage layer in MLCS of low-level radioactive waste NSDF.

4.6 Summary

1) Long-term flow tests of different soil-geotextile systems indicated that the variation in permeability with time for the three soils was found to be consistent with all the geotextiles.
2) The equilibrium permeability (k_{eq}) was observed to decrease with increase in fine contents of given soil.
3) The use of different geotextiles resulted in the comparable value of k_{eq}, which indicates that the influence of geotextiles on k_{eq} is marginal. However, higher improvement in permeability was observed in the case of geotextile with higher opening size (AOS) and vice versa.
4) It was noted that the trends of long-term permeability test results in centrifuge (N-g condition) was similar to that of conventional 1-g laboratory results. This proves that the interaction of soil-geotextile in long-term permeability test conducted in centrifuge under enhanced gravity is similar as that of 1-g for the range of gravity considered in this study. In addition, the time required for stabilization of permeability was much less in N-g as compared to 1-g (≈600 minutes in 72-g as against 30 days in 1-g).
5) Based on the test results obtained in this study, effort was made to determine the scale factor for equilibrium permeability and equilibrium time for centrifuge modeling. It was noted that scale factor for permeability for various soil-geotextile combinations were found to be close to unity, which is same as the expected theoretical value for permeability. This demonstrates the usefulness of geotechnical centrifuge for quick evaluation of long-term hydraulic performance of soil-geotextile combinations.
6) Hydro-mechanical evaluation of drainage layer aggregates indicated that the large sized aggregates exhibited a better performance both in terms of shear and seepage characteristics. Further, from shear strength and seepage results for large size particle used in this study, it was found that a relative density close to 60% would be optimal for drainage layer.

Chapter 5

Field performance of surface layer of multi-layered cover system

5.1 General

In this study, a pilot multi-layered cover system (MLCS) was constructed and exposed to field conditions for studying the influence of atmospheric factors on its stability. There are only limited field studies in assessing the performance of surface soils in cover system, especially in tropical regions receiving high amounts of rainfall. The MLCS was subjected to natural and simulated rainfall event, growth of natural vegetation for studying their impact on erosion of surface soil layer. Though vegetation is one of the proven erosion management practice, there are relatively few studies relating to quantitative evaluation of vegetation and its effect on erosion and infiltration of surface soils in MLCS. Considering the longer design periods of MLCS, there is immense need to estimate the soil loss in future. Hence, this study attempts to evaluate the efficiency of the commonly used empirical model to predict future erosion. The detailed field-monitoring program in evaluating MLCS is shown in Figure 5.1.

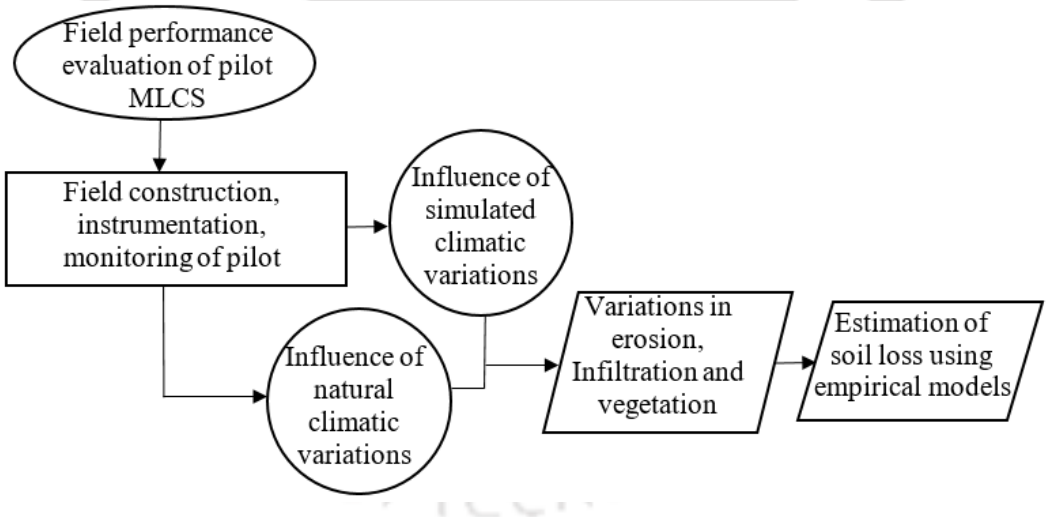

Figure 5.1 Experimental program to evaluate field performance of surface layer in MLCS

5.2 Materials

The materials used in this study were selected after a detailed evaluation of their laboratory performance, satisfying the preliminary recommendations of USEPA (1989). It includes local red soil (RS) in surface protection layer, a mixture of bentonite clay (B) – red soil (RS) in 30:70 proportion for barrier layer, and river sand (SS) for drainage layer. In

addition, a layer of geosynthetic clay liner (GCL) was provided above the barrier layer, geotextile drainage layer was provided below the drainage layer and a non-woven geotextile filter layer was provided under surface protection layer for improved performance. The geotechnical properties of soil materials and properties of geosynthetic materials are summarized in Table 5.1and Table 5.2, respectively. All the materials were tested according to the procedures detailed in American standards for testing materials (ASTM).

Table 5.1 Summary of geotechnical properties of various cover soils

Physical properties		**Measured result**		
	Designation	RS	SS	B
	Specific gravity (G)	2.69	2.64	2.88
Particle Size distribution (%)	Coarse sand (2.00 mm – 4.75 mm)	0	4	0
	Medium sand (0.425mm – 2.00mm)	6	4	0
	Fine sand (0.075 mm – 0.425 mm)	19	64	5
	Silt (0.002 mm – 0.075 mm)	51	32	31
	Clay (< 0.002mm)	24	0	64
Atterberg limits %	Liquid limit (LL)	41	-	295
	Plastic limit (PL)	25	-	43
	Shrinkage limit (SL)	23	-	11
	Plasticity index (PI) [%]	16	-	252
Compaction characteristics				30:70 mix
Optimum moisture content (%)		16.92	-	33.2
Maximum dry density (g/cm^3)		1.73	1.67	1.35
Saturated hydraulic conductivity (m/s)		2.9×10^{-8}	3×10^{-6}	1.9×10^{-12}
Angle of internal friction		32°	26°	11°

Table 5.2 Summary of general properties of geosynthetic specimens

Sl. No.	Property of geosynthetic material		Geosynthetic drainage	Non-woven geotextile	Geosynthetic clay liner
1	Thickness (mm)		3.870	1.440	7.157
2	Specific gravity		0.651	0.332	2.064
3	Mass per unit area (g/m^2)		790	425	6000
4	Dynamic puncture resistance (mm)		5.67	12.67	8.67
5	Static puncture resistance (kN)		0.46	0.68	1.22
6	Inplane permeability (m^2/sec)		3.95	0.93	-
7	Cross plane permeability (sec^{-1})		0.0019	0.0007	-
8	Grab tensile strength (kN/m)	Machine direction	27.45	25.91	27.83
		Cross machine direction	31.75	32.23	28.44

5.3 Methodology

5.3.1 Construction of MLCS

The configuration of MLCS considered in this study is as per the recommendations of USEPA (1989) and detailed in Table 5.3.

Table 5.3 Configuration of multi-layered cover system

Sl. No.	Layer	Thickness	Purpose
1	Surface protection layer	0.4m	To safeguard the remaining layers from direct interaction with atmospheric variants
2	Filter layer	~0.005m	To protect the drainage layer from clogging due to piping of surface soil
3	Drainage layer	0.3m	To divert the rain water infiltrated from surface soil layer outside cover system
4	Additional drainage	~0.005m	For extra safety, considering the long design life of MLCS
5	Additional Barrier	~0.01m	Composite GCL that has multiple protection facilities compacted in thin membrane
6	Conventional Barrier	0.4m	Low permeable clay layer that restricts moisture transfer into deeper sections.
7	Fill soil	~0.1m	The foundation layer, that bears the soil layers above it.

The usual recommendation of cover slope angle is 3 to 7° (USEPA 1989), however to understand the worst probable performance a slope of 10° is adopted in this study. The schematic representation of field cover system is depicted in Figure 5.2. Figure also details the position of rainfall simulator, the erosion collection chamber, and the vegetated surface.

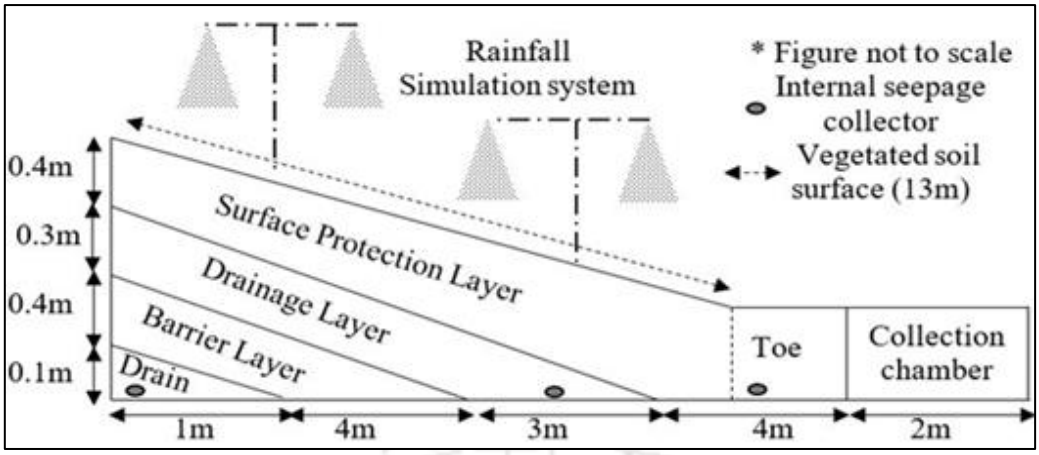

Figure 5.2 Schematic representation of field cover system

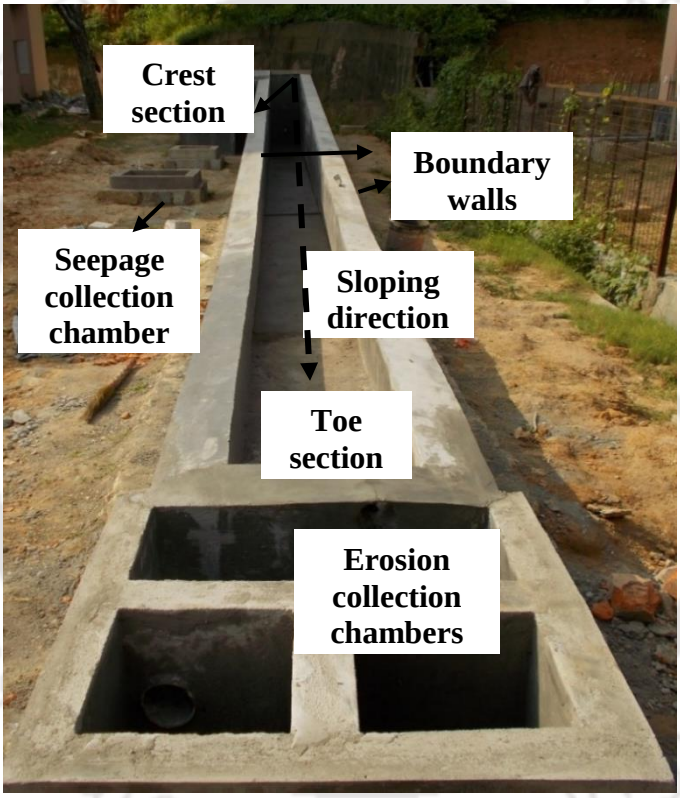

Figure 5.3 Pictorial image of constructed field setup

The photograph of the constructed setup is shown in Figure 5.3. Facility was provided for collecting eroded soil at the toe portion and collecting seepage water from drainage layers as shown in Figure 5.3. The construction sequence and calibration of rainfall simulator are detailed in forthcoming sections. Mixing of the soil in definite proportions to desired water contents was done as shown in Figure 5.4 (a) and Figure 5.4 (b). Care was taken to avoid clod formation while mixing cohesive soil with water shown in Figure 5.4 (c). The whole

mixture was transferred into closed drums and isolated for 7 days as shown in Figure 5.4 (d) for uniform distribution of moisture.

Figure 5.4 (a)

Figure 5.4 (b)

Figure 5.4 (c)

Figure 5.4 (d)

Figure 5.4 Preparation of materials to be filled in multi-layer cover system

The filling and compaction of barrier soil was done as shown in Figure 5.5 (a). The water content was verified at regular instants during filling. After reaching about half the depth, the sensors for monitoring moisture variations were laid in position exactly at the center of the barrier layer along its length. The placement of sensor was done by taking care of the zone of influence from the boundary walls, bottom surface, and from the adjacent sensor as shown in Figure 5.5 (b). The soil layer immediately above the sensors needs to be gently compacted as shown in Figure 5.5 (c). After completion of barrier layer, a layer of GCl was laid above it for additional protection as shown in Figure 5.5 (d). The profile probe casings were provided at designated location as shown in Figure 5.5 (e). The alignment of profile probe casings was repeatedly verified at every stage of compaction, to avoid any leakage along casing surface and easy insertion of probe through it. Immediately above GCl, a layer of geosynthetic drain layer (GDL) was laid as displayed in Figure 5.5

(e). The GDL layer was overlaid by a thick layer of river sand with the position of sensors in as shown in Figure 5.5 (f). The toe of the drainage layer sand is prefilled with fine gravel and covered with thick nonwoven geotextile layer to avoid any animal intrusion from drainage outlets as shown in Figure 5.5 (g). The completed drainage surface was covered by a nonwoven geotextile filter layer (GFL) as shown in Figure 5.5 (h) to avoid piping from surface protection layer. The surface protection layer was filled and compacted similar to other soil layers. The completed cover surface is as shown in Figure 5.5 (i).

Figure 5.5 (a)

Figure 5.5 (b)

Figure 5.5 (c)

Figure 5.5 (d)

Figure 5.5 (e)

Figure 5.5 (f)

Figure 5.5 (g)

Figure 5.5(h)

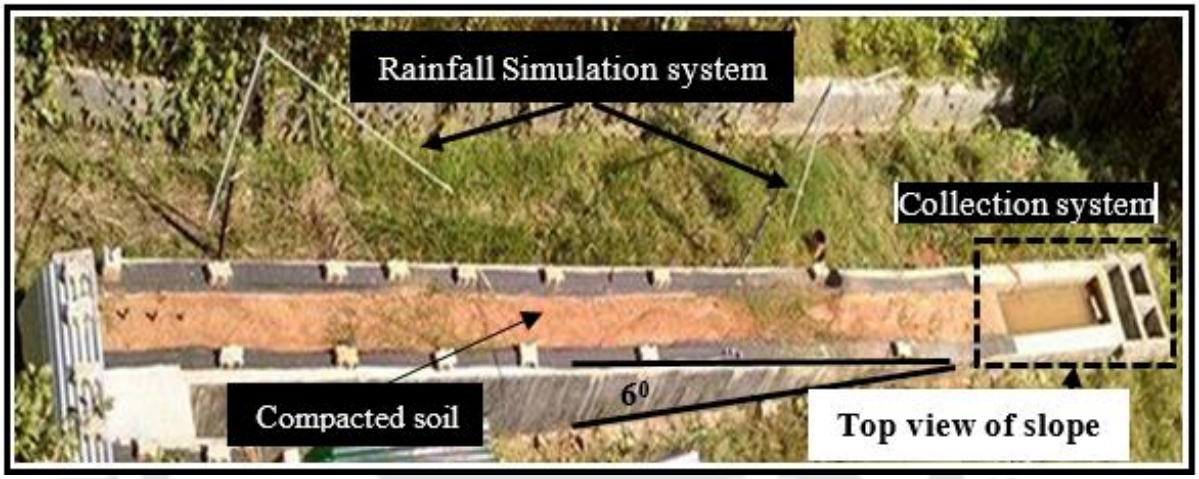

Figure 5.5 (i)

Figure 5.5 Construction of field cover system

5.3.2 Rainfall simulator

Figure 5.6 Experimental setup for evaluating erosion and infiltration of surface soil in multi-layered cover system

The rainfall simulator as shown in Figure 5.6 was made with four "Full Cone square spray - 1/2HH-40WSQ" nozzles procured from Spraying Systems Co. fitted to a 12mm pipe at a height of 2m from ground surface (Strauss et al. 2000; Francisco et al. 2010). The inlet pressure for rain simulator was controlled by an interferential, single jet, super dry straight reading type, hermetically sealed water meter confirming to ISO-4064. The spatial uniformity is established in-terms of coefficient of uniformity (*Cu*) defined by Christiansen (1941) as shown below

$$Cu = \left(1 - \frac{\sum_1^N |X_i - \bar{X}|}{N\bar{X}}\right) 100 \qquad \textbf{5.1}$$

where, X_i is the rainfall at any measurement location, $\bar{X}$ is the mean rainfall amount and N is the number of locations chosen for measuring rainfall.

The rainfall characteristics of simulated events are summarized in Table 5.4. From the table it can be seen that simulated rainfall intensity and rainfall drop size increased with the inlet pressure. The uniformity of simulated rainfall was satisfactorily recorded between 80 to 90%. The raindrop size was evaluated using flour pellet method defined by Kincaid et al. (1996). A plate of fly ash was placed below the simulated rainfall for fraction of seconds. The observed raindrop impact was measured and the average value is reported in this study.

Table 5.4 Characteristics of simulated rainfall events

Nozzle type	Orifice diameter (mm)	Inlet pressure (kPa)	Flow (L/Min)	Rain drop size (mm)	Rainfall intensity (mm/hr.)	Coefficient of uniformity (*Cu*) %
Full Cone square spray - 1/2HH-40WSQ	6.4 mm (maximum free passage 3.2 mm)	70 kPa	15.2	2.1±0.1	60±5 mm/hr	87.3
		90 kPa	17.8	2.4±0.1	80±5 mm/hr	81.4
		120 kPa	19.7	2.9±0.2	100±5 mm/hr	89.7

5.3.3 Weather station

A micro weather station (Meter Group inc. 2017) as shown Figure 5.7 was equipped with rain gauge (ECRN 100 high-resolution double-spoon tipping bucket type rain gauge), temperature and relative humidity sensor (VP3 relative humidity and air temperature sensor), wind speed (Davis cup anemometer) and solar radiation (PYR solar radiation) sensors. The weather station was installed in the immediate vicinity of field MLCS. The

weekly average climatic variations recorded during the experimental period are depicted in Figure 5.8.

The average daily temperatures results presented in this study include day and night recordings. From the variation in average daily temperature, it can be observed that the average temperature varied between 28±5°C during the monsoon and pre-monsoon periods, while in winter session it varied between 22±4°C. However, during some days in June-October the maximum temperatures were nearly about 35°C with night temperatures around 25°C. These days contribute to significant evaporation. The days with minimum average temperatures during this period are mostly the days that received rainfall, which result in relatively low evaporation. The temperature variation was relatively low in winter, which contributes to constant rate of evaporation, there by helps in maintaining constant rate of drying in simulated rainfall experiments. The temperatures were low in December and January, where the average temperature was close to 20°C while November and February had close to 24°C.

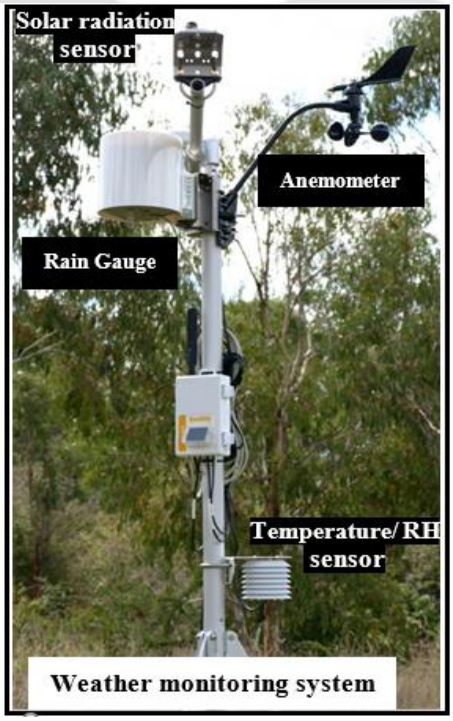

Figure 5.7 Micro weather station used in this study

The daily average relative humidity (RH) recorded at the test location broadly varied between 80±15% during monsoon and pre-monsoon periods while it varied between 75±10% during winter. The days with high RH corresponding to rainfall days and days with high temperatures during May-October. During November-December, the relative

humidity was almost constant around 78%, which gradually decreased until early February and reached about 68%. These constant and gradual variations result in similar climatic conditions during rainfall simulation experiments. The pre-monsoon in March has further shown higher RH close to 85%.

Figure 5.8 (d) summarizes the variation in daily average solar radiation with time. It was observed that except rainy days the solar radiation followed almost constant rate of decrement from June to December and then increased until March. The November-February session showed almost same amount of solar radiation providing similar climatic conditions during rainfall simulation experiments. Incoming solar radiation on days with rainfall was significantly affected due to presence of clouds.

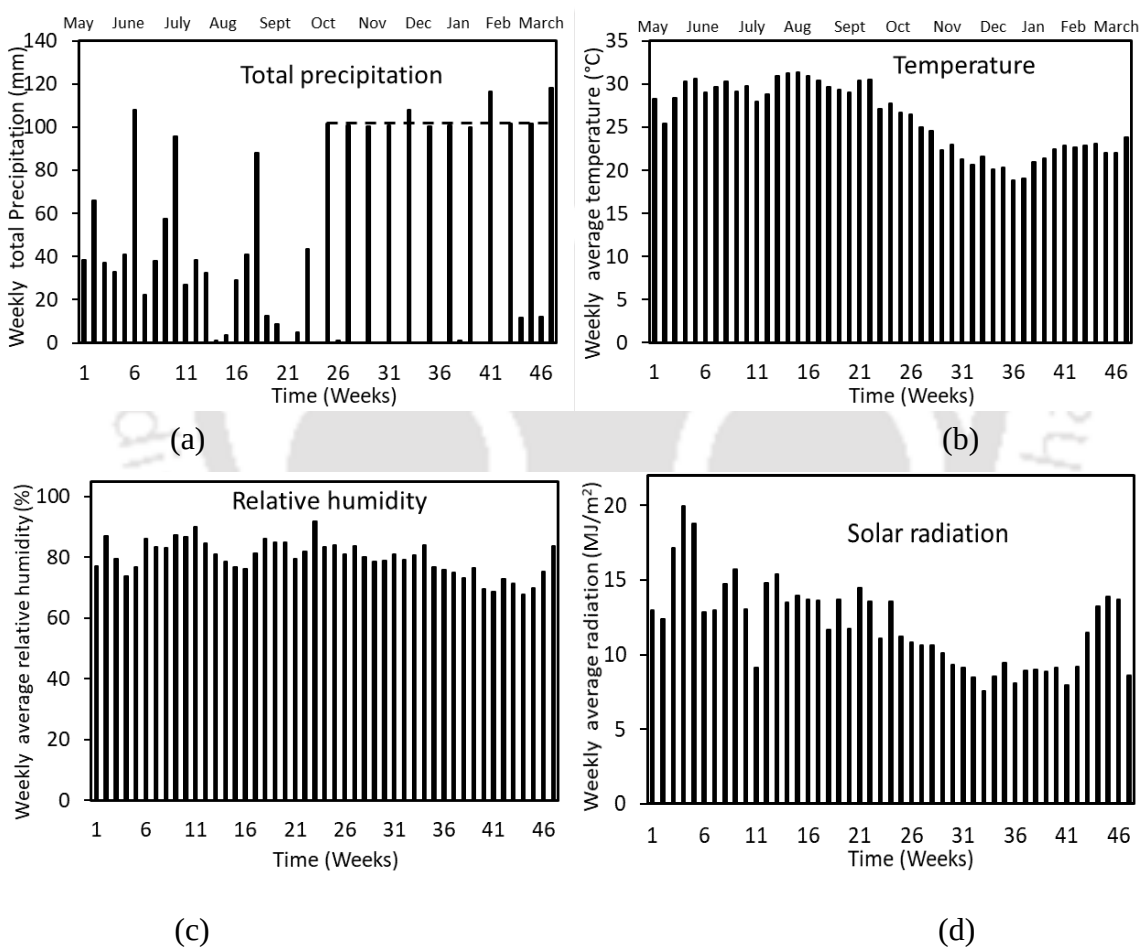

Figure 5.8 Weekly average climatic variations in the study area during the monitoring period

5.3.4 Vegetation measurements

Figure 5.9 illustrates the layout of 81 locations on surface layer of MLCS where the vegetation, infiltration, and depth of soil surface were measured. The surface area was categorized into small grids for quantifying spatial heterogeneity in vegetation growth, infiltration, and soil loss. The grid size was selected based on the initial measurements of vegetation and infiltration. Maximum area of grid size is 0.5 m × 0.125 m, that includes three monitoring locations. In case of cracks and high vegetation, number of recordings within grid was enhanced for better precision.

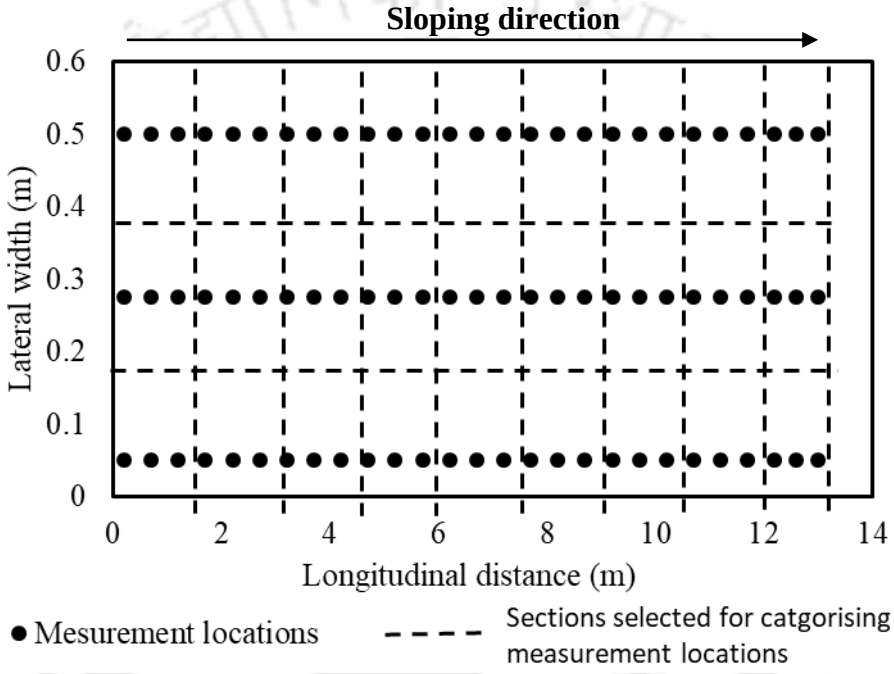

Figure 5.9 Schematic layout of measurement locations on the surface of MLCS

The vegetation percentage was evaluated using the images of nine sections (longitudinally as shown in Figure 5.9) captured using an advanced camera (NIKON D5200, Exposure time 1/4000 sec, FL-26 mm, Aperture 4.2, ISO 1000) on weekly basis. Images were analyzed using MATLAB image processing tool to evaluate the percentage of vegetated area based on the color index. The user steps involved in processing the vegetation index from images is described in Figure 5.10.

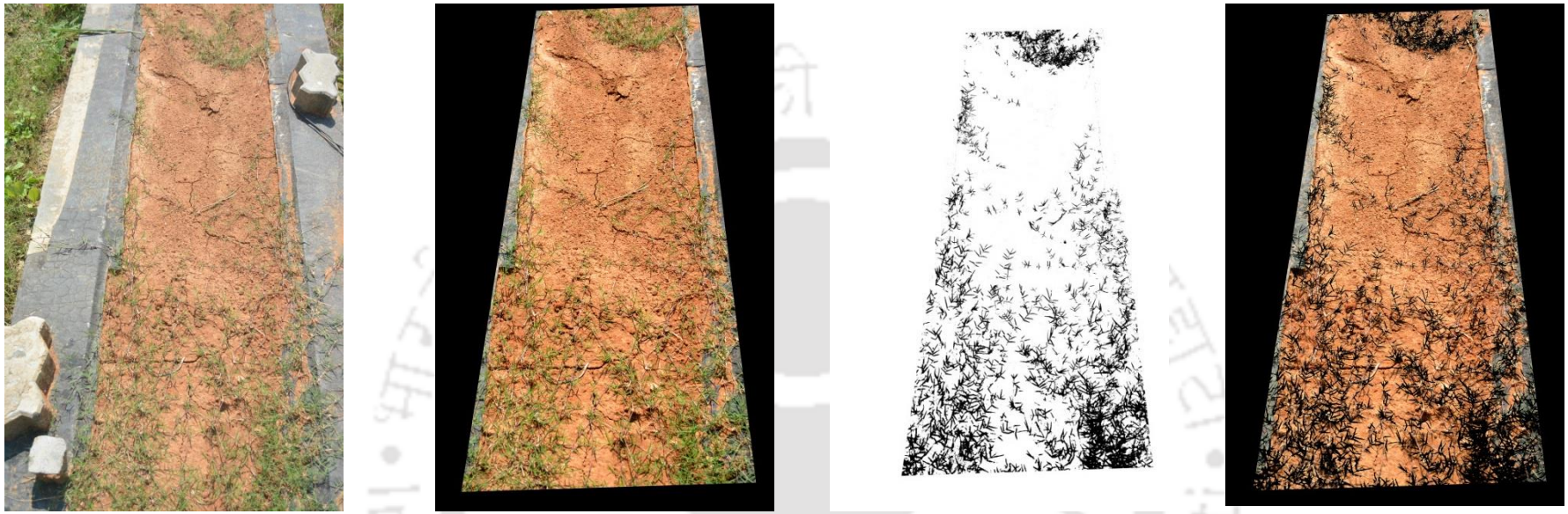

Figure 5.10 Schematic procedure for calculating vegetation index using image analysis

5.3.5 Infiltration monitoring

The infiltration in the testing locations was evaluated using Mini disk infiltrometer (Meter group inc. 2017) as shown in Figure 5.11. The monitoring and calculation method is similar to that explained earlier in section 3.4 of Chapter 3. The infiltration monitored from all 81 locations is averaged to attain infiltration rate for that week. The infiltration measurements were made before rainfall simulation for corresponding days of simulated rainfall. It was observed that desiccation cracks formed during drying tended to close with the initiation of surface erosion within 8 to 12 minutes of rainfall simulation, depending on the crack size. The time required for initiation of runoff collection varied from 5 to 10 minutes after rainfall started depending on the antecedent moisture content of the soil surface. For higher in-situ moisture contents runoff initiates quickly and vice versa.

Figure 5.11 Overview of infiltration measurement locations around crack and vegetated area

5.3.6 Erosion monitoring

Figure 5.12 depicts the eroded soil mass accumulated in the erosion collection chamber after series of rainfall events. The dry mass of soil accumulated in erosion collection chamber after series of rainfall events (natural/simulated) was measured at regular intervals of time to attain average erosion rate. Average erosion rate is calculated by taking the ratio of the amount of soil loss collected in erosion chamber and the cumulative duration of rainfall events. Further, the depth of soil surface is measured with ground surface of boundary wall as the reference datum using Vernier calipers.

Figure 5.12 Soil loss accumulated in the erosion collection chamber

5.4 Revised Universal Soil Loss Equation (RUSLE)

The Revised Universal Soil Loss Equation (RUSLE) is a spatially distributed model for estimating long-term average annual soil loss from inter-rill (sheet) and rill erosion caused by rainfall and associated overland flow. It has been recognized as the most widely used model due to its simplicity and limited data requirements. Renard et al. (1997) modified the Universal Soil Loss Equation (USLE, Wischmeier and Smith et al. 1965, 1978) to RUSLE. It computes the soil loss for a given site as the product of six major factors whose values depends on the particular study area. The annual average soil erosion rate (X) in tons per hectare year (t/ha-hr) is given by

$$X = R \,.\, K \,.\, LS \,.\, C. \, P \qquad \textbf{5.2}$$

where,

R is the rainfall–runoff erosivity factor;

K is the soil erodibility factor;

LS is the topographic factor defined as the ratio of the soil erosion amount between the actual conditions and the corresponding conditions of standard plots;

C is the vegetation cover factor;

P is the soil and water conservation factor.

5.4.1 Rainfall–runoff erosivity factor

The rainfall–runoff erosivity 'R' is the potential of a soil to be eroded due to rainfall. It is related to rainfall depth, rainfall duration, rainfall intensity, and rainfall kinetic energy. It reflects the impacts of the rainfall characteristics on soil erosion. R is the long-term annual average of the product of event rainfall kinetic energy (E) and the maximum rainfall intensity in 30 minutes (I_{30}) in mm per hour

$$R = \frac{1}{n}\left[\sum_{k=1}^{m}(E)(I_{30})_k\right] \quad \textbf{5.3}$$

where,

E is kinetic energy of rainfall;

I_{30} is the maximum rainfall intensity in 30 minutes in mm per hour;

k is the number of individual storm varying from 1 to m (total number of storm in a year);

n is the total number of years over which data has been collected.

Brown and Foster (1987) used a unit energy relationship to find the kinetic energy 'E' given by

$$E = 0.29\,[1 - 0.72\exp(-0.05\,i)] \quad \textbf{5.4}$$

where, i is the intensity in mm/hr of rainfall event.

5.4.2 Soil erodibility factor

The soil erodibility factor 'K' represents the measure of erosion that occurs during a rainfall or run off for a given type of soil. The parameter K is a complex factor describing the amount of soil detachment and transport by raindrop impact and surface flow, localized deposition due to topography, tillage-induced roughness, and rainwater infiltration into the soil profile. However, soil erodibility should be viewed as the change in the soil mass per unit area of applied external force or energy. Theoretically, erodibility is the ratio of soil loss (tons per hectare hour, t/ha h) per unit rainfall erosivity (MJ mm ha^{-1} h^{-1}). Thus, reasonable estimates of K values (t ha h/MJ mm ha) can be computed from the total soil loss per total rainfall energy (Wischmeier and Smith 1978). There are several approaches to determine soil erodibility (K) by conducting field erosion studies, scouring experiment, empirical equations using physical and chemical properties of soil, and simulated rainstorm (Song et al. 2005). Present study estimate K based on the known texture and organic carbon content of soil as given by Eq. **5.5** (Sharply and Williams 1990).

$$K = 0.1317 \times \{0.2 + 0.3\exp[-0.0256Sd(1 - Si/100)]\} \times [Si/(Ci + Si)]^2 \times \{1.0 - 0.25C/[C + \exp(3.72 - 2.9C)]\} \times \{1.0 - 0.7Sn/[Sn + \exp(-5.51 + 22.9Sn)]\} \quad \textbf{5.5}$$

where,

K is the soil erodibility factor,(t•ha•h/ (ha•MJ•mm)),

Sn=1−*Sd*/100

Sd is the percentage of sand particles (0.05–2.0 mm) content (%),

Si is the percentage of silt particles (0.002–0.05 mm) content (%),

Ci is the percentage of clay particles (<0.002 mm) content (%),

C is the percentage of soil organic carbon content (%).

5.4.3 Topographic factor 'LS'

The effect of topography on soil erosion in the RUSLE is accounted by the topographic factor LS, which is defined as the product of the slope length factor (L) and the slope steepness factor (S). The combined LS factor in RUSLE represent the ratio of soil loss on a given slope length and steepness to soil loss from a bare soil. Slope length is defined as the horizontal distance from the origin of overland flow to the point where either the slope gradient decreases enough that deposition begins or the runoff becomes concentrated in a defined channel (Wischmeier and Smith 1978). Wang et al. (2002) proposed relationship to calculate L and S as shown below

$$L = \left(\frac{\lambda}{22.13}\right)^m \quad \textbf{5.6}$$

$$S \text{ is } \begin{cases} 10.8\times \sin\acute{\emptyset} + 0.13 & \acute{\emptyset} < 9\% \\ 16.8\times \sin\acute{\emptyset} - 0.5 & 9\% < \acute{\emptyset} < 18\% \\ 21.91\times \sin\acute{\emptyset} - 0.96 & \acute{\emptyset} \geq 18\% \end{cases} \quad \textbf{5.7}$$

where,

L is the slope length factor,

λ is the slope length in meters,

m is the slope length exponent and its values are related to the slope gradient Ǿ as described below

m is 0.2 for $\acute{\emptyset} < 1\%$

0.3 for $1\% < \acute{\emptyset} < 3\%$

0.4 for $3\% < \acute{\emptyset} < 5\%$

5.4.4 Vegetation cover management factor 'C'

Vegetation cover management factor 'C' is defined as the ratio of soil loss from the land cropped under specific conditions to the corresponding loss from clean-tilled, continuous fallow land (Wischmeier and Smith 1978). Several studies assigned crop cover (vegetation cover) C factor based on land use/land cover types (Millward and Mersey 1999; Kumar and Khushwaha 2013; Durigon et al. 2014). The 'C' factor within the RUSLE is used to reflect the effect of cropping and management practices on soil erosion rates and is the factor used most often to compare the relative impacts of management options on conservation plans. Its value usually lies between 0 and 1. Yang (1999) and Cai et al. (2000) gives a relationship to determine C factor as follows

$$C = \sum_{i=1}^{12} \frac{R_i}{R} C_i \qquad \textbf{5.8}$$

C_i= 1 if c_i=0

0.658-0.3436 log(c_i) if $0 < c_i < 78.3\%$

0 if $c_i \geq 78.3\%$

where,

C_i is the monthly value of the vegetation cover-management factor;

c_i is the monthly vegetation cover (%);

C is the annual value of the vegetation cover-management factor;

R_i is the monthly value of the rainfall–runoff erosivity factor;

R is the annual value of the rainfall–runoff erosivity factor.

5.4.5 Support practice factor P

The support practice factor (P) for water conservation measures in the RUSLE is defined as the ratio of the soil loss amount for a specific soil with and without water conservation measures. Its value ranges from 0 to 1. Better the conservation practice, lesser is the value of P. For site without any water conservative practice, P has been assigned a value of 1. From the study of Cai et al. (2000) and Hong et al. (2008), the values of P for different land use types have been determined and shown in Table 5.5. Accordingly, the value of P for the current study has been considered as 0.5 (grassland).

Table 5.5 Support practice factor P for various land use types

Land use	Urban land	Farm land	Grass land	Forest land	Water land	Waste land
P	1	0.3	0.5	0.8	0	1

5.5 Results and discussion

5.5.1 Vegetation characteristics

Figure 5.13 depicts the variation in green vegetation cover on the surface layer of MLCS. From figure, it is evident that the percentage vegetation consistently increased during the testing period except in the months of January and February. This may be due to drop in photosynthetic action of grass, commonly observed in deep winter season, resulting in dry grass as shown in Figure 5.14. The drop in solar radiation during winters (as observed in Figure 5.8 (d)) strongly supports this.

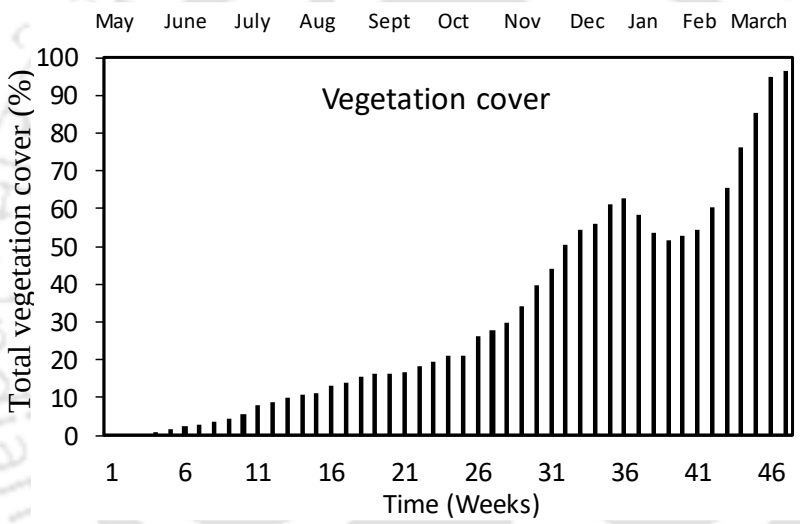

Figure 5.13 Temporal variation in percentage vegetation cover on the surface layer of MLCS

Figure 5.14 Section of surface layer with mixture of green and dry grass

5.5.2 Infiltration characteristics

The effect of seasonal variations on surface infiltration behaviour of MLCS was evaluated using mini disk infiltrometer, results of which are presented in Figure 5.15. From figure, it can be understood that the days that received low to moderate rainfall depicted significant infiltration attributed to the low in-situ water contents. In addition, the days with significant rainfall have higher water contents, which led to minimal infiltration. The months of July and August, that received low rainfall and high temperatures (as observed in Figure 5.8) have resulted in the development of cracks on its surface, which has led to multifold increase in infiltration (about 10 to 100 times) than the initial. Increase in infiltration would decrease the runoff and thereby decrease the runoff induced erosion.

From field observation it was noted that, mild cracks formed earlier during the drying spell was found to close when high intensity rainfall was simulated in the months of November and December resulting in decrease of infiltration rate. Increase in in-situ moisture contents lead to multifold decrease in infiltration rate. Further, the rates of infiltration are also observed to increase gradually to the end of test period for days of similar rainfall, likely due to increased surface vegetation. Similar observations were reported in Gadi et al. (2017) while studying hydraulic conductivity in green infrastructures. Increased vegetation also helped in reduction of desiccation cracks (visual observation), which further led to decrease in infiltration as observed in Figure 5.15.

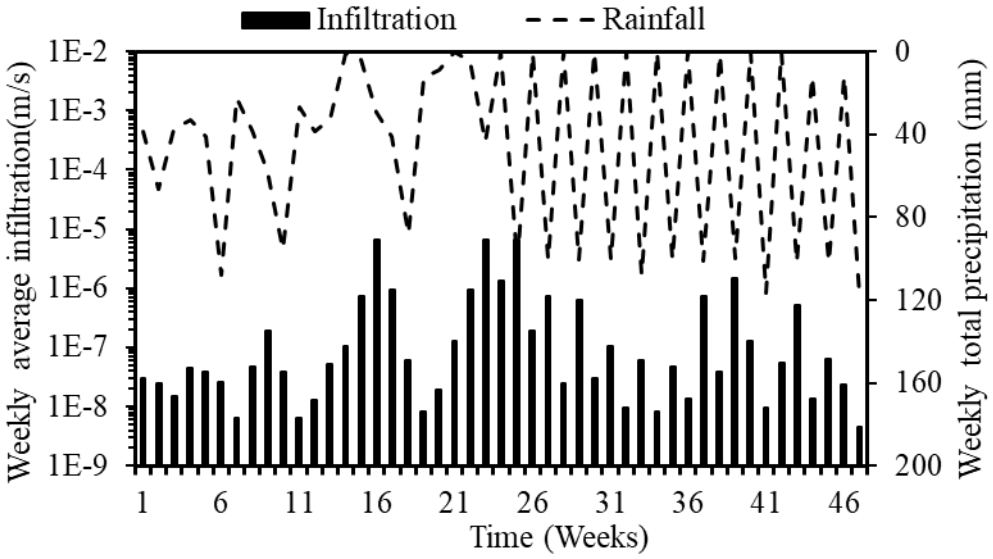

Figure 5.15 Temporal variation of weekly average infiltration against weekly total rainfall

5.5.3 Erosion characteristics

5.5.3.1 Erosion rate behaviour

Figure 5.16 details the variation in weekly erosion rate of surface layer of field MLCS. From figure, it can be clearly understood that the erosion rate is mostly effected by the rainfall behaviour. However, the effect of surface dryness is also evident in some events. For example, 16th week received similar amount of rainfall as in 17th week but resulted in higher amount of erosion indicating the increase in erosion with change in surface dryness ascertained from the temperature recordings depicted in Figure 5.8.

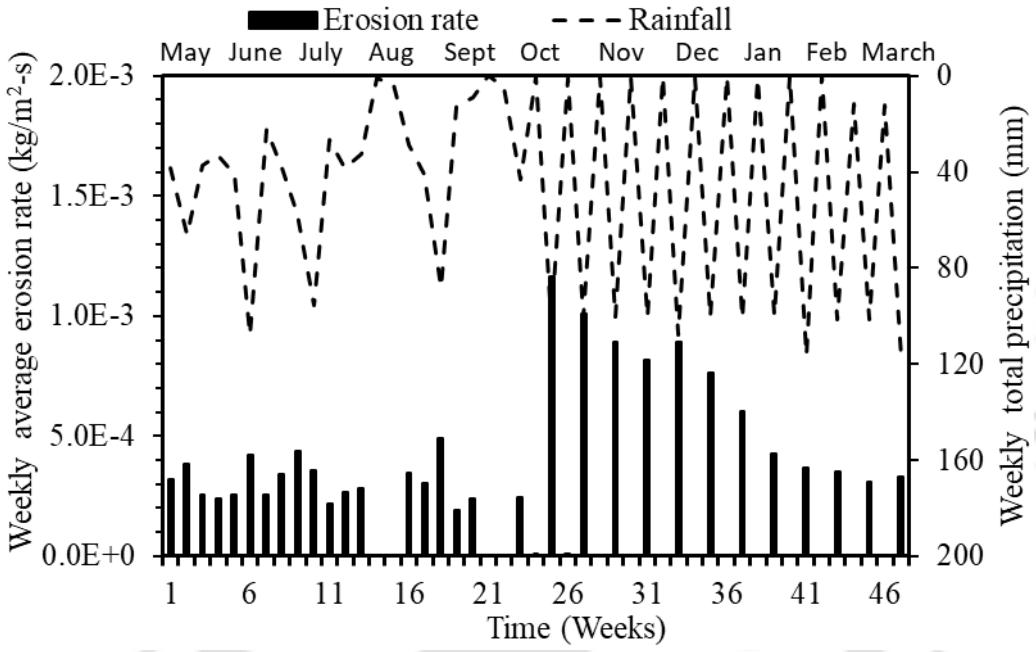

Figure 5.16 Temporal variation of weekly average erosion rate against weekly total rainfall

From figure, it is also observed that simulated rainfall of high intensity has resulted in significant amount of erosion, which however has decreased with further growth in vegetation. The drop in growth of vegetation in month of January has effected the relative decrease in erosion. Further drop in evapotranspiration in February has likely retained higher moisture within surface soil, which would have resulted in significant drop in erosion. In summary, it is understood that there is a strong interplay of vegetation, infiltration, desiccation, and erosion behaviors of surface soil, which necessitates an integrated model to consider continuous changes of these parameters on resulting erosion.

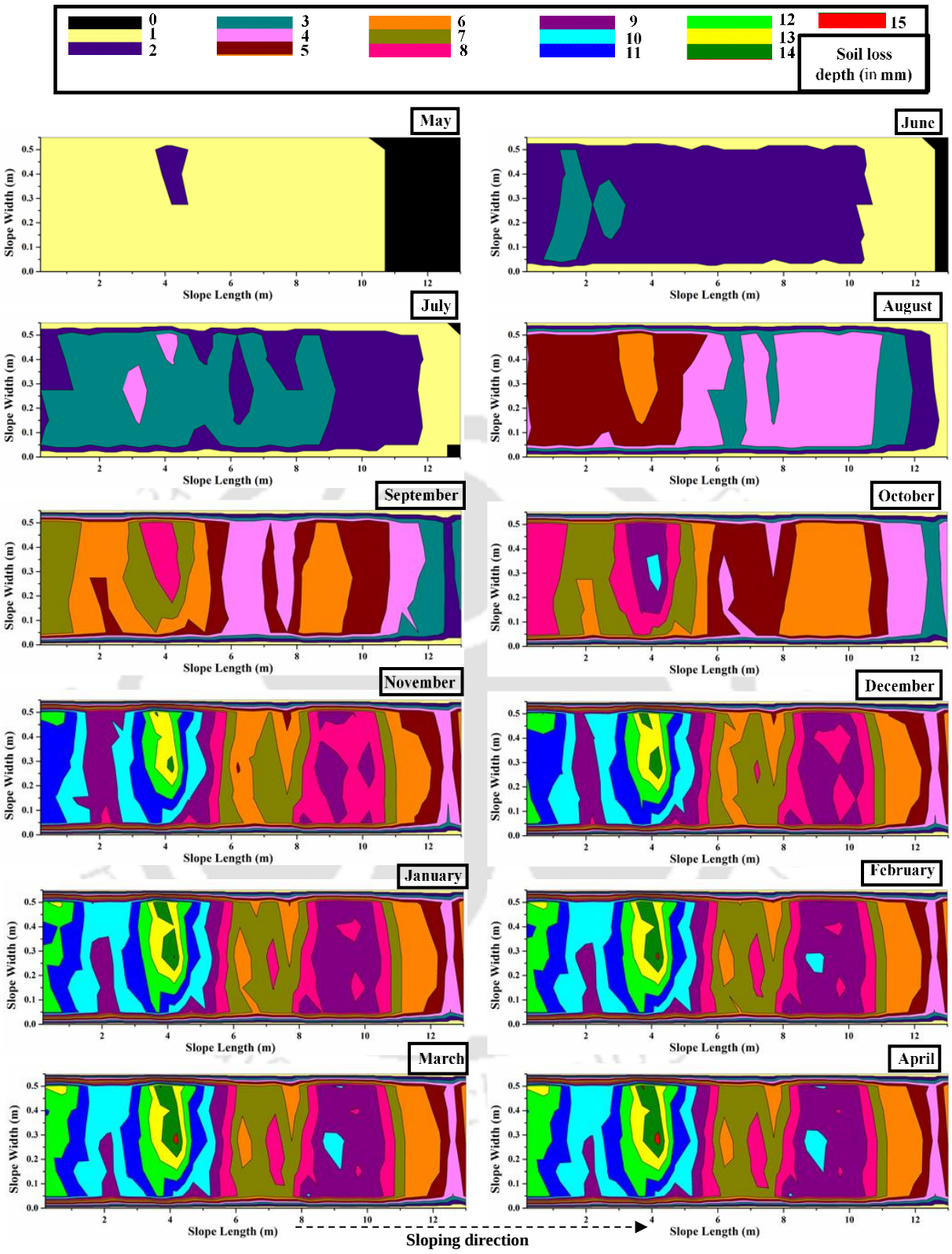

Figure 5.17 Variation in soil loss depth due to erosion for a period of 12 months

5.5.3.2 Surface erosion profile

The measurements of soil loss depth from different locations are interpolated to acquire 2D colour indexed contour profile of soil loss as illustrated in Figure 5.17. Figure indicates that the erosion is significant in the crest region and becomes minimal as it reaches toe. This could be likely due to deposition of particles rolled from the crest near the toe region, minimizing erosion. Further the width being smaller has resulted in rills of 'S' shape when the flow intersects the rigid boundaries. The central eroded portions of 'S' shaped rills are observed to possess mild vegetation as depicted in Figure 5.18, clearly indicating the influence of vegetation in resisting erosion.

However, the boundaries are not truly rigid, as the asphalt sheet provided on the masonry walls (to restrict boundary seepage) has helped in protecting the layer of soil from spill erosion thereby resulting a soil wall along the boundary. Figure 5.17 clearly depicts the reduced erosion along the boundaries.

Figure 5.17 also depicts that as the time passes the variation in soil profile within a section reduces, resulting in uniform soil profile along the slope. The increased vegetation and uniformly simulated rainfall could have influenced the uniformity in soil loss profile. The influence of vegetation on erosion rate (as described in Figure 5.16) can be demonstrated from decreased variation in erosion profile in Figure 5.17, for the months of January to April 2017.

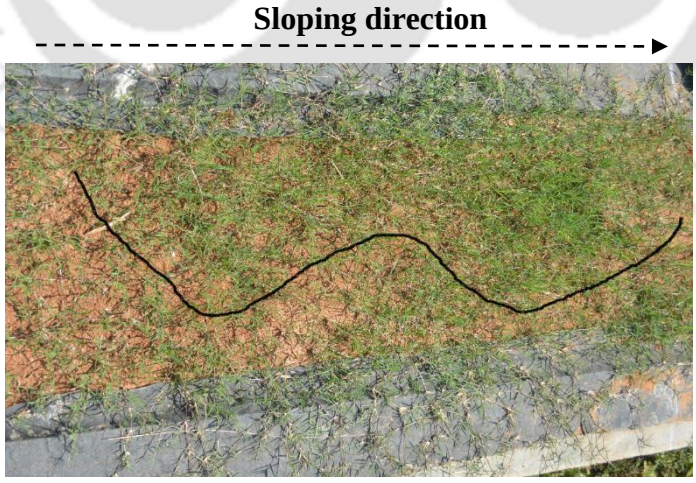

Figure 5.18 Rill profile of a section describing influence of vegetation and boundary

5.6 Soil loss estimation using RUSLE

Rainfall–runoff erosivity factor 'R' factor for each month has been evaluated by using the two formulae described in Eq. 5.3 and Eq. 5.4 and corresponding values are summarized in Table 5.6.

Table 5.6 Summary of rainfall–runoff erosivity and vegetation management factors

Month	Rainfall–runoff erosivity (R) (MJ• mm/ha•h)	Vegetation management factor C_i
May-16	1251.98	0.1105
Jun-16	1470.64	0.1019
Jul-16	2313.16	0.1435
Aug-16	430.28	0.0249
Sep-16	2010.93	0.1114
Oct-16	315.93	0.0170
Nov-16	2097.00	0.1075
Dec-16	2236.00	0.1062
Jan-17	2159.00	0.0954
Feb-17	2376.00	0.1095
Mar-17	2097.00	0.0913

Based on the grain size distribution defined in Table 5.1, surface layer red soil constitutes 25 % sand, 51 % silt, 24 % clay, and 0.5 % organic content. Accordingly using Eq. 5.5, the 'K' value is obtained to be 0.23. The 13.5m length slope at 10% gradient used in the study would result in 'LS' of 1.887 with L and S equal to 0.78 and 2.42, respectively as given by Eq. 5.6 and Eq. 5.7. The field measurements of vegetation as described in Figure 5.13 were used for determining c_i value in Eq. 5.8. Accordingly, the monthly vegetation management factor 'C_i' is calculated according to Eq. 5.8 using real field data and the results are listed in Table 5.6. Broadly, with the increase in area of vegetation, the results portray a decrease in 'C_i' i.e. as vegetation increases it would lead to decrease in corresponding soil erosion.

The RUSLE factors 'R', 'K', 'LS', 'C' and 'P' were together used to estimate the monthly soil loss according to Eq. 5.2. Corresponding results are reported in Table 5.7 along with field measured soil loss in the test plot. The efficiency of RUSLE estimation is further established by comparing the observed and estimated soil loss as depicted in Figure 5.19. The RUSLE is observed to be partly efficient in estimating the field soil loss of surface layer of MLCS with a coefficient of determination 'R^2' of 0.38, if correlated on monthly basis. However, the RUSLE model is quite acceptable in estimating cumulative annual soil loss as can be seen from the table.

Table 5.7 Observed versus estimated soil loss for surface layer of filed pilot MLCS

Month	Estimated soil loss RUSLE (kg/m^2-month)	Field observed soil loss (kg/m^2-month)
May-16	2.63	3.20
Jun-16	3.03	4.33
Jul-16	6.67	4.36
Aug-16	0.22	1.11
Sep-16	4.53	3.48
Oct-16	0.11	0.61
Nov-16	4.57	7.54
Dec-16	5.09	5.92
Jan-17	4.7	5.74
Feb-17	5.61	3.57
Mar-17	4.20	2.20
Annual soil loss	**41.36**	**42.06**

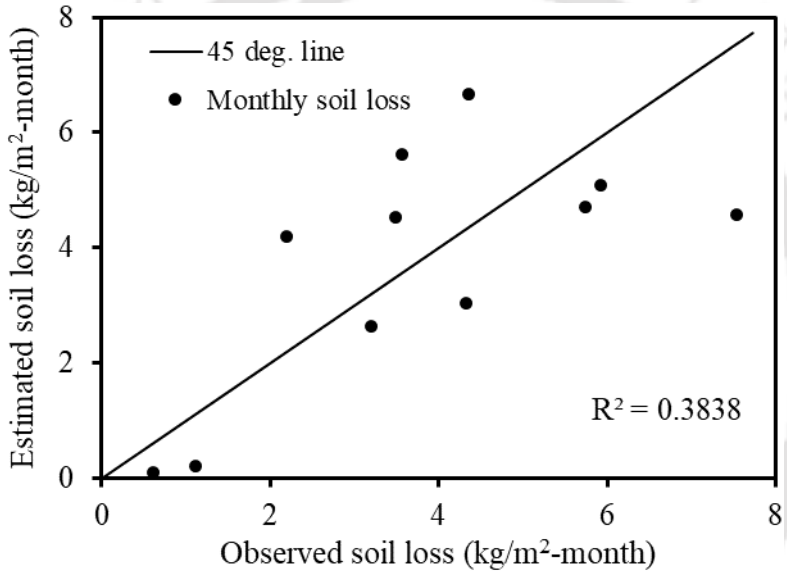

Figure 5.19 Observed versus estimated soil loss for surface layer of filed pilot MLCS

During the period of natural rainfall from May-16 to September-16, the RUSLE model shows a higher rate of soil erosion as compared to the observed soil erosion rate. This result resembles the findings of Mondal et al. (2016), which estimated the soil loss at a site in Narmada river basin. During the simulated rainfall period of intensity of the order of 100 mm/hr from November to January, the RUSLE model shows a lower rate of soil erosion than the observed soil loss rate. This can be due to the limitation of energy calculation 'E' described in Eq. 5.4, which uses the rainfall intensities up to a maximum of 72 mm/hr. The effect of rainfall higher than this intensity is not captured, leading to underestimation of cumulative soil loss. Further, it can be noted that RUSLE has

overestimated the soil loss in months of February and March, where the vegetation is on higher side.

In summary RUSLE is observed to overestimate the rain induced soil loss by about 30% in instants of high vegetation and underestimate by about 20% in high intensity rainfall conditions. Moreover, the present study is limited to a small-scale field pilot MLCS for a limited duration. Likely, this could be another reason for difference in measured and estimated soil loss. Further investigations are required to appropriate estimation of field erosion behavior by considering the scale effects, alternate estimation equations predicted in literature, etc. However, RUSLE fails in estimating temporal variation in erosion behaviour can be used conveniently for evaluating annual soil loss with errors in acceptable range.

5.7 Summary

This chapter deals with the field evaluation of surface soil layer of a pilot MLCS in terms of its erosion and infiltration under the influence of natural and simulated rainfall for a period of one year. The field-measured data were used to evaluate the efficiency of an erosion estimation model 'RUSLE'. Following are the important observations from this chapter.

1) The rate of infiltration was observed to increase during days of no rainfall due to the formation of surface desiccation cracks and low in-situ water contents. Further, the infiltration was found to decrease with partial closure of desiccation cracks and increase antecedent water contents owing to high intensity rainfall during simulated rainfall study.
2) The high erosion during simulated rainfall events decreased significantly, as the vegetation increased. Vegetation was found to have significant effect on reducing the soil loss of surface soil layer of MLCS. The study indicates the need of bioengineering for protecting the surface layer of MLCS.
3) The revised universal soil loss equation (RUSLE) gave satisfactory estimate of annual soil loss for surface soil. However, the monthly estimate of soil loss was found to be influenced by high intensity of rainfall and vegetation for which RUSLE under performed. This discrepancy gets averaged while estimating yearly soil loss.

Chapter 6

Translational slope stability analysis of MLCS

6.1 Preface

Stability and serviceability of geotechnical structures is always a key issue commonly encountered in different geotechnical structures (Stolle and Guo 2008). Multi-layered cover systems (MLCS) constructed above a shallow low-level hazardous waste disposal facility after reaching its full capacity of waste intake (USEPA 1989) is also susceptible to these issues. The MLCS include layers of soils and geosynthetics for performing specific functions such as protection, drainage, barrier, separation, and filtration (Koerner and Daniel 1997; Boulanger-Martel et al. 2015; Xie et al. 2017). MLCS are constructed with mild to moderate slope, to eliminate both ponding and rainwater ingress into the waste (Tami et al. 2004; USEPA 2015). The interfaces of different layers in MLCS are weak and prone to failure at soil-geosynthetic and geosynthetic-geosynthetic interfaces (Bussière et al. 2003; Bergado et al. 2006; Dixon et al. 2006). Numerous translational slope failures of MLCS along such interfaces are reported in the literature (Filz et al. 2001; Blight 2007; Qian and Koerner 2009). Hence, it is of utmost importance to precisely assess the translational stability of MLCS for affirming the safety of the structure (Mitchell et al. 1990; Qian and Koerner 2015).

Koerner and Hwu (1991) have formulated a systematic procedure to evaluate the translational stability of reinforced barrier system for a single layer of soil over a geosynthetic layer. In this study, the formulation developed by Koerner and Hwu has been extended for their application in MLCS of a near surface low-level radioactive waste disposal facility, anticipating multiple failure planes along the various interfaces of MLCS. The extended formulations were then used to study the stability of Resource Conservation and Recovery Act (RCRA) subtitle 'C' MLCS under different scenarios experienced during its life cycle as suggested by Koerner and Soong (2005). The RCRA subtitle 'C' cover system is selected in this study, as it should perform well under tropical wet climatic conditions with heavy rainfall and high temperatures (Landreth and Carson 1991; USEPA 2000; Dwyer 2003).

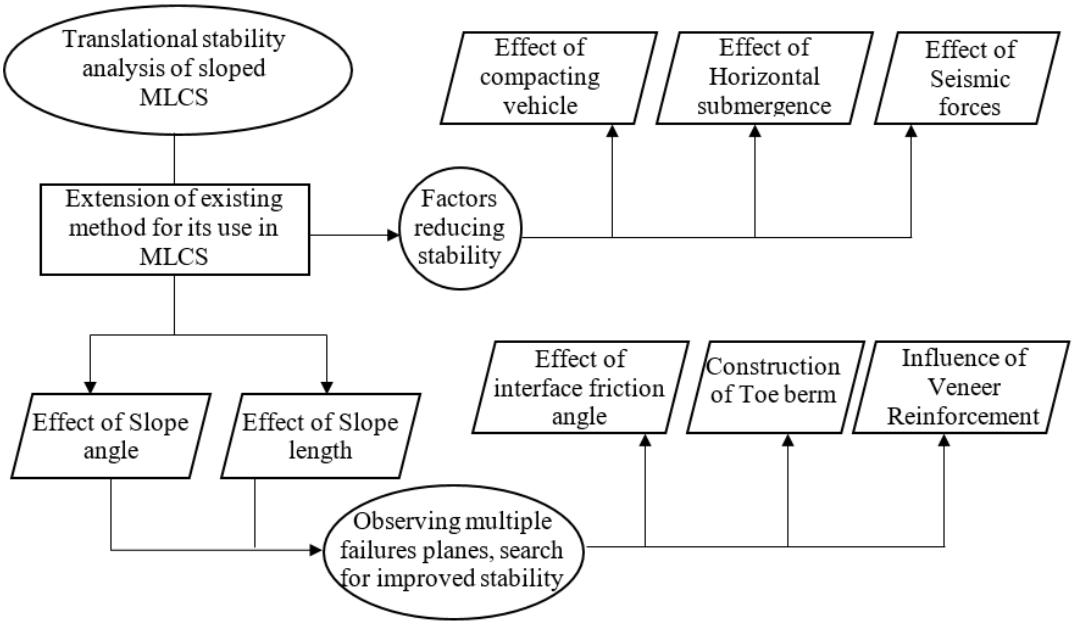

Figure 6.1 Experimental program to evaluate translation slope stability of MLCS

The complete analytical program followed for evaluating the translational stability of MLCS under different scenario is detailed in Figure 6.1. In the extended analysis, factor of safety (FoS) is determined at all the interfaces of MLCS by considering the changes in dimensions of both active and passive wedges contributing to stability. The FoS along every interface in MLCS is evaluated using extended analysis, anticipating the possibility of multiple failure planes. The stability of MLCS, influenced by slope configuration, material characteristics, and specific conditions experienced during its lifetime, has been studied. Design curves are developed for Resource Conservation and Recovery Act (RCRA) subtitle 'C' cover system under different scenarios that improve or deteriorate the stability. Suggestions for modifications in existing materials, and suitable materials to reinforce different layers, of MLCS are also reported in this study. Performance of MLCS under seepage induced by heavy rainfalls and earthquake situations is further described.

6.2 Analytical model

In this section, the analytical model developed by Koerner and Hwu (1991) for translational stability analysis of uniformly laid soil over geomembrane layer was extended for MLCS. The two-dimensional layout of the MLCS considered in this study is depicted in Figure 6.2. The major extension to the existing model is the inclusion of changes in dimensions of active wedges (A_1, A_2, ...A_n) and passive wedges (P_1, P_2, ...P_n), incorporating multiple pre-defined failure interfaces (α=1 to n), while determining FoS. This procedure enables to

understand the change in FoS for every interface, and thereby appropriately identifying the weak zone. The lengths of passive wedges (L_{p0}, L_{p1},….$L_{p(n-1)}$) and active wedges (L_{a0}, L_{a1},….$L_{a(n-1)}$) at different interfaces, as shown in Figure 6.2, are evaluated as described in Eq. 6.1 and Eq. 6.2 for all the layers (with interfaces α =1 to n).

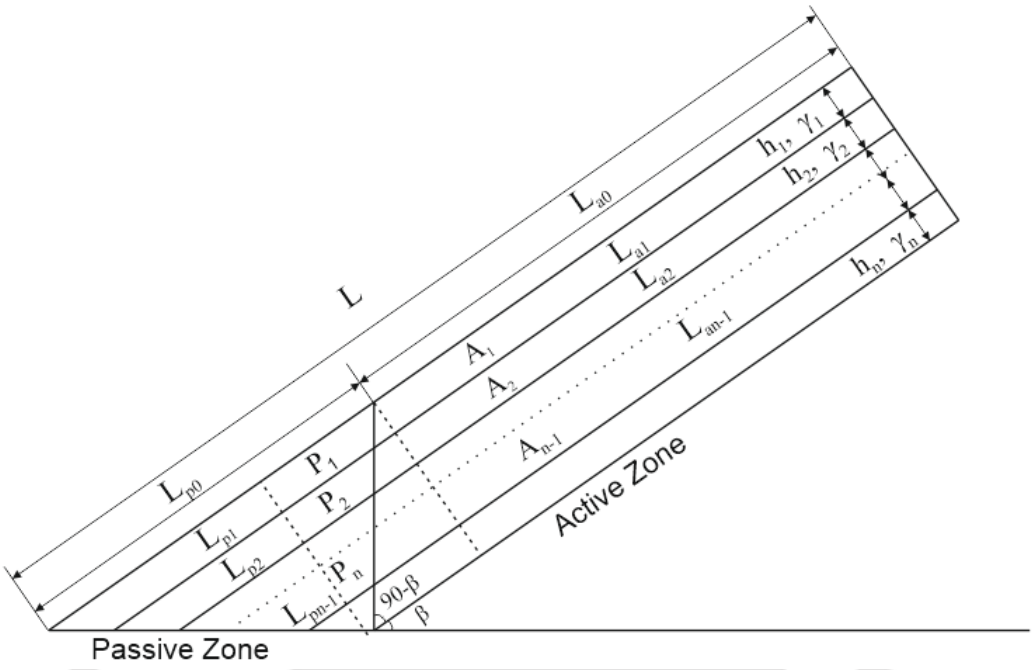

Figure 6.2 Schematic outline of multi-layered cover system (MLCS)

For interfaces α = 1 to n,

$$L_{p(\alpha-1)} = \frac{2\sum_{\alpha}^{n} h_\alpha}{\sin 2\beta} \qquad \textbf{6.1}$$

For interface α = 1,

$$L_{a(\alpha-1)} = L - L_{p(\alpha-1)} \qquad \textbf{6.2 a}$$

For other interfaces α = 2 to n,

$$L_{a(\alpha-1)} = L_{a(\alpha-2)} + h_{(\alpha-1)} \tan\beta \qquad \textbf{6.2 b}$$

Using these lengths, the areas of passive wedges (A_{p1}, A_{p2},….A_{pn}) and active wedges (A_{a1}, A_{a2}, ….A_{an}) are calculated as detailed in Eq. **6.3** for all layers (α =1 to n).

$$A_{p\alpha} = \left(L_{p(\alpha-1)} h_\alpha - \frac{h_\alpha^2}{\sin 2\beta}\right) \qquad \textbf{6.3 a}$$

$$A_{a\alpha} = \left(L_{a(\alpha-1)}h_\alpha + \frac{h_\alpha^2 \tan\beta}{2}\right) \qquad \textbf{6.3 b}$$

Knowing the geometry of active and passive wedges, the FoS for different interfaces are determined. The assumptions made in this analysis are:

i) The interface between different soil layers or soil-geosynthetic layers is a weak plane and is recognized as a pre-defined failure surface.

ii) There is no relative movement at the different overlying or underlying interfaces during slippage i.e., the movement occurs only at the pre-defined failure interface

iii) All the layers are of uniform thickness and are at the same slope angle, being parallel to one another even during and after the deformation.

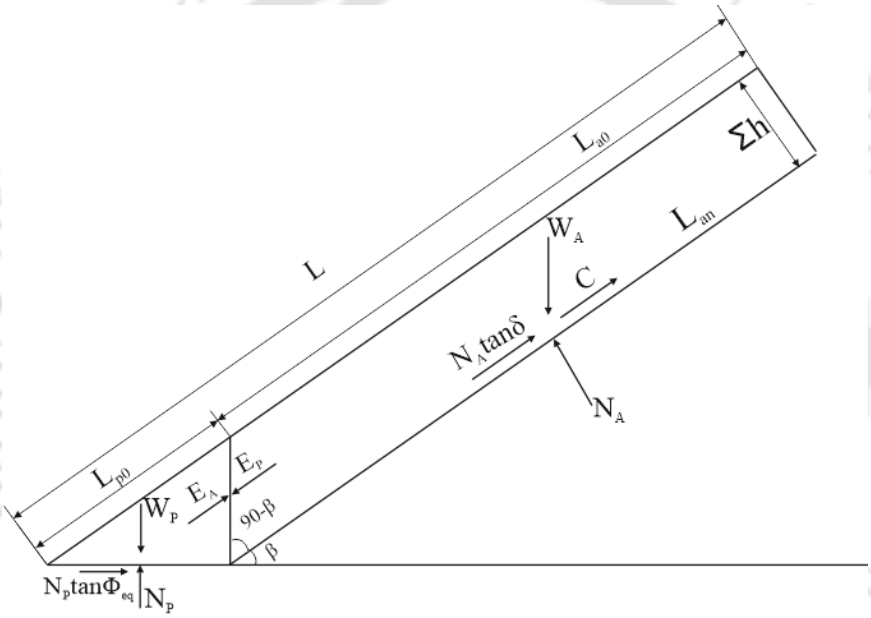

Figure 6.3 Simplified MLCS for stability analysis along the n^{th} interface

Figure 6.3 depicts the method by which different layers of MLCS above the pre-defined failure surface (any n^{th} interface) are considered as individual section. The method is adopted for all the interfaces during the analysis, to avoid the relative movement between the different layers during failure, according to the second assumption. The weights of active wedges (W_{A1}, W_{A2}, ...W_{An}) and passive wedges (W_{P1}, W_{P2}, ...W_{Pn}) are evaluated using Eq. 6.4 for all the layers, using their corresponding unit weights (γ_1, γ_2, ...γ_n).

$$W_{A\alpha} = (A_{a1}\gamma_1 + A_{a2}\gamma_2 + ------ + A_{a\alpha}\gamma_\alpha) \qquad \textbf{6.4 a}$$

$$W_{P\alpha} = (A_{p1}\gamma_1 + A_{p2}\gamma_2 + ------ + A_{p\alpha}\gamma_\alpha) \qquad \textbf{6.4 b}$$

These weights are then resolved into normal and tangential forces acting on the sliding plane. The normal force acting on active and passive wedge is given in Eq. 6.5. The determination of resisting force along the base of passive wedge is complex, since it includes the interaction of each layer with the corresponding base soil layer, as shown in Figure 6.4. It can be noted that the materials of each layer in passive wedge would interact with the base soil layer resulting in interactions I_1, I_2,.....I_n. Each interaction would have different resisting properties ϕ_1, ϕ_2.....,ϕ_n; which would lead to rigorous and complex equations for solution. To avoid such complexities, the combined resistance offered by all interactions at any n^{th} interface is represented by an equivalent resisting interface friction angle (ϕ_{eq}), as described in Eq. 6.6.

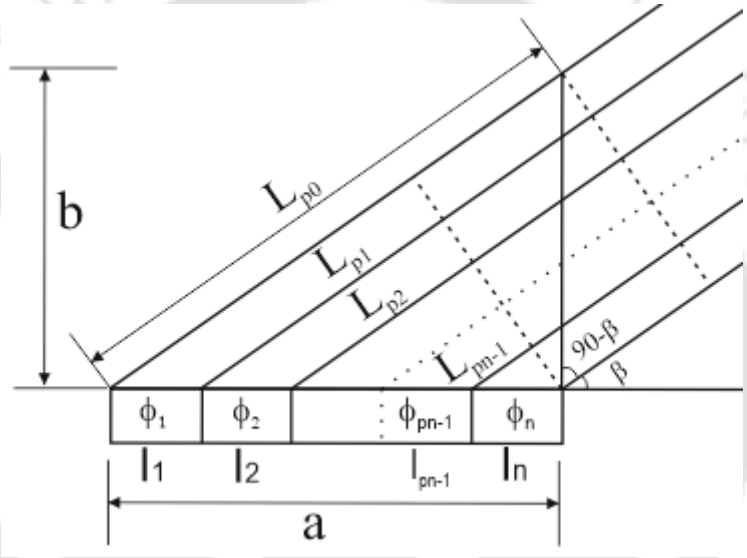

Figure 6.4 Interactions of MLCS at the base of the passive wedge

$$N_A = W_A \cos\beta \qquad \textbf{6.5 a}$$

$$N_P = W_p \cos\beta \qquad \textbf{6.5 b}$$

$$N_p \tan\phi_{eq} = \frac{N_p}{W_p} \sum_{1}^{n} \frac{(L_{p(\alpha-1)} + L_{p\alpha}) h_\alpha \tan(\phi_\alpha) \gamma_\alpha}{2\sin\beta} \qquad \textbf{6.6}$$

Finally, the FoS at n^{th} interface is evaluated similar to Koerner and Hwu (1991), from the roots of quadratic equation as described below

$$aFoS^2 + bFoS + c = 0 \qquad \textbf{6.7}$$

where,

$$a = (W_A - N_A \cos\beta)\cos\beta \qquad \textbf{6.8 a}$$

$$b = -[(W_A - N_A \cos\beta)\sin\beta\tan\phi_{eq} + (N_A \tan\delta + C_a)\sin\beta\cos\beta + (C + W_p \tan\phi_{eq})\sin\beta] \quad \textbf{6.8 b}$$

$$c = (N_A \tan\delta + C_a)\sin^2\beta\tan\phi_{eq} \quad \textbf{6.8 c}$$

The Factor of Safety (FoS) will be expressed as

$$FoS = \frac{-b \pm \sqrt{b^2 - 4ac}}{2a} \quad \textbf{6.9}$$

6.3 Analysis of critical FoS for cover system

In the present analysis, the critical failure plane of RCRA subtitle 'C' cover system is evaluated using the extended equations described in the earlier section. The low-level radioactive waste has a huge potential to cause moderate radiation and contamination in surroundings, and, hence, is initially encapsulated in concrete, and for added protection, sealed with a MLCS. The multiple layers of the cover system selected for the analysis is shown in Figure 6.5. The shear and interface shear characteristics of MLCS materials required for slope stability analysis were respectively determined using direct shear and modified direct shear tests, the results of which are summarized in Table 6.1.

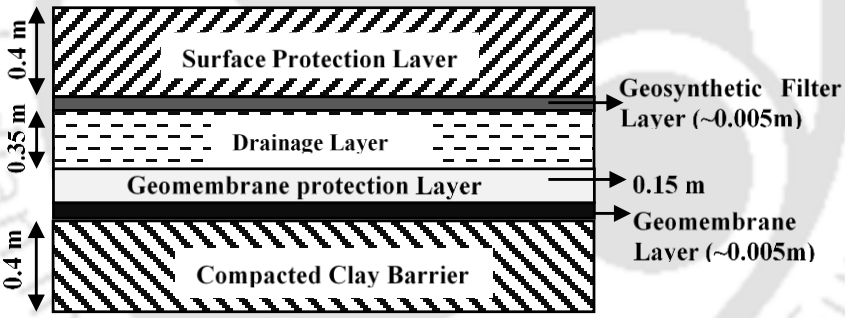

Figure 6.5 Typical configuration of RCRA subtitle C cover system

Table 6.1 Details of different interfaces in multi-layered cover system (MLCS)

Interface	Upper component	Unit weight γ (kN/m^3)	Friction angle	Lower component	Interface friction angle	Cohesion/ adhesion (kPa)
***n*=1**	Red soil	16.68	14.2°	Geotextile	12º	14
***n*=2**	Geotextile	6.50	-	Aggregate	9 º	-
***n*=3**	Aggregate	13.16	29.5°	Sand	22 º	-
***n*=4**	Sand	14.58	26.9°	Geomembrane	17 º	-
***n*=5**	Geomembrane	2.20	-	Bentonite	20 º	29

A locally available lateritic red soil was used as surface protection layer, to shield the bottom layers from direct interaction with atmospheric variants. Immediately beneath

surface protection layer, a geosynthetic filter layer is provided to prevent piping of fines from the overlying surface soil. Together, red soil-geosynthetic interface forms the first preferential failure plane (n=1). The stability analysis of this layer has relatively greater significance, owing to its direct interaction with atmospheric variants. In continuation, a drainage layer made of coarse aggregate is made to divert the rainwater infiltrated from surface layers. The geosynthetic-aggregate interface (n=2) can result in weak bond owing to lower contact area and the same is evident from low interface friction angle, as can be seen in Table 6.1. Coarse sand can also be adopted for drainage layer, however considering significantly heavy rainfalls in tropical region; aggregate is adopted for drainage layer. The aggregates in drainage layer might puncture the geomembrane placed underneath, and hence, to avoid such a scenario, a thin layer of river sand is sandwiched between them. The thin layer of sand would result in aggregate-sand (n=3) and sand-geomembrane (n=4) interfaces. Marginal thickness of sand may sometimes lead to critical failure emerging in between these layers, and thus, to avoid such circumstance, an optimum thickness needs to be adopted. A minimum thickness, twice the maximum size of aggregate in drainage layer, is commonly adopted to avoid puncture of geosynthetic surface present underneath. Finally, a thick layer of compacted clay is provided below the geomembrane as a conventional hydraulic barrier acting as the bottom layer preventing interaction of the waste with the atmosphere. The geomembrane-bentonite interface (n=5) becomes the final probable failure interface as considered in this analysis. All the materials selected in this study satisfy the permeability requirements of 40CFR258.60 (2002).

6.4 Effect of slope inclination

USEPA (2015) recommends a mild slope inclination 'tan (β)' of 3-7 % for the surface cover system. However, under certain circumstances, due to excess waste storage or unavailability of land, the slope inclination can be as high as 30% as reported in the literature (Seed et al. 1990; Di Trapani et al. 2013). Therefore, the FoS is evaluated for three different slope inclinations viz. 10%, 20% and 30%, which corresponds to slope angles 5.7°, 11.3° and 16.7°, respectively. In this analysis, the length of the outer face 'L' is considered as 30 m. The effect of the change in slope on the variation in FoS for different interfaces is presented in Figure 6.6. As expected, it can be noted that the FoS of various interfaces decreased with an increase in slope angle. The sensitivity of slope angle on FoS was found to be more prominent for mild slopes as compared to the steeper ones. This is likely due to the relative increase in proportion of normal forces against active and passive

wedges in steeper slopes in comparison to the same obtained for mild slopes. Such a trend was found to be reported by Michalowski (1995) obtained from translational failure analysis of sloped embankment using kinematic approach.

Based on the present analysis, the critical failure plane is identified as the geotextile-aggregate interface (n=2) overlying the drainage layer, and is subscribed as the weakest interface. However, in addition, the sand-geomembrane interface (n=4) also failed to satisfy the minimum requirement of FoS>1.5 for a 30% slope. This observation clearly brings out the importance of the stability analysis to be mandatorily conducted for all the interface layers for identifying multiple failure planes of MLCS, rather than limiting to the determination of a single interface. Similar observations were made by Qian and Koerner (2015) for multi-layered liner system.

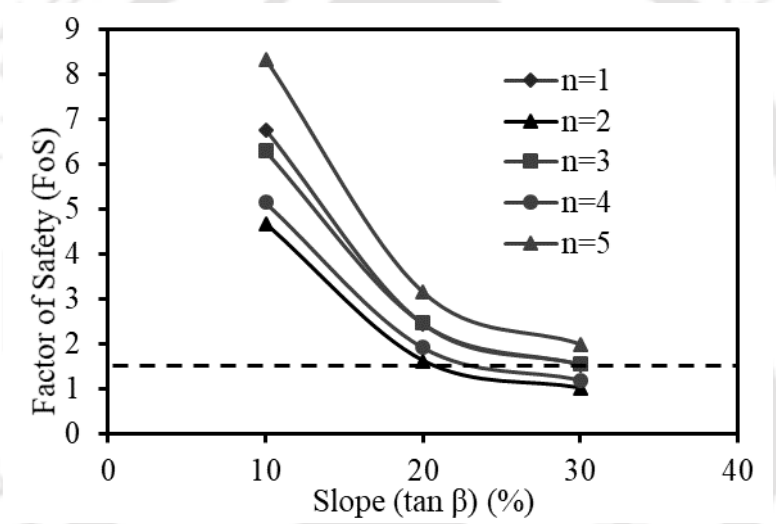

Figure 6.6 Design curves for FoS of MLCS with change in slope

6.5 Effect of length of MLCS

It may be noted in the earlier section that the influence of length of the slope '*L*' on FoS is not explicit. Therefore, effort was made to determine the variation of FoS with varying '*L*' for different interfaces of MLCS corresponding to maximum slope angle (30%), the results of which are presented in Figure 6.7. It can be observed that the FoS is significantly affected in small sections rather than in the longer ones. This is likely attributed to the increase in the weight of active wedge due to change in '*L*', contributing to the destabilization. In the small sections, the increase of length in active wedge would significantly destabilize the resistance offered by passive wedge. On the other hand, in the larger sections, the increase in length would show relatively equal contribution to active and passive forces (passive

forces formed due to the normal component acting against slope increases equally with that of active forces). In addition, change in '*L*' has shown minimal effect on the FoS of the interfaces comprising of cohesionless soils (*n*=3, 4). Further, as the length increased beyond 30 m, multiple interfaces (*n*=1, 2, 3, 4) are observed to fail (FoS<1.5), suggesting the necessity for adopting measures to substantially improve the stability of MLCS.

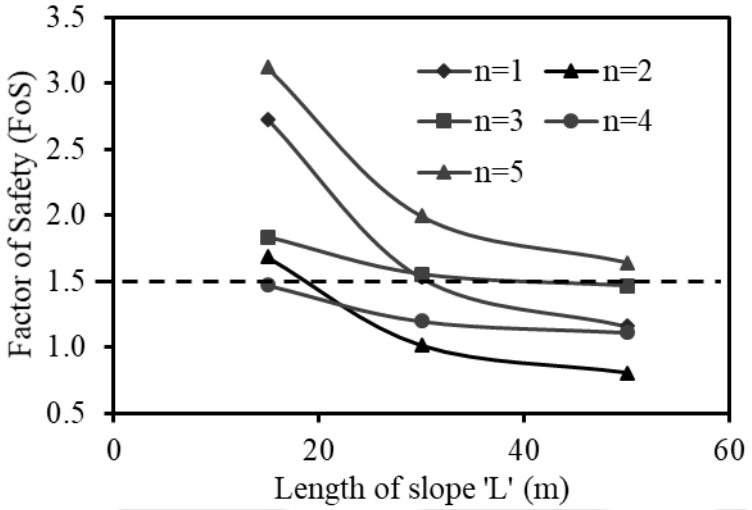

Figure 6.7 Design curves for FoS of MLCS with change in slope length

6.6 Alternate methods for enhancing stability of MLCS

The different possible ways of improving the stability of cover design may include the use of improved materials, construction of a toe berm or buttress, by constructing tapered cover system or by intentional veneer reinforcement (Koerner and Soong 2005). The method of analysis would remain same as adopted in the present study; however, the formulations are required to be modified for including the changes in the loading patterns imposed by modifications, which may lead to the alteration of FoS. This has been investigated and discussed below.

6.6.1 Effect of interface friction angle (Use of improved materials)

The interface friction angle of every interfaces in the selected RCRA cover system was varied by a possible range on either side of the experimentally determined values. The possible range of variation is selected based on the probable range of interface strength reported in the literature that used similar materials (Koutsourais et al. 1991; Dixon et al. 2006; Dixon 2010; Qian and Koerner 2015). The configuration of slope is considered same as in previous section with slope 30% and length 30 m. Figure 6.8 details the variation in FoS of different interfaces with change in interface friction angle of corresponding

interfaces. It can be observed that interfaces '*n*=2' and '*n*=4' are required to have interface friction angles of 17.5° and 21.5°, respectively, to form a stable slope of 30 m length at 30% inclination. The remaining interfaces are observed to satisfy the minimum requisite (FoS>1.5) with the existing and chosen interface friction angles. These observations help to make a decision about the proper choice of the materials required for the overall stability of the MLCS, especially when weak interfaces are encountered.

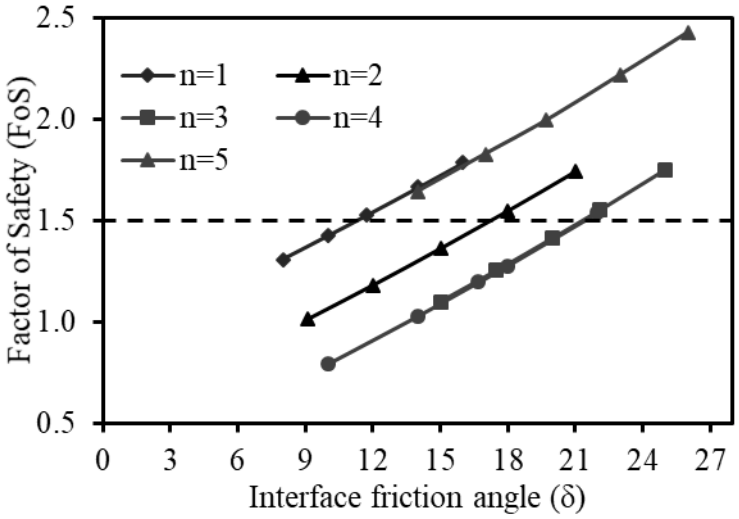

Figure 6.8 Design curves for FoS of MLCS with change in interface shear strength

6.6.2 Construction of toe-berm

In case of berm/buttress construction, there exist two different cases based on the extent of berm being constructed: (1) The extent of berm limited to passive zone and (2) the berm extending beyond passive wedge. Improper design of berm may lead to more critical stability issues in comparison to that generated by the original cover. The additional parameters defined in this section are the horizontal extent of the berm '*x*', vertical extent of berm '*y*' and unit weight of berm 'γ_b', as shown in Figure 6.9.

For incorporating the modifications induced by berm construction, Eq. 6.5 is modified as shown in Eq. 6.10 and Eq. 6.11. Eq. 6.10 represents the case for which the berm is constructed within passive zone, while 6.11 represents the case where berm is extended beyond the passive zone. The calculation of FoS follows the earlier procedure as described for Eq. 6.7, Eq. 6.8, Eq. 6.9.

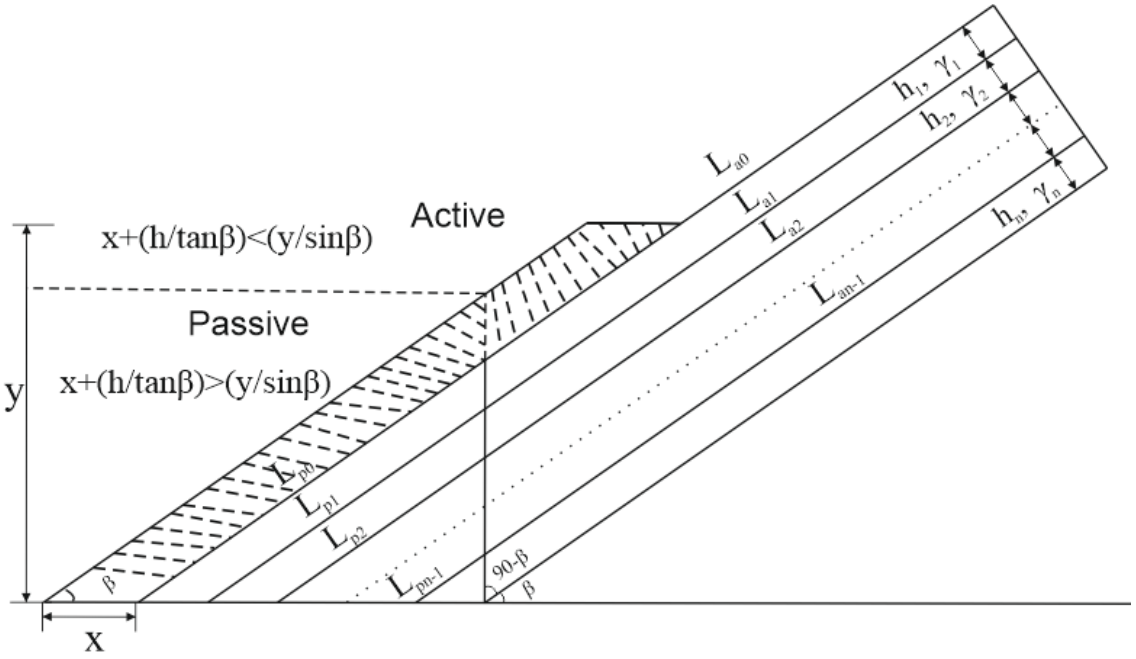

Figure 6.9 Stability enhancement of MLCS using toe berm installation

The weight of active and passive wedge, when a toe berm is introduced, are represented by

For $x+\frac{\sum h}{\sin\beta} > \frac{y}{\tan\beta}$

$$W_A = (A_{a1}\gamma_1 + A_{a2}\gamma_2 + ------ + A_{an}\gamma_n) \quad \textbf{6.10 a}$$

$$W_p = (A_{p1}\gamma_1 + A_{p2}\gamma_2 + ------ + A_{pn}\gamma_n) + (xy)\gamma_b \quad \textbf{6.10 b}$$

For $x+\frac{\sum h}{\sin\beta} \leq \frac{y}{\tan\beta}$

$$W_A = (A_{a1}\gamma_1 + A_{a2}\gamma_2 + ------ + A_{an}\gamma_n) + (xy - xL_{p0}\sin\beta - x^2\tan\beta)\gamma_b \quad \textbf{6.11 a}$$

$$W_p = (A_{p1}\gamma_1 + A_{p2}\gamma_2 + ------ + A_{pn}\gamma_n) + (xL_{p0}\sin\beta + x^2\tan\beta)\gamma_b \quad \textbf{6.11 b}$$

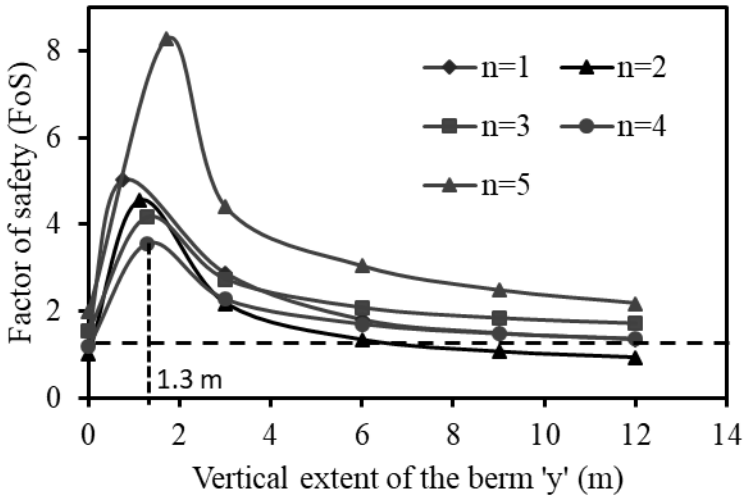

Figure 6.10 Design curves for FoS of MLCS using toe berm of unit width at various vertical extents

Figure 6.10 details the variation in FoS of different interfaces with varying vertical extent '*y*' of the berm, having unit base width (*x*=1 m). It can be observed that the FoS increases till the berm lies within passive zone, and then tend to decrease as the extent of the berm enters active zone. The FoS value reaches an asymptote, where further extension of berm would contribute equally in the generation of the active and passive forces. It can be observed that the initiation of decrease in FoS for different interfaces occurs at different extents of '*y*'. This re-confirms the effect of change in length of passive zone with the change in interface of MLCS on the overall FoS. From Figure 6.10, it is clearly evident that for the fourth interface i.e., sand-geomembrane interface, the reversal point has the lower FoS corresponding to a vertical extent of 1.3 m. Construction of berm beyond this extent would jeopardize safety of structure.

Figure 6.11 summarizes the variation of FoS of first interface (i.e. red soil-geotextile interface) of MLCS with the change in vertical extent using berms of different widths. The results portray a marginal sensitivity towards width of berm on FoS as compared to the effect of vertical extent, which indicates construction of berms beyond unit width would not provide any added benefit on the stability, and hence would be uneconomical. Hence, it is suggested to construct toe berm of unit width within passive zone for an appropriate enhancement in the stability of a MLCS.

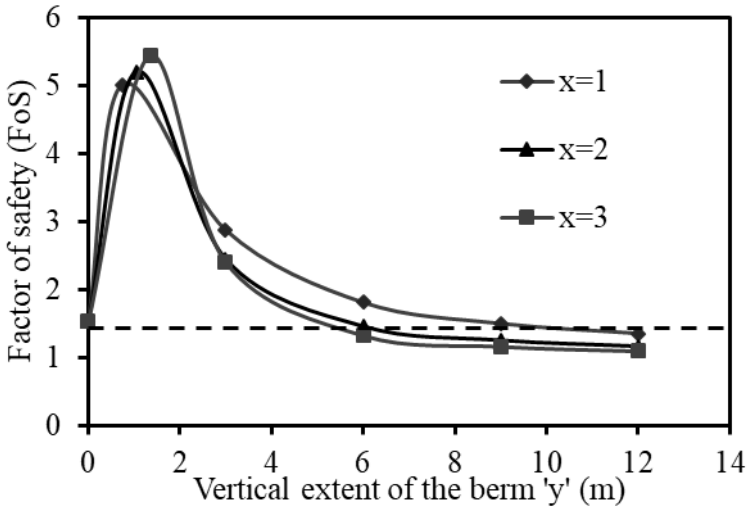

Figure 6.11 Design curves for FoS of first interface in MLCS using toe berms of various width

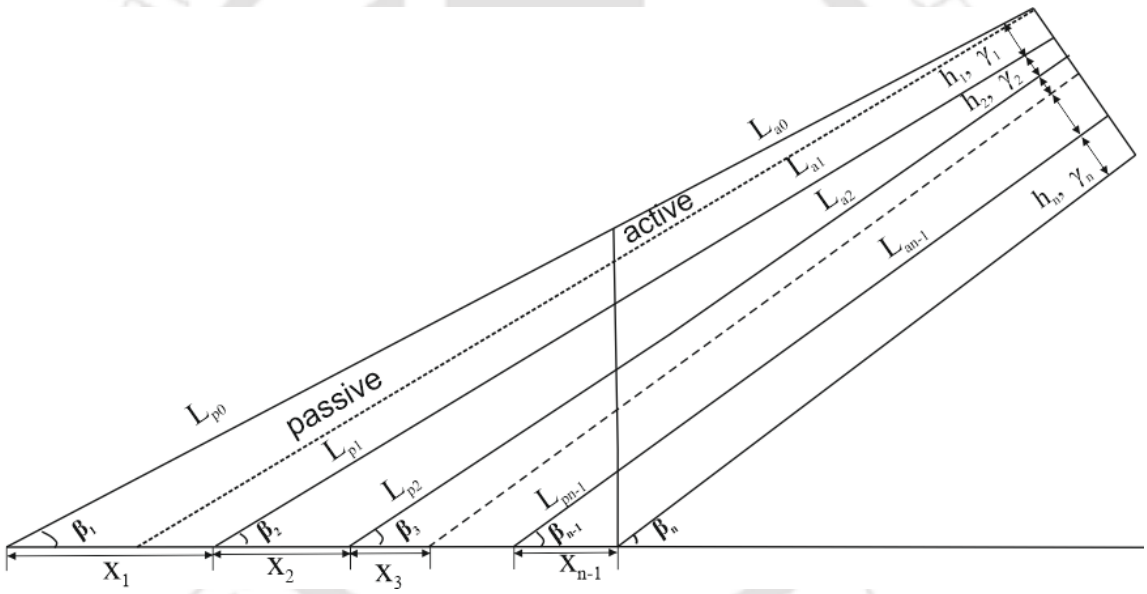

Figure 6.12 Multi-layered cover system with tapered layers from toe to crest to enhance stability

Alternatively, the stability of cover system can be improved by constructing a tapered cover system (Zhang et al. 2012), a method by which the base width of passive wedge is increased without altering the thickness of the layer at the crest. However, in case of MLCS the sloping angle of every layer changes with the amount of tapering of individual layers, as seen in Figure 6.12. The tapering of multiple layers would predominantly increase the complexity in construction and would be impractical to adopt. Henceforth, stability analysis of tapered cover system is not detailed in this study. Instead, it is suggested to

solely taper the critical layer of MLCS and go for case specific analysis as detailed in Koerner and Soong (2005).

6.6.3 Influence of veneer reinforcement on stability of MLCS

The simple and the most superior method of different improvement techniques is to provide additional veneer reinforcement such as geogrid, geocell, high capacity geotextile, or geomembrane for enhancing the stability (Carroll and Curtis 1991; Bouazza and Gassner 2005; Yu and Bathurst 2016).The important consideration in this method is to select the type of reinforcement based on the cover layer to be improved; improper selection would enhance the destabilization of MLCS (Christopher 1991; Koerner 2013). The reinforcing systems best suited for enhancing the stability of selected MLCS are shown in Figure 6.13. It includes geotextile/geogrid reinforcement in surface soil (Bhowmik et al. 2016); high-strength well-permeable geotextile above drainage layer (Luettich et al. 1992); composite geosynthetic drainage alongside conventional drainage (Paulson 2013); geosynthetic clay liner and composite geomembrane with enhanced surface roughness in barriers (Meer and Benson 2007). The reinforcing system is relatively more efficient in large-scale landfill cover systems. Eq. 6.8 were modified by incorporating the tensile strength of reinforcement, as shown in Eq. 6.12.

$$a = (W_A - N_A \cos\beta - T\sin\beta)\cos\beta \quad \textbf{6.12 a}$$

$$b = -[(W_A - N_A \cos\beta - T\sin\beta)\sin\beta\tan\phi_{eq} + (N_A \tan\delta + C_a)\sin\beta\cos\beta + (C + W_P \tan\phi_{eq})\sin\beta] \quad \textbf{6.12 b}$$

$$c = (N_A \tan\delta + C_A)\sin^2\beta\tan\phi_{eq} \quad \textbf{6.12 c}$$

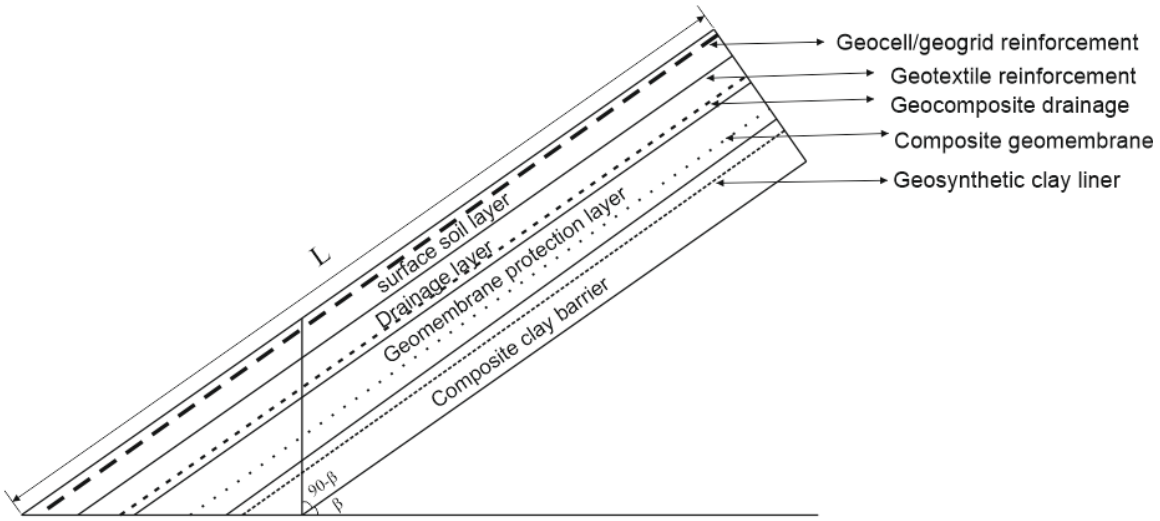

Figure 6.13 Best suited reinforcing systems for selected MLCS configuration

Considering the unavoidable degradation associated with the geosynthetics through its life cycle, a set-of reduction factors have been introduced to reduce the ultimate strength (T_{ult}) of reinforcing material as described in Eq. 6.13. The reduction factors in the strength modification equation include reduction factor for installation damage (RF_{ID}); reduction factor for creep (RF_{CR}); and reduction factor for chemical/biological degradation (RF_{CBD}), the cumulative effect would result in allowable value of reinforcing strength (T_{allow}). It is always suggested to use T_{allow} instead of T_{ult} in Eq. 6.13 to attain optimum FoS (Koerner and Daniel 1997).

$$T_{allow} = \frac{T_{ult}}{RF_{ID} \times RF_{CR} \times RF_{CBD}} \qquad \textbf{6.13}$$

Figure 6.14 describes the variation of FoS with the change in allowable tensile capacity of reinforcements in different layers of MLCS. It is evident that the stability is increased with the enhancement in the tensile capacity of reinforcement. Similar observations were witnessed by Koerner and Soong (2005). However, with the increase in the depth of reinforcement (location beneath the free surface), the amount of improvement is observed to decrease. This is likely due to the increased loads on the deeper layers, and thus, the increased demand resulting in a decrease in the amount of improvement.

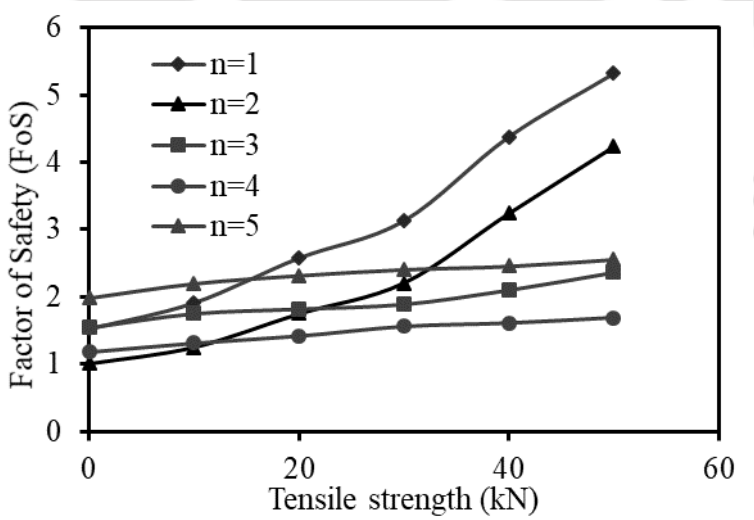

Figure 6.14 Design curves for FoS of MLCS with change in tensile strength of reinforcements

6.7 Factors leading to the reduction in slope stability of MLCS

This section deals with the factors negatively affecting the stability of MLCS. The additional situations considered for stability analysis are: a) Upward movement of

compacting vehicle from toe to crest, b) Downward movement of compacting vehicle from crest to toe, c) seepage forces (Horizontal submergence) and d) Seismic forces. The modifications in the analytical procedure made to consider these situations and their effect on FoS are explicitly detailed in this part of study.

6.7.1 Upward movement of compacting vehicle

The analysis of MLCS while a compacting vehicle is moving upwards along the MLCS slope will be similar and in continuation with the method developed by Koerner and Soong (2005). To evaluate the effect of vehicle movement on the stability of MLCS, a compaction equipment of weight 'W_b' = 72 kN; length 'l' = 1.2 m; and width 'w' = 0.5 m is considered moving upward at constant speed, as shown in Figure 6.15. The equivalent equipment force per unit width on an interface 'W_e', as included in Eq. 6.14 a, would depend on uniformly distributed vehicle load 'q' (Eq. 6.14 b) and the influence factor 'I', defined by Poulous and Davis (1974), as described in Eq. 6.14 c. According to the second assumption, irrespective of location of the vehicle in a given zone (active or passive), the weight of the vehicle is distributed uniformly ('q') along the whole area of the zone in consideration, as described by Eq. 6.14 b. The influence factor 'I' has been rephrased in this analysis to include the thickness of multiple layers, as described in Eq. 6.14 c. The equivalent weight of the vehicle moving on the sloped MLCS is expressed as

$$W_e = qlI \qquad \textbf{6.14 a}$$

where,

$$q = W_b / (2wl) \qquad \textbf{6.14 b}$$

$$I = \left(\frac{w}{\sum h} \right) \qquad \textbf{6.14 c}$$

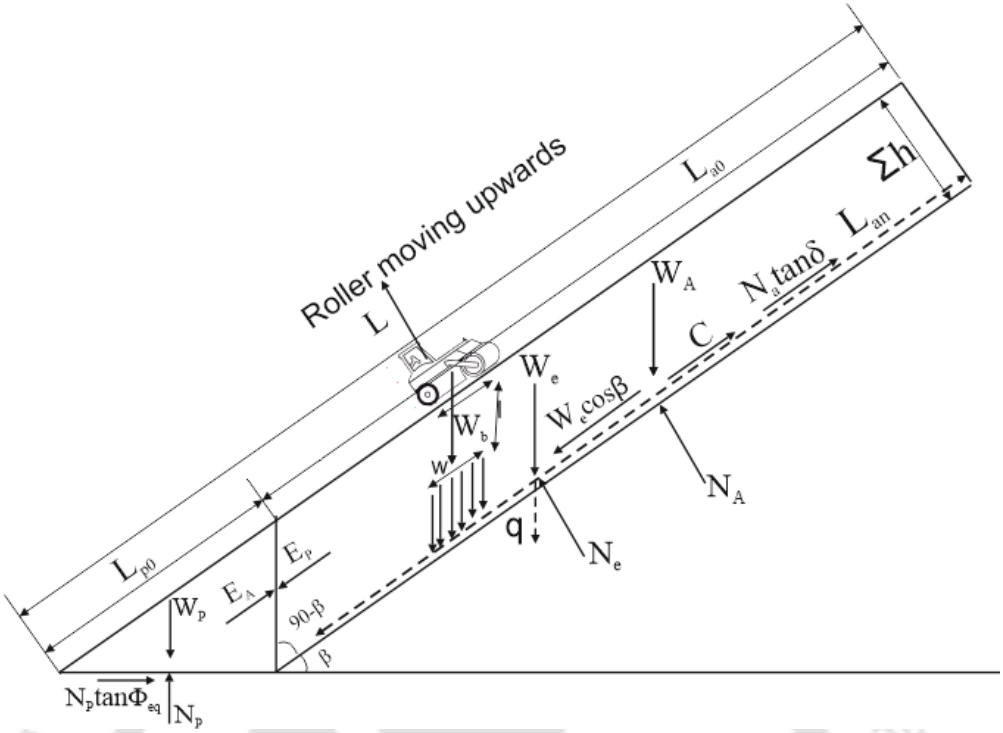

Figure 6.15 Force distribution for compacting vehicle ascending the slope

Upon determining the equipment forces 'W_e', according to Eq. 6.14 a, the FoS of MLCS is determined according to Eq.6.15 and Eq.6.16, similar to Eq. 6.8 described in the earlier section. The equations for FoS gets altered depending on the position of vehicle. The different equations for the vehicle located in the passive and active zone, signify the importance of the vehicle position in determining the FoS of MLCS, unlike Koerner and Soong (2005) where the stability analysis was limited to the active zone.

$H < \sum h \cos\beta$

$$a = (W_A - N_A \cos\beta)\cos\beta \qquad \textbf{6.15 a}$$

$$b = -[(W_A - N_A \cos\beta)\sin\beta \tan\phi_{eq} + (N_A \tan\delta + C_a)\sin\beta\cos\beta + \{C + (W_P + W_e)\tan\phi_{eq}\}\sin\beta] \qquad \textbf{6.15 b}$$

$$c = (N_A \tan\delta + C_A)\sin^2\beta \tan\phi_{eq} \qquad \textbf{6.15 c}$$

$H \geq \sum h \cos\beta$

$$a = [(W_A + W_e) - (N_A + N_e)\cos\beta]\cos\beta \qquad \textbf{6.16 a}$$

$$b = -[\{(W_A + W_e) - (N_A + N_e)\cos\beta\}\sin\beta\tan\phi_{eq} + \{(N_A + N_e)\tan\delta + C_a\}\sin\beta\cos\beta + (C + W_P \tan\phi_{eq})\sin\beta] \qquad \textbf{6.16 b}$$

$$c = [(N_A + N_e)\tan\delta + C_A]\sin^2\beta\tan\phi_{eq} \qquad \textbf{6.16 c}$$

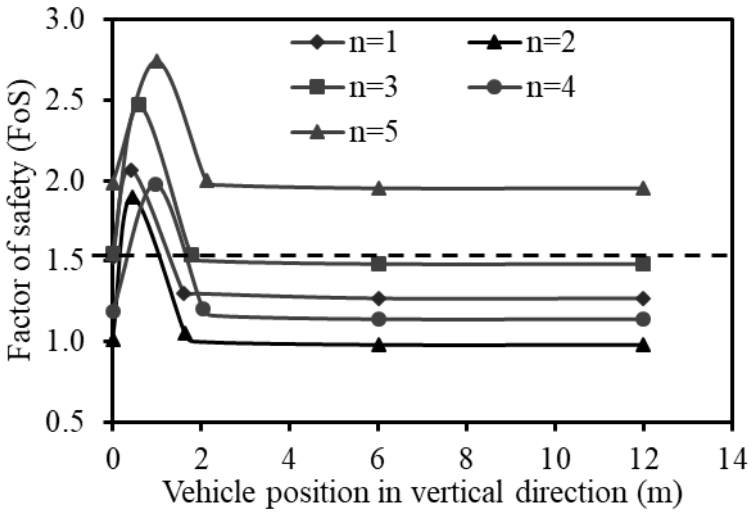

Figure 6.16 Design curves for FoS of MLCS while compacting vehicle is ascending the slope

Figure 6.16 details the variation in FoS for different positions of vehicle moving upward along the slope. It can be observed that the second interface is the most critical exhibiting minimal FoS, followed by first, third and fourth interfaces having FoS<1.5. This suggests that utmost care needs to be adopted during compaction of MLCS. Possibly the compactive efforts may be reduced or improved materials may be used in cover construction to avoid failure due to an ascending vehicle. Further, it is also observed that there is no change in FoS of the MLCS as the vehicle completely enters the active zone, which is due to the uniform distribution of vehicle weight along the whole area. Similar observations are evident in the outcome reported by Koerner and Soong (2005).

6.7.2 Downward movement of compacting vehicle

Vehicle moving downward is more unsafe to slope stability and not preferred (Koerner and Soong 2005). The vehicle tries to gain an additional acceleration while moving downward in contrary to its upward motion. Application of brakes to reduce the speed will cause abrupt traction loads that are highly detrimental to slope stability. For understanding the stability in this case, the configuration of vehicle is assumed same as in previous section. In addition, an acceleration component (a_c) is included in the descending vehicle (induced by gravitational force 'g'), which is included in terms of a fraction of gravity 'a_c=0.30g' in Eq. 6.17 a. Hence, the lateral component of the force increases by a component of 'F_e' that can be determined using Eq. 6.17 a, and corresponding normal component 'N_e' using Eq. 6.17 b. The additional force gained by the acceleration of the vehicle is given by

$$F_e = W_e\left(\frac{a_c}{g}\right) \quad \textbf{6.17 a}$$

$$N_e = W_e \cos\beta \quad \textbf{6.17 b}$$

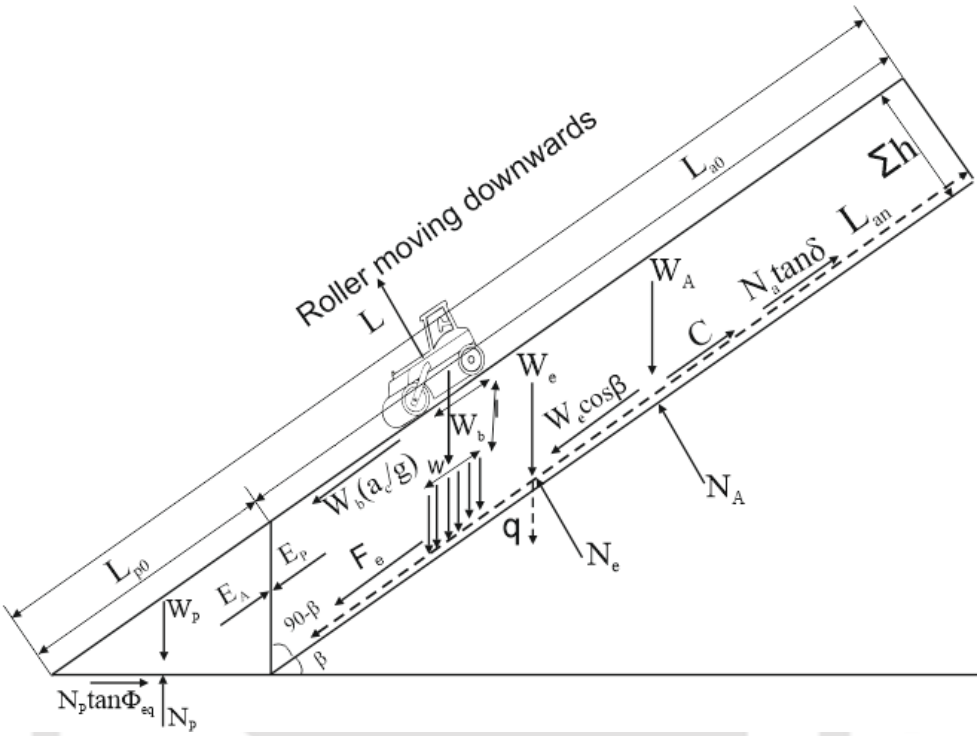

Figure 6.17 Force distribution for compacting vehicle descending the slope

This additional force component always acts in the driving direction, trying to destabilize the slope system, as shown in Figure 6.17. However, the vertical component of the equipment would enhance the stability as the vehicle enters the passive zone. The expression for determining FoS for this condition is described in Eq. 6.18 and Eq. 6.19, similar to Eq. 6.8. Upon calculating the amount of forces generated in different directions, the FoS of MLCS as the vehicle moves downwards of the slope is determined by

$H < \sum h \cos\beta$

$$a = (W_A \sin\beta + F_e)\cos\beta \quad \textbf{6.18 a}$$

$$b = -[(N_A \tan\delta + C_a)\cos\beta + (W_A \sin\beta + F_e)\sin\beta \tan\phi_{eq} + \{C + (W_P + W_e)\tan\phi_{eq}\}] \quad \textbf{6.18 b}$$

$$c = (N_A \tan\delta + C_a)\sin\beta \tan\phi_{eq} \quad \textbf{6.18 c}$$

$H \geq \sum h \cos\beta$

$$a = [(W_A + W_e)\sin\beta + F_e]\cos\beta \quad \textbf{6.19 a}$$

$$b = -[\{(N_A + N_e)\tan\delta + C_a\}\cos\beta + \{(W_A + W_e)\sin\beta + F_e\}\sin\beta \tan\phi_{eq} + (C + W_P \tan\phi_{eq})] \quad \textbf{6.19 b}$$

$$c = [(N_A + \mathrm{N}_e)\tan\delta + C_a]\sin\beta\tan\phi_{eq} \qquad \textbf{6.19 c}$$

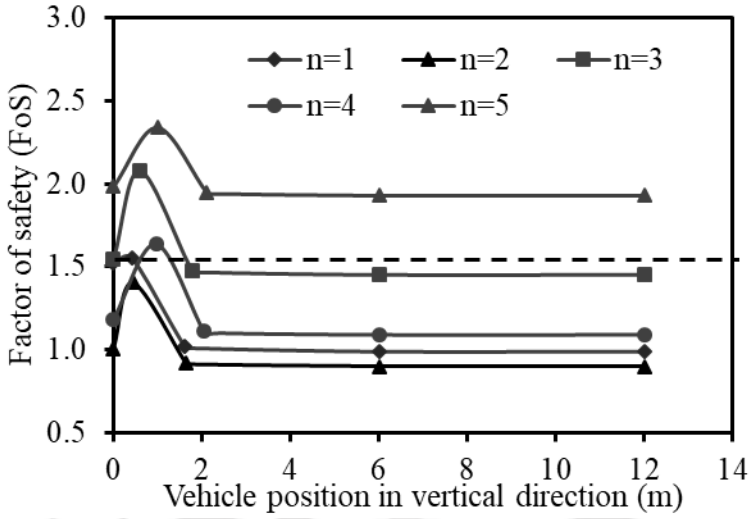

Figure 6.18 Design curves for FoS of MLCS while compacting vehicle is descending the slope

Figure 6.18 describes the change in FoS as the vehicle descends along the slope. It can be observed that the reduction of FoS at every interface is higher, as compared to that observed in the previous section on an ascending vehicle. Similar decrease in FoS with the change in direction of vehicular movement is reported in Koerner and Soong (2005). From Figure 6.16 and Figure 6.18, it can be understood that compacting passive zone would be relatively safer than active zone. Hence, higher compactive efforts can be utilized in passive zone and thereby achieve relatively higher densities in passive wedge, which in turn, would increase both the weight of passive wedge and the frictional strength of the soil present in passive zone. The angle of frictional resistance of a soil increases with increase in density (Bolton 1986). Combined increase in the weight and frictional resistance would augment FoS of particular interface layer in MLCS. (Zhang et al. 1998) In such circumstances, ample care should be taken to satisfy the permeability requirements of cover layers.

6.7.3 Seepage forces (horizontal submergence)

Tropical locations like India receive extensive monsoons in rainy seasons. At times, a rainfall depth of 1 m had been recorded in a single day (Bohra et al. 2006). Such occurrences would likely create a horizontal submergence of cover system. This part of study deals with analysis of horizontally submerged cover systems. Alternatively, in arid and semi-arid locations having low capacity or improper drainage, the layers of MLCS could sometimes get affected by parallel submergence as detailed in Koerner and Soong

(2005); which is hardly expected in tropics, and hence is avoided in this study. The correction for submergence is merely made by limiting the unit weight of submerged material to saturated unit weight (γ_{sat}) and the rest is considered dry; the heterogeneity in strength and saturation is not included in the analysis. Additional parameters like depth of submergence 'H_w' and vertical height of the slope 'H' are included to define horizontal submergence ratio, as described in Figure 6.19. The weights of active and passive wedge after submergence are calculated using subsequent Eq. 6.20.

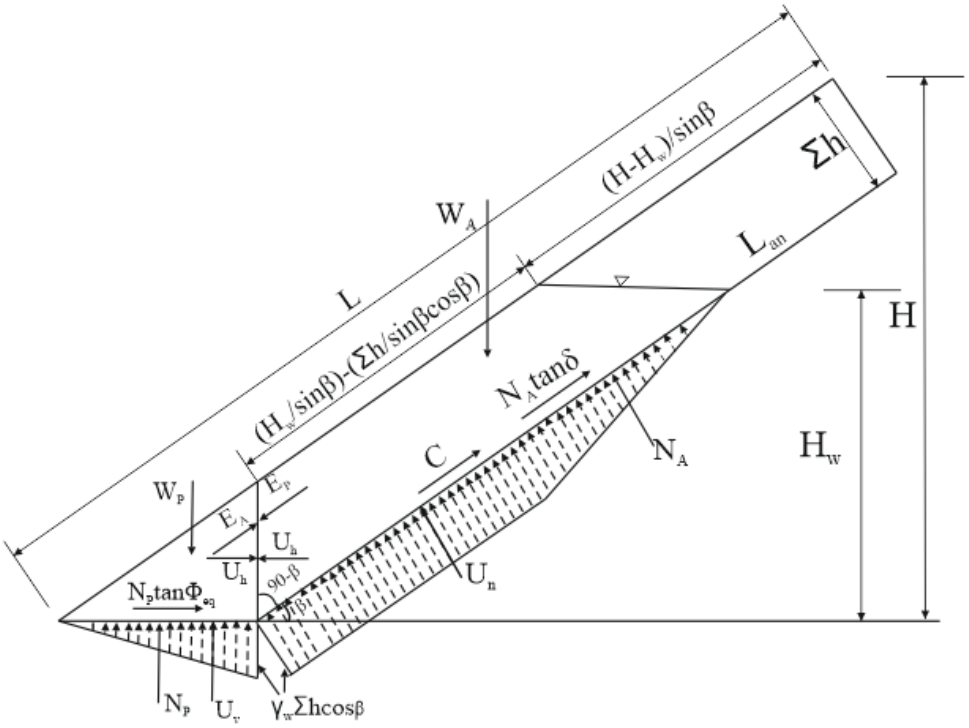

Figure 6.19 Force distribution during horizontal submergence of slope

$$W_{pn} = A_{pn}\gamma_{sat} \qquad \textbf{6.20 a}$$

$$W_{an} = \left(\frac{H_w h_n}{\sin\beta} - A_{pn}\right)\gamma_{sat} + \left(L_{a(n-1)}h_n + A_{pn} - \frac{H_w h_n}{\sin\beta}\right)\gamma_{dry} \qquad \textbf{6.20 b}$$

$$N_{An} = W_{an}\sin\beta + U_h \sin\beta - U_n \qquad \textbf{6.20 c}$$

The pore pressures at various locations, as detailed in Figure 6.19, are expressed as

$$U_h = \frac{\gamma_w \Sigma h^2}{2} \qquad \textbf{6.21 a}$$

$$U_v = U_h \cot\beta \qquad \textbf{6.21 b}$$

$$U_n = \frac{\gamma_w \Sigma h \cos\beta (2H_w \cos\beta - \Sigma h)}{\sin 2\beta} \qquad \textbf{6.21 c}$$

Analysis for FoS at n^{th} layer (Eq. 6.22) are defined similar to that described in Koerner and Soong (2005).

$$a = (W_A \sin\beta \cos\beta - U_h \cos^2\beta + U_h) \quad \textbf{6.22 a}$$

$$b = -W_A \sin^2\beta \tan\phi_{eq} + U_h \cos\beta \sin\beta \tan\phi_{eq} - (N_A \tan\delta + C_a)\cos\beta + (C + W_p - U_v)\tan\phi_{eq} \quad \textbf{6.22 b}$$

$$c = N_A \tan\delta \sin\beta \tan\phi_{eq} \quad \textbf{6.22 c}$$

To understand the effect of horizontal submergence on stability of MLCS, different horizontal submergence ratios are assumed. The configuration of MLCS and their strength characteristics are assumed the same as elucidated in previous sections (30% slope with outer length 30 m). Table 6.2 summarizes the variation in FoS of different layers of MLCS with the increase in horizontal submergence ratio (HSR). It can be observed that the FoS gradually increased till complete submergence of passive wedge is attained, followed by a significant decrease, up to an extent of near destabilization, and further followed by a near-asymptotic trend. Until complete submergence of passive wedge is achieved, the FoS increases since the passive resistance increases without any change in the weights of active wedges. In addition, it is assumed that there is no change in strength of MLCS with the change in saturation. The results portray the catastrophic failure of multiple interface layers expected during the hypothetical situation of complete submergence. Nevertheless, the MLCS considered for the present study is observed to be stable at HSR 0.18, i.e. a horizontal submergence height (H_w) of 1.62 m, which would outperform in case of 1 m rainfall recorded earlier (Bohra et al. 2006). Beyond HSR 0.18, there would be significant drop in FoS of first interface, followed by the progressive reduction at other layers, as detailed in Table 6.2. Similar observations were made by Koerner and Soong (2005) and Zhang et al. (2012) in seepage induced stability analysis of partially submerged cover systems.

Table 6.2 Variation in FoS of MLCS with change in horizontal submergence ratio

Interface	HSR=0	HSR=0.18	HSR=0.25	HSR=0.41	HSR=0.42	HSR=0.6	HSR=1
	H_w=0m	H_w=1.62m	H_w=2.25m	H_w=3.7m	H_w=3.8m	H_w=5.4m	H_w=9m
***n*=1**	1.52	3.96	0.95	0.92	0.92	0.89	0.83
***n*=2**	1.01	1.93	2.68	0.48	0.48	0.45	0.42
***n*=3**	1.54	2.40	3.34	5.48	1.20	1.18	1.15
***n*=4**	1.19	1.88	2.61	4.28	4.38	0.81	0.75
***n*=5**	1.98	2.04	2.69	4.41	4.52	6.45	1.36

6.7.4 Seismic forces

More than 50% landmass of India is vulnerable to earthquakes as per seismic zonation map given in IS 1893-1 (2002). Considering importance of landfills in India, the stability analysis of MLCS is extended by including anticipated pseudo-static horizontal earth pressures for various seismic intensities. The stability analysis is similar to the method explained in Koerner and Soong (2005). The manner in which seismic forces are accounted in the MLCS is represented in Figure 6.20. The existing method of calculating seismic forces is extended for multiple layers of MLCS, and thus, Eq. 6.8 are modified to Eq. 6.23 for the determination of the FoS.

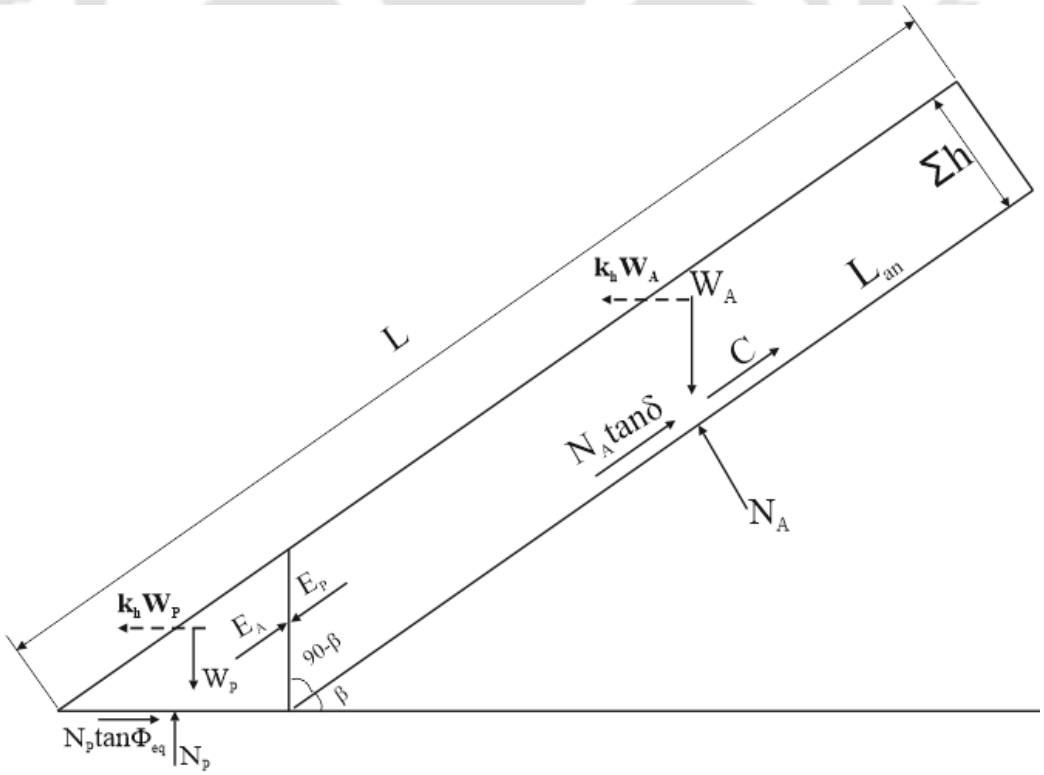

Figure 6.20 Force distribution for pseudo-static stability analysis

$$a = (k_h W_A + k_h W_p + N_A \sin\beta)\cos\beta \quad \textbf{6.23 a}$$

$$b = -[(k_h W_A + N_A \sin\beta)\sin\beta \tan\phi_{eq} + (N_A \tan\delta + C_a)\cos^2\beta + (C + W_p \tan\phi_{eq})\cos\beta] \quad \textbf{6.23 b}$$

$$c = (N_A \tan\delta + C_a)\cos\beta \sin\beta \tan\phi_{eq} \quad \textbf{6.23 c}$$

For determining the design curves of MLCS, in accordance with the seismic zonation map suggested in IS1893-1:2002, the design pseudo-static earthquake coefficients for different zones are calculated according to Eq. 6.24. In view of safeguarding the economy, importance, and safety of the intensive construction activities against earthquakes, Indian standards IS1893:1962 has developed a seismic zonation map with five zones evaluating seismicity of past events, which later were modified to four zones in IS1893-1:2002.

$$k_h = \frac{ZIS_a}{2Rg} \quad \textbf{6.24}$$

The design pseudo-static horizontal earthquake coefficients for a structure in these four zones are evaluated considering the zone factor '*Z*' for different zones as given in the standard. The importance factor '*I*' is considered as 1.5 taking into account the functional value of structure reported in the standard and the response reduction factor '*R*' is considered as 1.5 in view of the unreinforced cement concrete slab bearing the MLCS. Finally, the average seismic earthquake coefficient 'S_a/g' is considered to be 2.5, the maximum value based on the response spectra for any type of soil or rock strata with 5% damping ratio. Considering these parameters as per the specifications, the probable horizontal earthquake coefficient for different seismic zones in India are evaluated and represented as shown in Figure 6.21.

Figure 6.21 details the variation in FoS values of MLCS with change in horizontal seismic acceleration coefficients. As expected, it can be understood that as the severity of the earthquake increases, the FoS of the various interlayers of MLCS decreases. For the first, second and fourth interface, beyond an average seismic coefficient of 0.10, the FoS has been observed to reduce below 1 (one). In such scenario, the corresponding sloping layers of the MLCS would fail to withstand the seismic excitation caused by particular event, and thereby undergo a lateral displacement governed by the ground acceleration generated from the corresponding earthquake. Based on the amount of deformation and progressive failure mechanism, necessary changes in MLCS design need to be adopted (Koerner and Soong 2005).

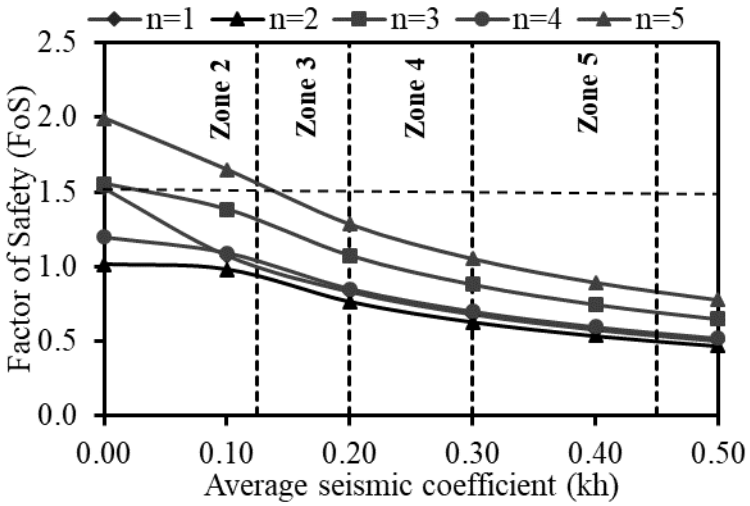

Figure 6.21 Design curves for FoS of MLCS with varying pseudo-static seismic coefficients

6.8 Summary

In this study, the existing method of translational stability analysis of uniformly laid soil over geosynthetic liner is extended to cater the analysis of multi-layered cover systems (MLCS). The effect of changes in passive wedge on FoS is brought forth. The formulation was used to evaluate the FoS of RCRA subtitle 'C' cover system, for their application in near-surface low-level hazardous waste disposal facilities. Different possibilities were incorporated in the analysis for enhancing the stability of MLCS wherever applicable. Based on the brief analysis and results obtained, the following conclusions are derived.

1) The effect of change in slope inclination or its length on the response of all interface layers of the MLCS is observed to be significant on mild slopes or slopes with relatively shorter lengths.
2) The stability analysis illustrates that it is important to decipher the behaviour of multiple failure planes of MLCS under various circumstances, thus signifying the need for intricate and rigorous extension of existing stability analysis for all the possible interfaces.
3) The effect of change in materials, application of reinforcement, and construction of toe berm are presented with design curves established for RCRA subtitle 'C' MLCS configuration.
4) Design curves for destabilising cases viz., vehicle ascending and descending the slope, horizontally submerged slope, and seismically active slope have been developed.

5) The new method of slope stabilisation suggests improving the capacity of the passive wedge by applying higher compactive efforts and limiting densities within allowable permeability criteria.

Chapter 7

Conclusions and future scope

7.1 General

This research was initiated to evaluate the performance of individual components and translational stability of multi-layered cover system (MLCS) for hazardous waste disposal facilities. The effects of atmospheric variants on long-term performance of MLCS were investigated. Based on the systematic laboratory, field and analytical studies, the following conclusions were drawn from this study.

7.2 Conclusions

1) Soils of moderate plasticity compacted at optimal water contents to higher densities displayed relatively superior performance in terms of erosion resistance.
2) The long-term hydraulic evaluation of soil-geotextile system demonstrated higher improvement in permeability in the case of geotextile with higher opening size (AOS).
3) The equilibrium permeability (k_{eq}) of soil-geotextile system was found to reduce with increase in soil fines.
4) The scale factor for k_{eq} in centrifuge was found closer to unity proves the efficiency of geotechnical centrifuge in long-term performance studies of soil-geotextile system.
5) Aggregates of large size compacted close to 60% relative density exhibited optimal performance for drainage layer in MLCS.
6) Rate of infiltration and erosion of surface soils in field MLCS were significantly affected by antecedent moisture content and desiccation cracks attributed to climatic variations.
7) Revised universal soil loss equation (RUSLE) was found to predict the annual soil loss satisfactorily for MLCS. However, on monthly basis RUSLE was found to underperform soil loss prediction especially during high intensity rainfall and for higher vegetation cover.
8) The effect of change in slope inclination and length or its length is observed to be significant on the translational stability of all interface layers of the MLCS specifically for mild slopes or slopes with relatively shorter lengths.
9) The analytical translational stability analysis performed in this study helps to identify the weakest interface of MLCS under various factors that causes instability.

7.3 Major contributions

1) A methodology was developed for selecting suitable soil type and its compaction state for surface layer of MLCS by incorporating erosion resistance of soil.
2) This study proposed a quick method using geotechnical centrifuge for long-term hydraulic performance evaluation of soil-geotextile system for its use as filter layer in MLCS.
3) Combined shear and seepage based design criteria for drainage layer of MLCS was proposed in this study.
4) Efficiency of RUSLE model in predicting annual soil loss of surface layer in MLCS was established and the need for bioengineering in protecting the surface layer of MLCS is brought forth.
5) Modified translational stability analysis was presented for identifying multiple failure plane and weakest inteface in MLCS.

7.4 Limitations of present study

1) The surface soil evaluation is limited to 5 types of local soils with plasticity index 16 to 26. More soils need to be tested for confirming the proposition made in this study.
2) The erosion study in laboratory, both using pin hole test and jet erosion test were limited to flow rates corresponding to 3 typical rainfall intensities.
3) The field performance study of pilot MLCS is limited to 1 year of study and under local climatic scenario. This needs to be extended for further validation.
4) Field soil loss estimation was limited to an empirical model RUSLE. Process and physics based soil loss estimation methods need to be studied for effective estimation.
5) The translational slope stability analysis performed in this study did not consider the direct effect of rainfall. The climate change impact need to be considered keeping in view the design life of MLCS.

7.5 Future scope

1) Erosion based criterion for surface layer in MLCS need to be extended for different soil classification which is appropriate as surface layer with suitable automation of the present set up.
2) The field studies on pilot MLCS needs to be extended for different configurations under various climatic conditions.

REFERENCES

40CFR258.60 (2002). Standards for owners and operators of hazardous waste treatment, storage and disposal facilities, United states Government Printing Office, Washington D.C.

Agassi, M., and Bradford, J. M. (1999). "Methodologies for interrill soil erosion studies." Soil and Tillage Research, 49(4), 277-287.

Akram, M. and Kemper, W. D. (1979). "Infiltration of soils as affected by the pressure and water content at the time of compaction." Soil Sci. Soc. Am. J., 43(6), 1080-1086.

Albrecht, B. A. and Benson, C. H. (2001). "Effect of desiccation on compacted natural clays." Journal of Geotechnical and Geoenvironmental. Engineering, ASCE, 127(1), 67-75.

Albright, W. H., Benson, C. H., Gee, G. W., Roesler, A. C., Abichou, T., Apiwantragoon, P., and Rock, S. A. (2004). "Field water balance of landfill final covers." Journal of Environmental Quality, 33(6), 2317-2332.

Almeida, M.S.S., Spada, J. and Ehrlich, M. (1995). "Geotextile Filtration Tests on Two Brazilian Soils and Current Filter Criteria." Geosynthetics International, 2(1), 357-377.

Alonso, E. E., Olivella, S., and Pinyol, N. M. (2005). "A review of Beliche Dam." Geotechnique 55(4), 267–285.

Amadi, A. A., and Eberemu, A. O. (2013). "Characterization of Geotechnical Properties of Lateritic Soil-Bentonite Mixtures Relevant to Their Use as Barriar in Engineered Waste Landfills." Nigerian J Tech., 32(1), 93-100.

Anderson, S. A., T Samuel Holder, P. E., and Gene Dodd, P. E. (2000). "Rapid Reactivation of a Large Composite Earth Slide—Earth Flow." ASCE.

Angulo-Jaramillo, R., Vandervaere, J. P., Roulier, S., Thony, J. L., Gaudet, J. P., and Vauclin, M. (2000). "Field measurement of soil surface hydraulic properties by disc and ring infiltrometers: A review and recent developments." Soil and Tillage Research, 55(1), 1-29.

Arnaez, J., Lasanta, T., Ruiz-Flaño, P., and Ortigosa, L. (2007). "Factors affecting runoff and erosion under simulated rainfall in Mediterranean vineyards." Soil and Tillage Research, 93(2), 324-334

Arslan, H., Baykal, G., and Sture, S. (2009). "Analysis of the influence of crushing on the behavior of granular materials under shear." Granular Matter, 11(2), 87-97.

Assouline, S., and Ben-Hur, M. (2006). “Effects of rainfall intensity and slope gradient on the dynamics of interrill erosion during soil surface sealing.” Catena, 66(3), 211-220.

ASTM D 4632 (2008). Standard test method for grab breaking load and elongation of geotextiles. Annual Book of ASTM Standards, Vol. 04.08, ASTM International, West Conshohocken, PA, USA.

ASTM D 6574-00 (2011). Standard test method for determining the (In-Plane) hydraulic transmissivity of a geosynthetic radial flow. Annual Book of ASTM Standards, Vol. 04.13, ASTM International, West Conshohocken, PA, USA.

ASTM D2166/D2166M (2016) Standard Test Method for Unconfined Compressive Strength of Cohesive Soil, ASTM International, West Conshohocken, PA, USA.

ASTM D2434-68 (2006) Standard Test Method for Permeability of Granular Soils (Constant Head), ASTM International, West Conshohocken, PA, USA.

ASTM D2487 (2011) Standard Practice for Classification of Soils for Engineering Purposes (Unified Soil Classification System), ASTM International, West Conshohocken, PA, USA.

ASTM D3080/3080M (2011). Standard test method for direct shear test of soils under consolidated drained conditions. Annual Book of ASTM Standards, Vol. 04.08, ASTM International, West Conshohocken, PA, USA.

ASTM D4254 (2016). Standard Test Methods for Minimum Index Density and Unit Weight of Soils and Calculation of Relative Density. Annual Book of ASTM Standards, Vol. 04.08, ASTM International, West Conshohocken, PA, USA.

ASTM D4318 (2010) Standard Test Methods for Liquid Limit, Plastic Limit, and Plasticity Index of Soils, ASTM International, West Conshohocken, PA, USA.

ASTM D4491 / D4491M (2009) Standard Test Methods for Water Permeability of Geotextiles by Permittivity, ASTM International, West Conshohocken, PA, USA.

ASTM D4647/D4647 (2013) Standard Test Methods for Identification and Classification of Dispersive Clay Soils by the Pinhole Test, ASTM International, West Conshohocken, PA, USA.

ASTM D5199 (2001). Standard Test Method for Measuring the Nominal Thickness of Geosynthetics. ASTM International, West Conshohocken, PA, USA.

ASTM D5261 (2010) Standard Test Method for Measuring Mass per Unit Area of Geotextiles, ASTM International, West Conshohocken, PA, USA.

ASTM D5567 (1994). Standard test method for determining Hydraulic conductivity ratio of soil/geotextile systems, Annual Book of ASTM Standards, ASTM International, West Conshohocken, PA, USA.

ASTM D698 (2012) Standard Test Methods for Laboratory Compaction Characteristics of Soil Using Standard Effort (12 400 ft-lbf/ft3 (600 kN-m/m3)), ASTM International, West Conshohocken, PA, USA.

ASTM D7928 (2016) Standard Test Method for Particle-Size Distribution (Gradation) of Fine-Grained Soils Using the Sedimentation (Hydrometer) Analysis, ASTM International, West Conshohocken, PA, USA.

ASTM D854 (2014) Standard Test Methods for Specific Gravity of Soil Solids by Water Pycnometer, ASTM International, West Conshohocken, PA, USA.

ASTM, D. 5852 (2000) Standard test method for erodibility determination of soil in the field or in the laboratory by the jet index method. ASTM International, West Conshohocken, PA, USA.

ASTM, D. 6913 (2004). Standard test methods for particle size distribution of soils using sieve analysis. ASTM International, West Conshohocken. PA, USA.

Aydilek, A. H. (2006). "A semi-analytical methodology for development of woven geotextile filter selection criteria", Geosynthetics International, 13(2), 59–72.

Aydilek, A. H., Madden, E. T., and Demirkan, M. M. (2006). "Field evaluation of a leachate collection system constructed with scrap tires." Journal of geotechnical and geoenvironmental engineering, 132(8), 990-1000.

Bagarello, V., Ferro, V., Giordano, G., Mannocchi, F., Pampalone, V., Todisco, F., and Vergni, L. (2011). "Effect of plot size on measured soil loss for two Italian experimental sites." Biosystems engineering, 108(1), 18-27.

Bear, J. (1972). "Dynamics of fluids in porous materials." Society of Petroleum Engineers: Dallas, TX, USA.

Beikae, M. (2000). "A numerical technique for two-dimensional slope stability problems." Geotechnical Special Publication, 33-47.

Benson, C. H., Bosscher, P. J., Lane, D. T., and Pliska, R. J., (1994) "Monitoring System for Hydrologic Evaluation of Landfill Covers," Geotechnical Testing Journal, 17(2), 138-149.

Benson, C. H., Sawangsuriya, A., Trzebiatowski, B., and Albright, W. H. (2007). "Postconstruction changes in the hydraulic properties of water balance cover soils." Journal of Geotechnical and Geoenvironmental engineering, 133(4), 349-359.

Benson, C., Abichou, T., Albright, W., Gee, G., and Roesler, A. (2001). "Field evaluation of alternative earthen final covers." Int. J. Phytoremediation, 3(1), 105-127.

Bergado, D. T., Ramana, G. V., and Sia, H. I. (2006). "Evaluation of interface shear strength of composite liner system and stability analysis for a landfill lining system in Thailand." Geotextiles and. Geomembranes, 24(6), 371-393.

Bergado, D.T., Manivannan, R., and Balasubramaniam, A.S., (1996). "Filtration Criteria for Prefabricated Vertical Drain Geotextile Filter Jackets in Soft Bangkok Clay", Geosynthetics International, 3(1), 63-83.

Bhatia, S.K. and Smith, J.L. (1996). "Geotextile Characterization and Pore-Size Distribution: Part II. A Review of Test Methods and Results." Geosynthetics International, 3(2), 155-180.

Bhowmik, R., Sukumar, R., Datta, M., and Shahu, J. T. (2016). "The Use of Geosynthetic Reinforcement for Enhancing the Stability of the Geomembrane–Soil Interface along the Slopes of Cover Systems of MSW Landfills." In Geo-Chicago, ASCE, 307-318.

Blight, G. E. (2007). "Failures during construction of a landfill lining: a case analysis." Waste Management and Research, 25(4), 327-333.

Boardman, J. (2006). "Soil erosion science: Reflections on the limitations of current approaches." Catena, 68(2), 73-86.

Bohra, A. K., Basu, S., Rajagopal, E. N., Iyengar, G. R., Gupta, M. D., Ashrit, R., and Athiyaman, B. (2006). "Heavy rainfall episode over Mumbai on 26 July 2005: Assessment of NWP guidance." Current Science, 90(9), 1188-1194.

Bolton, M. D. (1986). "The strength and dilatancy of sands." Geotechnique, 36(1), 65-78.

Bonaparte, R., Daniel, D., and Koerner, R. M. (2002). "Assessment and recommendations for improving the performance of waste containment systems" EPA-Environmental Protection Agency.

Bordoloi, S. Yamsani, S.K. Garg, A. Sreedeep S. and Borah. S. (2015) “Study on efficacy of harmful weed species Eicchornia crasssipes for soil reinforcement.” Ecological Engineering, 85, 218-222.

Bouazza, A., and Gassner, F. (2005). “Geosynthetics Reinforcement in Landfills Design: Australasian Perspectives.” In International. Perspective on Soil Reinforcement Applications, ASCE, 1-15.

Bouazza, A., and Wojnarowicz, M. (2000). “Stability assessment of an old domestic waste slope in Warsaw (Poland).” Geotechnical Special Publication, 48-57.

Boulanger-Martel, V., Bussière, B., Côté, J., and Mbonimpa, M. (2015). “Influence of freeze–thaw cycles on the performance of covers with capillary barrier effects made of crushed rock–bentonite mixtures to control oxygen migration.” Canadian Geotechnical Journal, 53(5), 753-764.

Briaud, J. L. (2008). “Case histories in soil and rock erosion: woodrow wilson bridge, Brazos River Meander, Normandy Cliffs, and New Orleans Levees.” Journal of Geotechnical and Geoenvironmental Engineering, 134(10), 1425-1447.

Brown, L. C., and Foster, G. R. (1987). “Storm erosivity using idealized intensity distributions.” Transactions of the ASAE, 30(2), 379-0386.

Bussière, B., Aubertin, M., and Chapuis, R. P. (2003). “The behavior of inclined covers used as oxygen barriers.” Canadian Geotechnical Journal, 40(3), 512-535.

Butterfield, R. (2000). “Scale-modelling of fluid flow in geotechnical centrifuges.” Soils and foundations, 40(6), 39-45.

Cai, C. F., Ding, S. W., and Shi, Z. H. (2000). “Study of Applying USLE and Geographical Information System IDRISI to Predict Soil Erosion in Small Watershed.” Journal of Soil Water Conservation, 14(2), 19–24.

Cargill, K. W., and Ko, H. Y. (1983). “Centrifugal modeling of transient water flow.” Journal of Geotechnical Engineering, 109(4), 536-555.

Carroll, R. G., and Chouery-Curtis, V. (1991). “Geogrid reinforcement in landfill closures.” Geotextiles and. Geomembranes, 10(5-6), 471-486.

Carroll, R. G., Jr. (1983). "Hydraulic Properties of Geotextile," Geotextile Testing and the Design Engineer, ASTM STP 952, ASTM, Philadelphia, 7-20.

Carsel, R.F. and Parrish, R.S. (1988). “Developing joint probability distributions of soil water retention characteristics.” Water Resources Research, 24(5), 755-769.

Casagrande, A., and Shannon, W. L. (1948). “Research on stress-deformation and strength characteristics of soils and soft rocks under transient loading.” Pub. Harvard Univ. Grad. Sch. Eng. No. 447. 132 pp.

Cedergren, H., R. (1989). Seepage, drainage, and flow nets, John Wiley and Sons, Toronto.

Christiansen, J. E. (1942). Irrigation by sprinkling. California Agricultural Experimental Station Bulletin 670. University of California, Berkeley, California.

Christopher, B. R. (1991). “Geotextiles in landfill closures.” Geotextiles and. Geomembranes, 10 (5-6), 459-470.

Christopher, B. R. and Holtz, R. D. (1985). “Geotextile engineering manual.” Report No. FHWA-TS-86/203, US Federal Highway Administration, Washington, DC.

Cooper, C., Mira, R., and Low, T. (2012) “Draft Record of Decision for Parcel E-2”, Department of Navy, San Francisco.

CPCB (2010). “Pollution control acts, rules and notifications issued thereunder”, Central Pollution Control Board, Government of India, Delhi.

Daniel, D. E., and Wu, Y. K. (1993). “Compacted clay liners and covers for arid sites.” Journal of Geotechnical Engineering, ASCE, 119(2), 223-237.

David, A., and Stark, T. D. (2000). “Importance of Three-Dimensional Slope Stability Analyses in Practice.” ASCE.

Decagon-Devices inc. (2007) Mini disk infiltrometer, user’s manual versión 6. Decagon Devices, Pullman

Defersha, M. B., and Melesse, A. M. (2012). “Effect of rainfall intensity, slope and antecedent moisture content on sediment concentration and sediment enrichment ratio.” Catena, 90, 4.

Denkler, P., Bowders, J., and Loehr, E. (2000). “Geotextiles and Loess: Long-Term Flow.” In Mid–continent transportation symposium proceedings, 249-253.

Di Trapani, D., Di Bella, G., and Viviani, G. (2013). “Uncontrolled methane emissions from a MSW landfill surface: Influence of landfill features and side slopes.” Waste Management, 33(10), 2108-2115.

Dixon, N., (2010). “Soil-geosynthetic interaction: interface behaviour.” Proceedings of 9th International Conference on Geosynthetics, Guaruja, Brazil, 563-582.

Dixon, N., Jones, D. R. V., and Fowmes, G. J. (2006). “Interface shear strength variability and its use in reliability-based landfill stability analysis.” Geosynthetic International, 13(1), 1 - 14.

DOE (2000) U.S. Environmental Protection Agency Innovation technology summary report Alternative Landfill Cover, Sandia National Laboratories Report, DOE/EM-0558.

Dohnal, M., Dusek, J. and Vogel, T. (2010). “Improving hydraulic conductivity estimates from minidisk infiltrometer measurements for soils with wide pore-size distributions.” Soil Science Society of America Journal, 74(3), 804-811.

D'souza, V. P. C., and Morgan, R. P. C. (1976). “A laboratory study of the effect of slope steepness and curvature on soil erosion.” Journal of agricultural engineering research, 21(1), 21-31.

Durigon, V. L., Carvalho, D. F., Antunes, M. A. H., Oliveira, P. T. S., and Fernandes, M. M. (2014). “NDVI time series for monitoring RUSLE cover management factor in a tropical watershed.” International journal of remote sensing, 35(2), 441-453.

Dwyer, S. F. (2003). Water balance measurements and computer simulations of landfill covers. Doctoral dissertation, The University of New Mexico.

EIA, (2014). Monthly energy review. Energy Information Administration, US.

Ekwue, E. I., and Harrilal, A. (2010). “Effect of soil type, peat, slope, compaction effort and their interactions on infiltration, runoff and raindrop erosion of some Trinidadian soils.” Biosystems engineering, 105(1), 112-118.

Fannin, R. J., Vaid, Y. P., and Shi, Y., (1994) "A Critical Evaluation of the Gradient Ratio Test," Geotechnical Testing Journal, 17(1), 35-42.

Faure, Y. H., Farkouh, B., Delmas, P., and Nancey, A. (1999). “Analysis of geotextile filter behaviour after 21 years in Valcros dam.” Geotextile and Geomembranes, 17(5), 353-370.

Filz, G. M., Esterhuizen, J. J., and Duncan, J. M. (2001). “Progressive failure of lined waste impoundments.” Journal of Geotechnical and Geoenvironmental Engineering, ASCE, 127(10), 841-848.

Fischer, G. R., Holtz, R. D., and Christopher, B. R. (1996). "Evaluating geotextile pore structure. In Recent developments in geotextile filters and prefabricated drainage geocomposites." ASTM International.

Forman, A. D., and Anderson, J. E. (2005). "Design and performance of four evapotranspiration caps." Pract. Period. Hazardous, Toxic, Radioactive Waste Management, ASCE, 9(4), 263-272.

Forrester, K. (2001). "Drain Construction Materials. Subsurface Drainage for Slope Stabilization." ebooks, ASCE press: pp. 101-111. doi: 10.1061/9780784400166.ch11.

Francisco. P. J., de Castro, L., and Delgado, A. (2010). "A comparison of two variable intensity rainfall simulators for runoff studies." Soil and Tillage Research, 107(1), 11-16.

Freitag, D. R. (1986). "Soil randomly reinforced with fibers." Journal of Geotechnical Engineering., ASCE, 112(8), 823-826.

Fujisawa, K., Kobayashi, A., and Yamamoto, K. (2008) "Erosion rates of compacted soils for embankments." Jpn Soc. Civil Engs. P., 64(2), 403-410.

Gadi, V. K., Tang, Y. R., Das, A., Monga, C., Garg, A., Berretta, C., and Sahoo, L. (2017). "Spatial and temporal variation of hydraulic conductivity and vegetation growth in green infrastructures using infiltrometer and visual technique." Catena, 155, 20-29.

Gaucher, J., Marche, C., and Mahdi, T. F. (2010)." Experimental investigation of the hydraulic erosion of noncohesive compacted soils." Journal of Hydraulic Engineering, 136(11), 901-913.

Geostudio (2007) Geostudio: user's guide for Sigma- W and Slope-W, version 8.0. Geoslope International, Calgary

Giroud, J. P. (2005). "Quantification of geosynthetic behaviour." Geosynthetics International, 12(1), 2-27.

Giroud, J. P., Zornberg, J. G., and Zhao, A. (2000). "Hydraulic design of geosynthetic and granular liquid collection layers", Geosynthetics International, 7(4-6), 285-380.

Gregory, J. H., Dukes, M. D., Jones, P. H., and Miller, G. L. (2006). "Effect of urban soil compaction on infiltration rate." Journal of Soil and Water Conservation, 61(3), 117-124.

Haghighi, I., Chevalier, C., Duc, M., Guédon, S., and Reiffsteck, P. (2013). “Improvement of hole erosion test and results on reference soils.” Journal of Geotechnical and Geoenvironmental Engineering, ASCE, 139(2), 330-339.

Hamed, Y., Albergel, J., Pépin, Y., Asseline, J., Nasri, S., Zante, P., and Balah, M. (2002). “Comparison between rainfall simulator erosion and observed reservoir sedimentation in an erosion-sensitive semiarid catchment.” Catena, 50(1), 1-16.

Hanson, G. J. (1990). “Surface erodibility of earthen channels at high stresses part II-developing an in situ testing device.” Transactions of the ASAE, 33(1), 132-0137.

Hanson, G. J., and Cook, K. R. (2004). “Apparatus, test procedures, and analytical methods to measure soil erodibility in situ,” Applied engineering in agriculture, 20(4), 455.

Hanson, G. J., and Simon, A. (2001). “Erodibility of cohesive streambeds in the loess area of the midwestern USA.” Hydrological processes, 15(1), 23-38.

Hardin, B. O. (1985). “Crushing of soil particles.” J Geotech. Eng.-ASCE, 111(10), 1177-1192.

Harshberger, K., Zietek, R., and Eichlberger, C. (2012) "An unprecedented design/build regulatory effort." Geosynthetics Magazine.

Ho, C. K., Arnold, B. W., Cochran, J. R., Taira, R. Y., and Webb, S. W. (2001). “Development of a Risk-Based Performance-Assessment Method for Long-Term Cover Systems–Application to the Monticello Mill Tailings Repository.” SAND2001-3032, Sandia National Laboratories.

Hong, H. S., Huang, J. L., and Cao, W. Z. (2008). “Agricultural Non-point Source Pollution Mechanism and Control Research in Jiulong River Watershed.” Beijing: Science Press.

Hsuan, Y. G., Schroeder, H. F., Rowe, K., Müller, W., Greenwood, J., Cazzuffi, D., and Koerner, R. M. (2008). “Long-term performance and lifetime prediction of geosynthetics.” In Proceeding of Euro Geo 4-4th European Geosynthetics Conference.

Indraratna, B., Sun, Q. D., and Nimbalkar, S. (2014). “Observed and predicted behaviour of rail ballast under monotonic loading capturing particle breakage.” Can. Geotech. J., 52(1), 73-86.

IS 11209 (1985). “Specification for mould assembly for determination of Permeability of soils.” Bureau of Indian Standards.

IS 2720 part 13 (1986). “Methods of Test for Soils: Direct shear test for soils.” Bureau of Indian Standards.

IS 2720 part 17 (1986) “Methods of Test for Soils: Laboratory determination of permeability.” Bureau of Indian Standards.

IS 2720 part 39 (1977). “Methods of Test for Soils: Direct shear test for soil containing gravel.” Bureau of Indian Standards.

IS1893 (1962) Indian Standard Recommendations for Earthquake Resistant Design of Structures. Bureau of Indian Standards, New Delhi.

IS1893-1 (2002) Criteria for earthquake resistant design of structures. Bureau of Indian standards, New Delhi.

Ishihara, K. (1996). Soil behaviour in earthquake geotechnics, Oxford science publications.

Islam, M. N., Siddika, A., Hossain, B., Rahman, A., and Asad, M. A. (2011). “Effect of particle size on the shear strength behavior of sands.” Aust. Geomech., 46(3), 75-86.

ISO 4064 (2005) Measurement of water flow in fully charged closed conduits—meters for cold potable water and hot water. International Organization for Standardization.

ITRC (Interstate Technology and Regulatory Council) (2003) Technical and regulatory guidance for design, installation, and monitoring of alternative final landfill covers. www.itrcweb.org/GuidanceDocuments/ALT-2.pdf. Accessed April 2, 2016

Jesionek, K. S., and Dunn, R. J. (1998). “Final cover systems for municipal solid waste landfills. In Contaminated and Derelict Land,” The Proceedings of GREEN 2: The Second International Symposium on Geotechnics Related to the Environment Held in Kraków, Poland, September 1997 (p. 391). Thomas Telford.

Joshi, V. U., and Tambe, D. T. (2010). “Estimation of infiltration rate, run-off and sediment yield under simulated rainfall experiments in upper Pravara Basin, India: Effect of slope angle and grass-cover.” Journal of earth system science, 119(6), 763-773.

Kincaid, D.C., Solomon, K.H., and Oliphant, J.C. (1996). “Drop size distribution for irrigation sprinklers.” Transactions of ASAE 39 (3), 839–845.

Kleppe, J. H., and Olson, R. E. (1985). “Desiccation cracking of soil barriers.” In Hydraulic barriers in soil and rock. ASTM Int.. STP34583S.

Kodikara, J. K., Barbour, S. L., and Fredlund, D. G. (2000). "Desiccation cracking of soil layers." Unsaturated soils for Asia, 90(5809), 139.

Koerner, G. R., and Koerner, R. M. (1992). "Leachate flow rate behavior through geotextile and soil filters and possible remediation methods." In Geosynthetics in Filtration, Drainage and Erosion Control (pp. 65-94).

Koerner, R. M. (2013). Landfill Closures: Geosynthetics, Interface Friction and New Developments. Elsevier.

Koerner, R. M. and Daniel, D. E. (1997) Final covers for solid waste landfills and abandoned dumps, ASCE press, Reston Virginia, ISBN 0784402612.

Koerner, R. M., and Hwu, B. L. (1991). "Stability and tension considerations regarding cover soils on geomembrane lined slopes." Geotextiles and Geomembranes, 10(4), 335-355.

Koerner, R. M., and Koerner, G. R. (2013). "A data base, statistics and recommendations regarding 171 failed geosynthetic reinforced mechanically stabilized earth (MSE) walls." Geotextiles and Geomembranes, 40, 20-27.

Koerner, R. M., and Soong, T. Y. (1998) "Analysis and design of veneer cover soils." In proceedings of the Sixth International Conference on geosynthetics, 1-26.

Koerner, R. M., and Soong, T. Y. (2005) "Analysis and design of veneer cover soils." Geosynthetics International, 12(1), 28-49.

Koerner, R. M., Koerner, G. R., and Hsuan, Y. G. (2005). "Lifetime prediction of exposed geo-membranes." Geosynthetics research and development in progress, Geofrontiers 2005, ASCE

Koerner, R. M., Lord, A. E., and Halse, Y. H. (1988). "Long-term durability and aging of geotextiles." Geotextiles and Geomembranes, 7(1), 147-158.

Koerner, R.M. (1998) Designing with Geosynthetics, 4TH Ed., Prentice Hall, Upper Saddle River, NJ.

Koutsourais, M. M., Sprague, C. J., and Pucetas, R. C. (1991). "Interfacial friction study of cap and liner components for landfill design." Geotextiles and Geomembranes, 10(5), 531-548.

Kumar, P. R. (2007). "Scaling laws and experimental modelling of contaminant transport mechanism through soils in a geotechnical centrifuge." Geotechnical and Geological Engineering, 25(5), 581.

Kumar, S., and Kushwaha, S. P. S. (2013). “Modelling soil erosion risk based on RUSLE-3D using GIS in a Shivalik sub-watershed.” Journal of Earth System Science, 122(2), 389-398.

Lambe T. W. (1958) “The structure of compacted clay.” J Soil Mech. Founds. Div., ASCE, 84(SM2):1-34.

Landreth, R. E., and Carson, D. A. (1991). “RCRA cover systems for waste management facilities.” In Landfill Closures (pp. 1-9).

Lavigne, F., Wassmer, P., Gomez, C., Davies, T. A., Hadmoko, D. S., Iskandarsyah, T. Y. W., Gaillard, J. C., Fort, M., Texier, P., Heng, M. B. and Pratomo, I. (2014). “The 21 February 2005, catastrophic waste avalanche at Leuwigajah dumpsite, Bandung, Indonesia.” Geoenvironmental Disasters, 1(1), 1-12.

Lei, T. W., Zhang, Q. W., Yan, L. J., Zhao, J., and Pan, Y. H. (2008). “A rational method for estimating erodibility and critical shear stress of an eroding rill.” Geoderma, 144(3), 628-633.

Leonard, J., and Richard, G. (2004). “Estimation of runoff critical shear stress for soil erosion from soil shear strength.” Catena, 57(3), 233-249.

Li, X. S., and Dafalias, Y. F. (2000). “Dilatancy for cohesionless soils.” Geotechnique, 50(4), 449-460.

Luettich, S. M., Giroud, J. P., and Bachus, R. C. (1992). “Geotextile filter design guide.” Geotextiles and. Geomembranes, 11(4-6), 355-370.

Maheshwari, B, K., and Gunjagi, D. A. (2008). “Filtration and clogging behavior of geotextiles with roorkee soils.” Geotech. Geol. Eng., 26(1), 101-107.

Mannering, J. V., and Meyer, L. D. (1963). “The Effects of Various Rates of Surface Mulch on Infiltration and Erosion 1.” Soil Science Society of America Journal, 27(1), 84-86.

Meer, S. R., and Benson, C. H. (2007). “Hydraulic conductivity of geosynthetic clay liners exhumed from landfill final covers.” Journal of Geotechnical and Geoenvironmental Engineering, ASCE, 133(5), 550-563.

Merry, S. M., Kavazanjian Jr, E., and Fritz, W. U. (2005). “Reconnaissance of the July 10, 2000, Payatas landfill failure.” Journal of Performance of constructed Facilities, 19(2), 100-107.

Meter Group Inc. (2017) ATMOS 41 all in one mini weather station, user manual. METER Group, Inc. 2365 NE Hopkins Ct. Pullman, WA USA

Michalowski, R. L. (1995). “Slope stability analysis: a kinematical approach.” Geotechnique, 45(2), 283-93.

Millward, A. A., and Mersey, J. E. (1999). “Adapting the RUSLE to model soil erosion potential in a mountainous tropical watershed.” Catena, 38(2), 109-129.

Mitchell, J. K., Seed, R. B., and Seed, H. B. (1990). “Kettleman Hills waste landfill slope failure. I: Liner-system properties.” Journal of Geotechnical Engineering, ASCE, 116(4):647–668.

Młynarek, J., BogumiłLewandowski, J., Rollin, A., and Bolduc, G. (1991). “Soil-geotextile system interaction.” Geotextiles and Geomembranes, 10(2), 161-176.

Mondal, A., Khare, D., and Kundu, S. (2016). “A comparative study of soil erosion modelling by MMF, USLE and RUSLE.” Geocarto International, 1-15.

Morris, C. E., and Stormont, J. C. (1997). “Capillary barriers and subtitle D covers: estimating equivalency.” Journal of Environmental Engineering, ASCE, 123(1), 3-10.

Nandakumaran, P., and Richardson. G. N. (1999) "Landfill cover failure prompts standards upgrade." Designer’s Forum, Geotechnical Fabrics Report. Vol. 17. No. 7.

Narejo, D., Li, M., Zimmel, E., and Wu, Y. (2013). “A monolithic layered nonwoven–woven geotextile for use with drainage geocomposites in coal combustion residual projects.” Geotextiles and Geomembranes, 37, 16-22.

O’Kane, M., Ayres, B., Christensen, D., and Meiers G., (2002). “CANMET – CETEM Manual on Cover System Design for Reactive Mine Waste” O’Kane Consultants Inc. OKC Report No. 689-01.

Ören, A. H., Önal, O., Özden, G., and Kaya, A. (2006). “Nondestructive evaluation of volumetric shrinkage of compacted mixtures using digital image analysis.” Engineering geology, 85(3-4), 239-250.

Osinubi K. J. and Nwaiwu, C. M. (2008). “Desiccation-induced shrinkage in compacted lateritic soils.” Geotechnical and Geological Engineering, 26(5), 603-611.

Paulson, J. N. (2013). “New geocomposite drains.” Landfill Closures: Geosynthetics, Interface Friction and New Developments, 10, 243-251.

Peck, R. B., Hanson, W. E., and Thornburn, T. H. (1974). Foundation engineering. 2nd Ed., John Wiley & Sons, Inc., New York, N.Y.

Piet, S. J., Breckenridge, R. P., Jacobson, J. J., White, G. J., and Inyang, H. I. (2005). "Design principles and concepts for enhancing long-term cap performance and confidence." Practice Periodical of Hazardous, Toxic, and Radioactive Waste Management, 9(4), 210-222.

Qian, X., and Koerner, R. M. (2009). "Stability analysis when using an engineered berm to increase landfill space." Journal of Geotechnical and Geoenvironmental Engineering, ASCE, 135(8), 1082-1091.

Qian, X., and Koerner, R. M. (2015). "Critical interfaces and waste placement in landfill design." Environmental Geotechnics. ICE, 2(2), 118-126.

Rahardjo, H., Satyanaga, A., and Leong, E. C. (2013). "Effects of flux boundary conditions on pore-water pressure distribution in slope." Engineering Geology, 165, 133-142.

Rahardjo, H., Satyanaga, A., Harnas, F. R., and Leong, E. C. (2015) "Use of Dual Capillary Barrier as Cover System for a Sanitary Landfill in Singapore." Indian Geotechnical Journal,1-11.

Rahimi, A., Rahardjo, H., and Leong, E. C. (2010). "Effect of antecedent rainfall patterns on rainfall-induced slope failure." Journal of Geotechnical and Geoenvironmental Engineering, 137(5), 483-491.

Raisinghani, D.V., and Viswanadham, B.V.S. (2010). "Evaluation of permeability characteristics of a geosynthetic- reinforced soil through laboratory tests." Geotextiles and Geomembranes, 28(6), 579-588.

Ramsey, B. and Narejo, D. (2005) "Using Woven and Heat-Bonded Geotextiles in Geonet Geocomposites." Waste Containment and Remediation: Geofrontiers 2005, ASCE 1-8

Rao, B. H., and Singh, D. N. (2012). "Establishing soil-water characteristic curve and determining unsaturated hydraulic conductivity of kaolin by ultracentrifugation and electrical measurements." Canadian Geotechnical Journal, 49(12), 1369-1377.

Rao, G.V., Gupta, K.K., and Pradhan, M.P.S. (1991), "Long term filtration behavior of soil-geotextile system." Geotechnical Testing Journal, 15(3), 238-247.

Raymond, C. W., and Tang, W. H. (2000). "Bayesian calibration of slope failure probability." Geotechnical Special Publication, 72-85.

Reddi, L. N., Lee, I-M., and Bonala, M. V. S., (2000) “Comparison of Internal and Surface Erosion Using Flow Pump Tests on a Sand-Kaolinite Mixture.” Geotechnical Testing Journal, 23(1), 116–122.

Reddy, K. R., Stark, T. D., and Marella, A. (2009). “Beneficial use of shredded tires as drainage material in cover systems for abandoned landfills.” Pract. period. hazard., toxic, radioact. waste manag., 14(1), 47-60.

Renard, K. G. (1997). Predicting soil erosion by water: a guide to conservation planning with the revised universal soil loss equation (RUSLE). USDA, U.S. Govt. Office, Washington, DC.

Reynolds, W.D., D.E. Elrick, E.G. Youngs, A. Amoozegar, H.W.G. Booltink, and J. Bouma. (2002). Saturated and field-saturated water flow parameters, Methods of Soil Analysis, Part 4. 797-801.

Richardson, Gregory N., Stacey A. Smith, and Pieter K. Scheer. (2008) "Active LFG control: An unreliable aid to veneer stability." Geosynthetics Magazine.

Rollin, A., and Lombard, G. (1988). “Mechanisms affecting long-term filtration behavior of geotextiles.” Geotextiles and Geomembranes, 7(1-2), 119-145.

Romero-López, A. A., Rodríguez-Palacios, E., Alarcón-Gutiérrez, E., Geissert, D., and Barois, I. (2015). “Effects of White Grubs on Soil Water Infiltration.” Neotropical entomol., 44(2), 134-139.

Römkens, M. J. M., Dabney, S. M., Govers, G., and Bradford, J. M. (2002). Soil erosion by water and tillage. Methods of Soil Analysis: Part 4 Physical Methods, 1621-1662.

Rowe, R. K. (1998) “From the past to the future of landfill engineering through case histories”, Proceedings: Fourth International Conference on Case Histories in Geotechnical Engineering, St. Louis, Missouri.

Rowe, R. K. (2005). “Long-term performance of contaminant barrier systems.” Geotechnique, 55(9), 631-678.

Rowe, R. K., and Yu, Y. (2012). “Modeling of leachate characteristics and clogging of gravel drainage mesocosms permeated with landfill leachate.” Journal of Geotechnical and Geoenvironmental Engineering, 139(7), 1022-1034.

Sanchez-Moreno, J. F., Mannaerts, C. M., Jetten, V., and Löffler-Mang, M. (2012).” Rainfall kinetic energy–intensity and rainfall momentum–intensity relationships for Cape Verde.” Journal of Hydrology, 454, 131-140.

Sansone, L. J. and Koerner, R.M. (1992). “Fine fraction filtration test to assess geotextile filter performance.” Geotextiles and Geomembranes, 11(4-6):371-393.

Sarihan, H. N., and Stark, T. D. (2008). “Back analyses of landfill slope failures.” In Proceedings of 6th international case histories conference (pp. 11-16).

Seed, R. B., Mitchell, J. K., and Seed, H. B. (1990). “Kettleman hills waste landfill slope failure. II: stability analyses.” Journal of Geotechnical Engineering, ASCE, 116(4), 669-690.

Sharply, A. N. and Williams, J. R. (1990). EPIC-Erosion/Productivity Impact Calculator I, model documentation. U.S. Department of Agriculture Technical Bulletin, No. 1768. (Washington, DC:USDA Agricultural Research Service), 235 pp.

Sherard, J. L., Steele, E. F., Decker, R. S., and Dunnigan, L. P. (1976). “Pinhole test for identifying dispersive soils.” Journal of the Geotechnical Engineering Division, 102(1), 69-85.

Siebecker (2005) http://waste360.com/mag/waste_final_caps_fail (accessed 14-04-2016)

Singh, D. N., and Gupta, A. K. (2000). “Modelling hydraulic conductivity in a small centrifuge.” Canadian Geotechnical Journal, 37(5), 1150-1155.

Singh, D. N., and Kuriyan, S. J. (2002). “Estimation of hydraulic conductivity of unsaturated soils using a geotechnical centrifuge.” Canadian Geotechnical Journal, 39(3), 684-694.

Singh, M. K., Sharma, J. S., and Fleming, I. R. (2009). “A design chart for estimation of horizontal displacement in municipal landfills.” Waste management, 29(5), 1577-1587.

Skempton, A. W., and Bishop, A. W. (1950). “The measurement of the shear strength of soils.” Geotechnique, 2(2), 90-108.

Smith, M.E., and Christos A. (2013) "Evaluations of engineered cover systems for mine waste rock and tailings." Geosynthetics Magazine.

Smyth, J. A., and Smith, S. A. (2012) "The basis for landfill closure, remediation, and redevelopment." Geosynthetics Magazine.

Song, Y., Liu, L., Yan, P., and Cao, T. (2005). "A review of soil erodibility in water and wind erosion research." Journal of Geographical Sciences, 15(2), 167-176.

Stolle, D., and Guo, P. (2008). "Limit equilibrium slope stability analysis using rigid finite elements." Canadian Geotechnical Journal, 45(5), 653-662.

Stormont, J. C. (1995). "The performance of two capillary barriers during constant infiltration." In Landfill Closures@ sEnvironmental Protection and Land Recovery (pp. 77-92). ASCE.

Strauss, P., Pitty, J., Pfeffer, M., and Mentler, A. (2000). "Rainfall simulation for outdoor experiments." Current research methods to assess the environmental fate of pesticides, 329-333.

Suter, G. W., Luxmoore, R. J., and Smith, E. D. (1993). "Compacted soil barriers at abandoned landfill sites are likely to fail in the long term." J. Env. Qual., 22(2), 217-226.

Sutherland, R. A., Wan, Y., Ziegler, A. D., Lee, C. T., and El-Swaify, S. A. (1996). "Splash and wash dynamics: an experimental investigation using an Oxisol." Geoderma, 69(1), 85-103.

Take, W. A., Rowe, R. K., Brachman, R. W. I., and Arnepalli, D. N. (2015). "Thermal exposure conditions for a composite liner with a black geomembrane exposed to solar radiation", Geosynthetics International, 22(1), 93-109.

Tami, D., Rahardjo, H., Leong, E. C., and Fredlund, D. G. (2004). "Design and laboratory verification of a physical model of sloping capillary barrier." Canadian geotechnical journal, 41(5), 814-830.

Tang, C. S., Shi, B., Liu, C., Suo, W. B., and Gao, L. (2011). "Experimental characterization of shrinkage and desiccation cracking in thin clay layer." Applied Clay Science, 52(1-2), 69-77.

Tao M, Abu-Farsakh M, and Zhang Z (2008) "Optimize drainable unbound aggregate through laboratory tests." Characterization, Monitoring, and Modeling of Geosystems, Proc GeoCongress 2008, ASCE 28–35

Tatsuoka, F., Enomoto, T., and Kiyota, T. (2006). "Viscous property of geomaterial in drained shear." In Geomechanics II Testing, Modeling, and Simulation (pp. 285-312). ASCE

Tay, Y. Y., Stewart, D. I., and Cousens, T. W. (2001). "Shrinkage and desiccation cracking in bentonite–sand landfill liners." Engineering Geology, 60(1-4), 263-274.

Taylor, R. E. (Ed.). (2003). Geotechnical centrifuge technology. CRC Press.

Tedder, R. (2005) "Use of Geosynthetic Drainage Materials at Landfills in Florida." Waste Containment and Remediation: pp. 1-7. doi: 10.1061/40789(168)12

Thoman, R. W., and Niezgoda, S. L. (2008). "Determining erodibility, critical shear stress, and allowable discharge estimates for cohesive channels: Case study in the Powder River basin of Wyoming." Journal of Hydraulic Engineering, 134(12), 1677-1687.

Traynham, B., Clarke, J., Burger, J. and Waugh, J. (2012), "Engineered containment systems: Identification of dominant ecological processes for long-term performance assessment and monitoring." Remediation, 22: 93–103.

USBR-DSO (2008) "Determining Erosion Indices of Cohesive Soils with the Hole Erosion Test and Jet Erosion Test" Dam Safety Technology Development Program, Report DSO-08-05, U.S. Department of the Interior Bureau of Reclamation Technical Service Center Denver, Colorado.

USEPA (1989). Final Covers on Hazardous Waste Landfills and Surface Impoundments, Technical Guidance Document, EPA/530/SW-89/047, United States Environmental Protection Agency, Office of Solid Waste and Emergency Response, Washington, D.C., 39 p.

USEPA (2000). "Summary report on Alternative landfill covers." www.epa.nsw.gov.au

USEPA (2015). "Draft Environmental Guidelines Solid waste landfills." www.epa.nsw.gov.au

Wan, C. F., and Fell, R. (2004). "Investigation of rate of erosion of soils in embankment dams." Journal of Geotechnical and Geoenvironmental Engineering, ASCE, 130(4), 373-380.

Wang, N., Zhu, Y. M., and Xu, C. G. (2002). "Appling GIS to the quantity study of runoff pollutants in watershed." Journal of Northeast Normal University (Natural Science Edition), 34(2), 92–98.

Williams, N.D., and Abouzakhm, M.A. (1989). "Evaluation of Geotextile/Soil filtration characteristics using the hydraulic conductivity ratio analysis." Geotextiles and Geomembranes, 8(1), 1-26.

Wischmeier, W. H. and Smith, D. D. (1965) "Predicting rainfall erosion losses from cropland east of the Rocky Mountains." USDA Agriculture Handbook, 282. U.S. Govt. Office, Washington, DC.

Wischmeier, W. H. and Smith, D. D. (1978) “Predicting rainfall erosion losses- A guide for conservation planning.” USDA Agriculture Handbook, 282. U.S. Govt. Office, Washington, DC.

Wu, C. S., Hong, Y. S., and Wang, R. H. (2008). “The influence of uniaxial tensile strain on the pore size and filtration characteristics of geotextiles.” Geotextiles and Geomembranes, 26(3), 250-262.

Xie, H. J., Wang, Q., Yan, H., and Chen, Y. M. (2017). “Steady-state analytical model for vapour-phase VOCs diffusion in layered landfill composite cover systems.” Canadian Geotechnical Journal.

Yang, Z. S. (1999). Crop-Planting Factor of Soil Erosion of Sloping Cultivated Land in the Northeast Mountain Region of Yunnan Province. Journal of Mountain Research, 17(S1), 19–21.

Younus, M. M., and Sreedeep, S. (2012). “Evaluation of bentonite-fly ash mix for its application in landfill liners.” J. Test. Eval., 40(3), 357-362.

Yu, Y., and Bathurst, R. J. (2016). “Influence of Selection of Soil and Interface Properties on Numerical Results of Two Soil–Geosynthetic Interaction Problems.” International Journal of Geomechanics, ASCE, 17(6), 04016136.

Yu, Y., and Rowe, R. K. (2012). “Effect of grain size on service life of MSW landfill drainage systems.” Canadian Geotechnical Journal, 50(1), 1-14.

Zekkos, D., Vasileios, S., Vlachakis, and Athanasopoulos, G. A. (2014) “The 2010 Xerolakka landfill slope instability,” Environmental Geotechnics, 1:1, 56-65.

Zhang, B., Gary, F., and Jones, D. R. V. (2012). “Landfill capping stability: tapered solution with seepage.” Proceedings of the Institution of Civil Engineering: Geotechnical Engineering, 165(3), 141-150.

Zhang, L., Yu, X., and Hu, T. (1998). “Optimization of compaction zoning in loess embankments.” Canadian Geotechnical Journal, 35(4), 611-621.

Zhang, R. (1997a). “Determination of soil sorptivity and hydraulic conductivity from the disk infiltrometer.” Soil Science Society of America Journal, 61(4), 1024-1030.

Zhang, R. 1997b). “Infiltration models for the disk infiltrometer.” Soil Science Society of America Journal, 61(6), 1597-1603.

Zhu, Y., Lu, J., Liao, H., Wang, J., Fan, B., and Yao, S. (2008). “Research on cohesive sediment erosion by flow: An overview.” Science in China Series E: Technological Sciences, 51(11), 2001-2012.

Zornberg, J. G., and McCartney, J. S. (2010). “Centrifuge permeameter for unsaturated soils. I: Theoretical basis and experimental developments.” Journal of Geotechnical and Geoenvironmental Engineering, 136(8), 1051-1063.

Zornberg, J., Byler, B., and Knudsen, J. (2004). "Creep of Geotextiles Using Time–Temperature Superposition Methods." Journal of Geotechnical and Geoenvironmental. Engineering, 10.1061/(ASCE)1090-0241(2004)130:11(1158), 1158-1168.

LIST OF PUBLICATIONS

Journals

- **S. K. Yamsani,** S. Sreedeep and R. R. Rakesh (2016) "Shear and interface shear characteristics of Multi-layered cover system". International Journal of geosynthetics and ground engineering, Springer, 2(3), 23.
- **S. K. Yamsani,** S. Sreedeep and R. R. Rakesh (2017) "Combined shear and seepage characteristics for selecting drainage layer in near surface low level radioactive waste disposal facility". Geotechnical and Geological Engineering, Springer, 35(2), 871-878.
- Y. Gapak, **S.K. Yamsani,** S. Sreedeep and R. R. Rakesh (2017) "Long-term permeability characteristics of soil-geosynthetic combination used in landfill covers" Advances in Civil Engineering Materials, ASTM , 6(1), 296 –309.
- **S. K. Yamsani,** S. Kumar, S. Sreedeep and R. R. Rakesh (2017) "Soil erosion index for surface soils of landfill covers". Journal of Environmental Geotechnics-Special issue on Soil-Atmosphere interaction, ICE. (In Print)

Conferences

- **S. K. Yamsani** and S. Sreedeep. (2014) "Shear and seepage characteristics of multi-layered cover soils: A laboratory study" Indian geotechnical conference (IGC) December 2014, JNTU Kakinada.
- Y. Gapak, **S. K. Yamsani** and S. Sreedeep. (2016) "Comparative study of long-term and gradient ratio tests in hydraulic performance evaluation of soil- geotextile system" Northeast students Geocongress on advances in geotechnical engineering (NESGC) January 2016, NIT Agartala.
- **S. K. Yamsani** and S. Sreedeep (2016) "Understanding desiccation potential of a given soil compaction state" International Conference on Soil and Environment (ICSE) 2016, IISc. Bangalore.
- **S. K. Yamsani** and S. Sreedeep.(2017) "Evaluation of surface infiltration characteristics of Multi-layered cover system" Indian geotechnical conference (IGC) December 2017, IIT Guwahati.
- Himanshu. K, **S. K. Yamsani** and S.Sreedeep. (2017) "Erosion Indices of Surface Soils with Pin Hole Test" ASCE India Conference December 2017, IIT Delhi.